Functional analysis of L-type voltage-gated Ca^{2+} channel isoforms Cav1.2 and Cav1.3 in NG2 glia

DISSERTATION

zur Erlangung des akademischen Grades des
Doktors der Naturwissenschaften
(Dr. rer. nat.)
der Medizinischen Fakultät, Institut für Physiologie,
der Universität des Saarlandes

vorgelegt von
Na Zhao

Homburg
April 2017

1. Gutachter:
   Prof. Dr. Frank Kirchhoff, CIPMM
   Molekulare Physiologie
   Institut für Physiologie
   Universität des Saarlandes
   66421 Homburg/Saar

2. Gutachter:
   Prof. Dr. Peter Lipp
   Institut für Molekulare Zellbiologie
   Universität des Saarlandes
   66421 Homburg/Saar

Tag der Disputation: _____

敬献给我亲爱的父母

To my beloved parents

Zusammenfassung

NG2 Glia sind Zellen, die gleichmäßig im zentralen Nervensystem verteilt sind und dabei den Hauptanteil der proliferierenden Zellen darstellen. Sie haben die Fähigkeit sich in Oligodendrozyten zu differenzieren. NG2 Glia exprimieren eine Vielzahl von spannungsgesteuerten Na^+ und K^+- Kanälen, die bei der Differenzierung, Proliferation und Reifung der Zellen beteiligt sind. Des Weiteren werden aber auch spannungsgesteuerte Ca^{2+}-Kanäle (Cav, voltage gated Ca^{2+} channels, VGCC) des L- und T-Typs mit unbekannter Funktion exprimiert.

Unsere elektrophysiologischen Analysen zeigten, dass NG2-Zellen während der Entwicklung L-Typ-Ca^{2+}-Kanäle in der weißen und grauen Substanz exprimieren, sich die Dichte der Ca^{2+}-Ströme in kortikalen NG2 Glia allerdings mit dem Alter verringert. Cav1.2 (*cacna1c*) und Cav1.3 (*cacna1d*), als Hauptuntereinheiten der L-Typ Ca^{2+}-Kanäle, werden beide in NG2 Glia exprimiert, die pharmakologische Analyse ihrer Funktion ist aber schwierig. Eine Analyse der einzelnen Knockouts könnte durch kompensatorische Effekte beeinflusst werden. Daher wurden zur Funktionsanalyse von Cav1.2 und Cav1.3 in NG2 Glia, Tamoxifen-induzierbare Doppel-Knockout-Mäuse (dKO) durch Kreuzen von gefloxten Cav1.2 und geflexten Cav1.3 Mäusen mit der NG2-CreERT2-Knockin-Maus generiert.

Patch-Clamp-Messungen der dKOs im Vergleich zu den Kontrolltieren zeigten eine signifikante Reduktion von spannungsgesteuerten Ca^{2+}-Strömen nach Tamoxifen induzierter Genrekombination. Dies konnte durch bildgebende Ca^{2+}-Messungen bestätigt werden, in denen die Ca^{2+}-Signale der dKOs deutlich reduziert waren. Der Verlust von L-Typ Ca^{2+}-Strömen in Cav1.2/1.3 dKOs konnte zu zwei Zeitpunkten nachgewiesen werden, zum einen drei Wochen nach der Induktion der Rekombination an den postnatalen Tagen sieben und acht und zum anderen nach einer späteren Induktion im Alter von drei Wochen mit einer erfolgreichen Deletion der Untereinheiten nach zehn Wochen. Hier konnte zudem ein weiterer kompensatorischer Einwärtsstrom bei -40 mV gemessen werden, ein charakteristisches Merkmal von spannungsgesteuerten T-Typ Ca^{2+}-Kanälen.

Diese Ergebnisse beweisen die erfolgreiche Deletion der L-Typ Ca^{2+}-Kanal-Isoformen Cav1.2 und Cav1.3 in neonatalen und adulten NG2-Zellen.

Die Deletion von Cav1.2/1.3 in NG2-Zellen hatte keinen Einfluss auf die Differenzierung der NG2 Glia und die anschließende Myelinisierung, während die kortikale Proliferation der NG2-Zellen um 54% reduziert war. In dKO-Mäusen war die Morphologie insbesondere in den feinen Fortsätzen der Zellen weniger komplex, was vermutlich auf die erhöhte Expression von α-Tubulin zurückzuführen ist. Weiterhin waren im Corpus Callosum der dKO-Mäuse die Abstände zwischen den paranodalen Strukturen im Vergleich zu Kontrolltieren verkürzt, ohne jedoch die Leitungsgeschwindigkeit der Axone zu verändern. Auch konnten in dKOs keine NMDA-induzierten Langzeitdepressionen (LTD, long term depression) im Hippocampus und präfrontalem Cortex induziert werden. Verhaltenstests wiesen bei den dKOs im Vergleich zu den Kontrolltieren eine Verhaltensstörung auf, die Tiere waren gestresster und zeigten verstärkt Angstzustände.

Alle genannten Ergebnisse zeigen deutlich, dass die Ca^{2+}-Kanäle des L-Typs in NG2-Glia-Zellen wichtig sind für die funktionale Modulation der neuronalen Netzwerkaktivität durch NG2 Glia.

Abstract

NG2 glia are uniformly distributed in the central nervous system. They are the major proliferating cells in the brain with the potential to differentiate into oligodendrocytes. Numerous voltage-gated ion channels, e.g. K^+ and Na^+ channels are expressed in NG2 glia, which are involved in their differentiation, proliferation and maturation. In addition, L- and T-type voltage-gated Ca^{2+} channels (VGCCs) are also expressed, however, their functions remain unknown.

Electrophysiological analysis showed that NG2 glia expressed L-type VGCCs in white and gray matter during development, while the peak Ca^{2+} current density in cortical NG2 glia was decreased gradually in an age-dependent manner. Cav1.2 (*cacna1c*) and Cav1.3 (*cacna1d*) as the main subunits of L-type VGCCs are both expressed in NG2 glia, but pharmacological analysis of each subtype function is infeasible. Furthermore, analysis of the single knockout might be influenced by compensatory effects. Therefore, to understand the functional roles of Cav1.2 and Cav1.3 in NG2 glia, we generated double knockout (dKO) mice by crossbreeding floxed Cav1.2 and flexed Cav1.3 transgenic mice to NG2-CreERT2 knock-in mice.

When mice were treated with tamoxifen to induce Cre-activity at postnatal day (P7) and analyzed three weeks later (P7+ 3 weeks or P21+ 7 weeks), patch-clamp recordings and Ca^{2+} imaging of NG2 glia in dKO mice revealed a significant reduction of voltage-gated Ca^{2+} currents and Ca^{2+} elevations compared to controls. Additionally, another inward peak current with a characteristic feature of T-type VGCCs was elicited at -40 mV in NG2 glia of dKO mice (P21+ 7 weeks). These results proved successful deletion of L-type VGCC isoforms Cav1.2 and Cav1.3 from NG2 glia in neonatal and adolescent mice.

Deletion of Cav1.2 and Cav1.3 in NG2 glia did not influence their differentiation and subsequent myelination, while cortical proliferation of NG2 glia was reduced by 54%. Meanwhile, Cav1.2/1.3 deficient NG2 glia displayed a less complex morphology in branching of their fine processes, presumably due to the upregulated expression level of α-

Tubulin in dKO mice. In addition, callosal paired paranodes in dKO mice were significantly shortened compared to control mice. However, no change in the conduction velocity of callosal axons was detected. NMDA-dependent long-term depression could not be elicited in hippocampus and medial prefrontal cortex of Cav1.2/1.3 deficient mice, while the synaptic input to NG2 glia from axons remained unaltered. Furthermore, behavioral tests implied an anxiety-like disorder in Cav1.2/1.3 deficient mice. In summary, NG2 glia are playing key roles in the functional modulation of neuronal network activities via the activation of L-type VGCCs.

Contents

Zusammenfassung **i**

Abstract **iii**

Contents **v**

List of Figures viii

List of Tables xi

List of Abbreviations xii

1 Introduction **1**

1.1 The expression and function of voltage-gated K^+ channels in NG2 glia . . . 3

1.2 The expression and function of voltage-gated Na^+ channels in NG2 glia . . 4

1.3 The expression of voltage-gated Ca^{2+} channels in NG2 glia 4

1.4 Physiological and pathological functions of VGCCs in NG2 glia 5

1.5 Summary 7

2 Aims of the study **9**

3 Materials and Methods **11**

3.1 Materials 11

3.1.1 Chemicals and reagents 11

3.1.2 Drugs 11

3.1.3 Antibodies 12

3.1.3.1 Primary Antibodies 12

3.1.3.2 Secondary Antibodies 12

3.1.3.2.1 For immunohistochemistry: 12

3.1.3.2.2 For Western blot: 12

3.1.4 Mouse lines 13

3.2 Methods . . . 13
3.2.1 Tamoxifen administration . . . 13
3.2.2 In situ experiments . . . 13
3.2.3 Slice preparation . . . 13
3.2.4 Electrophysiology . . . 14
3.2.5 Ca^{2+} imaging . . . 16
3.2.6 FM1-43 and FM1-43FX staining . . . 16
3.2.7 5-bromo-2-deoxyuridine (BrdU) treatment . . . 17
3.2.8 Immunohistochemical analysis . . . 17
3.2.8.1 Preparation of vibratome slices . . . 17
3.2.8.2 Antibody incubation . . . 17
3.2.8.3 Imaging acquisition and analysis . . . 18
3.2.9 Morphology analysis . . . 18
3.2.10 SDS-PAGE and Western blotting analysis . . . 19
3.2.10.1 Tissue preparation and protein isolation . . . 19
3.2.10.2 Western blot and immunodetection . . . 19
3.2.11 Behavioral tests by the ErasmusLadder . . . 20
3.2.11.1 Introduction of the ErasmusLadder . . . 20
3.2.11.2 Data analysis for the ErasmusLadder . . . 22
3.2.12 Statistical analysis . . . 23

4 Results **24**
4.1 NG2 glia: a heterogeneous cell population . . . 24
4.2 L-type voltage-gated Ca^{2+} channel expression in NG2 glia . . . 26
4.3 Removal of Cav1.2 and Cav1.3 genes from NG2 glia *in vivo* . . . 30
4.4 L-type VGCCs as the main contributors to Ca^{2+} influx in NG2 glia . . . 36
4.5 Normal membrane properties of Cav1.2/1.3 deficient NG2 glia . . . 41
4.6 No changes of oligodendroglial differentiation in Cav1.2/1.3 deficient NG2 glia . . . 44
4.7 Inhibited proliferation of cortical NG2 glia in Cav1.2/1.3 deficient mice . . . 47
4.8 No requirement of Cav1.2 and Cav1.3 proteins for myelination . . . 49
4.9 Partial loss of fine processes in Cav1.2/1.3 deficient NG2 glia . . . 52
4.10 Shortened paranodes in Cav1.2/1.3 deficient mice in the corpus callosum . . . 53
4.11 No alteration of conduction velocity in callosal axon after ablation of Cav1.2 and Cav1.3 in NG2 glia . . . 59

4.12 No changes of synaptic input in the somatosensory cortex after removal of Cav1.2 and Cav1.3 . . . 62
4.13 NMDA-dependent long-term depression deficit in Cav1.2 and Cav1.3 knock-out mice . . . 62
4.14 Vesicular release of NG2 glia . . . 67
4.15 Cav1.2/1.3 knockout mice with anxiety-like behavioral abnormalities . . . 68

5 Discussion **73**
5.1 Conditional inactivation of Cav1.2 and Cav1.3 specifically in NG2 glia . . . 74
5.2 Reduced proliferation and no changes in differentiation in Cav1.2/1.3 deficient NG2 glia . . . 75
5.3 Myelination was not affected by knockout of Cav1.2/1.3 in NG2 glia . . . 76
5.4 Ablation of Cav1.2 and Cav1.3 impaired the cytoskeleton network . . . 78
5.5 The neuronal network was strongly influenced in Cav1.2 and Cav1.3 knock-out mice . . . 79
5.6 Anxiety-like behavior in Cav1.2/1.3 deficient mice after several stimulation . 80
5.7 Hypothetical functions of VGCCs in NG2 glia. . . . 81

6 Outlook **84**

7 Appendix **86**
7.1 Cav1.2/1.3 deficient mice behaved anxiety-like disorders . . . 86

References **91**

Appendix A: Publications **98**

Appendix B: Acknowledgment **100**

List of Figures

1.1 Cellular diversity of neurons and glial cells in the brain. 2
1.2 Voltage-gated ion channels expression by NG2 glia. 7

2.1 Induction of Cav1.2 and Cav1.3 conditional knockout in NG2 glia. 9

3.1 The ErasmusLadder used for analysis of motor coordination. 21
3.2 The default protocols. 21
3.3 The classification of steps. 23

4.1 Whole-cell membrane current profiles of cortical NG2 glia in young mice ($<$ P16). 25
4.2 Membrane properties of complex and passive NG2 glia in the neonatal cortex. 26
4.3 Whole-cell membrane current profiles of NG2 glia in the adult cortex. 27
4.4 The expression of voltage-gated Ca^{2+} channels in cortical NG2 glia. 28
4.5 Comparison of Ca^{2+} currents in different brain regions during the development. 29
4.6 NG2 glia retain stable membrane properties in different brain regions during CNS development. 30
4.7 Successful knockout of Cav1.2 and Cav1.3 in NG2 glia from neonatal mice. 32
4.8 dKO mice lost body weight after tamoxifen treatment. 33
4.9 Removal of Cav1.2 and Cav1.3 in NG2 glia of adolescent mice. 34
4.10 Failure to delete Cav1.2 and Cav1.3 in NG2 glia in adult mice. 35
4.11 Ca^{2+} elevation in cortical NG2 glia upon depolarization. 36
4.12 Ca^{2+} elevation in Cav1.2/1.3 deficient NG2 glia in the cortex upon depolarization. 37
4.13 Somatic Ca^{2+} elevations were decreased in Cav1.2/1.3 deficient NG2 glia. . 38
4.14 Ca^{2+} elevations were reduced in the processes of cortical NG2 glia. 39

4.15 Ca^{2+} elevations in neurons. 40
4.16 Somatic Ca^{2+} elevations in cortical NG2 glia is mediated by activation of L-type VGCCs. 41
4.17 Ca^{2+} elevations in the processes of NG2 glia is also mediated by the activation of L-type VGCCs. 42
4.18 Membrane currents of Cav1.2/1.3 deficient NG2 glia. 43
4.19 Membrane properties of Cav1.2/1.3 deficient NG2 glia. 44
4.20 NG2 glia retain the ability to differentiate into oligodendrocytes in dKO mice. 45
4.21 Percentages of GFP^{+} cells in dKO mice using EGFP reporter. 46
4.22 Cav1.2/1.3 deficient NG2 glia kept proliferating in the corpus callosum and cortex. 48
4.23 Inhibition of cortical NG2 glia proliferation in Cav1.2/1.3 deficient mice. . . . 49
4.24 Knockout of Cav1.2 and Cav1.3 in NG2 glia did not alter myelin protein expression. 50
4.25 Knockout of Cav1.2 and Cav1.3 in NG2 glia disturbed microtubule cytoskeleton in the corpus callosum. 51
4.26 Ca1.2/1.3 deficient NG2 glia exhibited less complex morphology. 54
4.27 Paranodes in corpus callosum of CTL and dKO mice. 55
4.28 The length of paired paranodes in corpus callosum from Cav1.2/1.3 deficient mice were shortened. 56
4.29 Paranodes in the spinal cord of CTL and dKO mice. 57
4.30 Deletion of Cav1.2 and Cav1.3 did not alter the length of paired paranodes and nodes of Ranvier in the spinal cord. 57
4.31 Paranodes in the optic nerve of CTL and dKO mice. 58
4.32 Deletion of Cav1.2 and Cav1.3 did not alter the length of paired paranodes and nodes of Ranvier in optic nerve. 58
4.33 Strategy of callosal compound action potential recordings. 59
4.34 Callosal conduction velocity was not influenced by the deletion of Cav1.2 and Cav1.3 in NG2 glia. 60
4.35 The stimulus-response upon current injection in corpus callosum from CTL and dKO mice. 61
4.36 Removal of Cav1.2/1.3 did not affect neuron-glia synapses in the somatosensory cortex. 63
4.37 LTD induced by low frequency stimulation in hippocampus. 64
4.38 LTD induced by NMDA perfusion in hippocampus. 65

4.39 LTD induced by LFS in the medial prefrontal cortex. 66
4.40 FM1-43 dye staining in NG2 glia. 67
4.41 FM1-43 dye staining in Cav1.2/1.3 deficient NG2 glia 68
4.42 Cav1.2/1.3 deficient mice showed unaltered motor learning on the ladder. . 69
4.43 Cav1.2/1.3 deficient mice showed unaltered motor coordination. 70
4.44 Cav1.2/1.3 deficient mice stayed longer on the ladder after cue. 71

5.1 Hypothetical functions of VGCCs in NG2 glia. 82

7.1 dKO mice made more undisturbed trials due to irregular walking on the ladder. 86
7.2 dKO mice triggered less perturbation trials. 87
7.3 dKO mice increased the percentage of short steps in perturbation trials. . . 88
7.4 dKO mice moved slower with short steps during perturbation sessions. . . . 89
7.5 No difference of the percentage of long steps between CTL and dKO mice. 89
7.6 dKO mice walked slowly with long steps during perturbation sessions. . . . 90
7.7 dKO mice did not show any difference on the percentage of Jumps from CTL mice. 90

List of Tables

3.1 Drugs used in electrophysiological studies 11
3.2 Primary antibodies 12
3.3 Mouse lines 13

4.1 Paranodal length in white matter 53

List of Abbrevations

$[Ca^{2+}]_i$	Intracellular Ca^{2+} concentration
ACSF	Artificial cerebral spinal fluid
AMPAR	α-amino-3-hydroxy-5-methyl-4-isoxazole propionic acid receptor
CAP	Compound action potential
CC	Corpus callosum
CS	Conditioned stimulus
CTL	Control
CTX	Cortex
dKO	Double knockout
EPSC	Excitatory postsynaptic current
ER	Endoplasmic reticulum
fEPSP	Field excitatory postsynaptic potential
FGF2	Fibroblast growth factor 2
GABAR	Gamma-aminobutyric acid receptor
GluR	Glutamate receptor
IV curve	Current-voltage curve
K_v	Voltage-gated potassium channel
LFS	Low-frequency stimulation
LTD	Long-term depression

mPFC	Medial prefrontal cortex
Na_v	Voltage-gated sodium channel
NMDAR	N-methyl-D-aspartate receptor
OL	Oligodendrocyte
OPC	Oligodendrocyte precursor cell
Pα	PDGFRα
P7	Postnatal 7 days
PDGFR	Platelet-derived growth factor receptor
RT	Room temperature
sKO	Single knockout
SVZ	Subventricular zone
US	Unconditioned stimulus
VGCC	Voltage-gated Ca^{2+} channel

All dimensions in this study were described according to the international system of units.

Chapter 1

Introduction

NG2 glia are an abundant class of glial cells in the central nervous system (CNS) which express the chondroitin sulfate proteoglycan NG2 and the alpha receptor for platelet-derived growth factor (PDGFR) (Dawson et al., 2000; Nishiyama et al., 2009). They are extensively distributed in CNS gray and white matter during development and differ from other glial cells, e.g. astrocytes, microglia and oligodendrocytes by their different morphological and physiological properties (Fig.1.1) (Hill and Nishiyama, 2014). The main known function of NG2 glia is the differentiation into oligodendrocytes in gray and white matter throughout life, thus they are often termed oligodendrocyte precursor cells (OPCs) (Kang et al., 2010; Zhu et al., 2008a). Embryonic NG2 glia can give rise to astrocytes which are mainly present in the gray matter of the forebrain and spinal cord (Huang et al., 2014; Zhu et al., 2008a,b). NG2 glia retain their physiological properties and keep self-renewing as the major proliferating cell population outside the neurogenic regions of subventricular zone and dentate gyrus of hippocampus under physiological (Clarke et al., 2012; Hill and Nishiyama, 2014; Huang et al., 2014; Zhu et al., 2008a) or pathological conditions (Tatsumi et al., 2008; Tripathi et al., 2010). However, they display regional heterogeneity in their proliferation (Young et al., 2013). It has been shown that the proliferation rates of NG2 glia exhibit regional differences in gray and white matter, decreasing with age in these regions(Dimou and Gallo, 2015; Hill and Nishiyama, 2014; Hill et al., 2013; Moshrefi-Ravasdjani et al., 2016).

NG2 glia can receive synaptic input from axons, which is downregulated after differentiation into oligodendrocytes (De Biase et al., 2010; Kukley et al., 2010). Recent evidence indicated that NG2 glia have the capability to modulate neuronal network activities. Pharmacological inhibition of NG2 or genetic ablation of NG2 protein resulted in striking reduction in N-methyl-D-aspartate receptor (NMDAR) dependent long term potentiation (LTP)

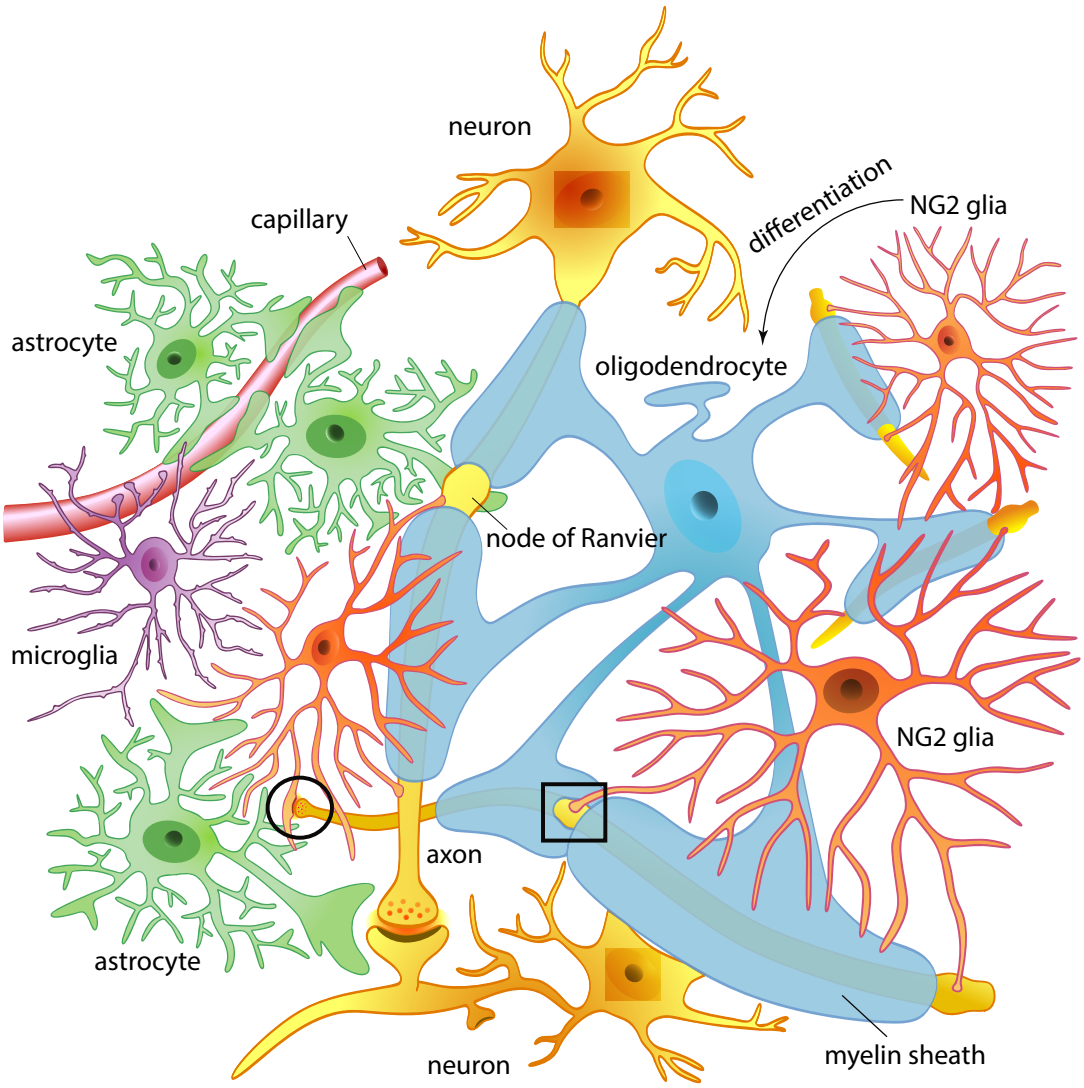

Figure 1.1 Cellular diversity of neurons and glial cells in the brain. NG2 glia (orange) are distinct from the other kinds of glial cells, e.g., astrocytes (green), microglia (purple) and oligodendrocytes (blue). During their lifespan, NG2 glia differentiate into oligodendrocytes in gray and white matter (arrow). They have synaptic contact with neurons (square box) or receive synaptic input from neurons (circle).

in pyramidal neurons of the somatosensory cortex and diminished NMDA and α-Amino-3-hydroxy-5-methyl-4-isoxazolepropionic acid receptor (AMPAR)-dependent current amplitudes in these neurons (Sakry et al., 2014). Ablation of NG2 glia causes deficits in the excitatory glutamatergic synaptic transmission in the prefrontal cortex (PFC) of the adult brain which results in depressive-like behaviors (Birey et al., 2015). Therefore, NG2 glia are playing a very important role in modulation of CNS homeostasis. However, the precise mechanism remains unknown.

1.1 The expression and function of voltage-gated K^+ channels in NG2 glia

NG2 glia express voltage-gated K^+ channels (K_v), namely large transient outward A-type K^+ (K_A) channels, outward delayed rectifier K^+ (K_{DR}) channels and inward delayed rectifier K^+ (K_{IR}) channels in gray (cortex and hippocampus) and white matter (corpus callosum) of mice (Attali et al., 1997; Berger et al., 1991; Chittajallu et al., 2004; Steinhauser et al., 1994). Transient outward A-type K^+ currents (I_{K_A}) display a peak amplitude due to rapid activation and inactivation, which can be blocked by 4-aminopyridine (4-AP) and internal Cs^+ (Steinhauser et al., 1994). Outward delayed rectifier K^+ currents ($I_{K_{DR}}$) exhibit sustained steady-state currents, characterized by slow activation and non-inactivation, which can be blocked by tetraethylammonium (TEA) and internal Cs^+ (Barres et al., 1990). Reverse transcription PCR cloning, immunocytochemical and Western blot analysis revealed that $I_{K_{DR}}$ channel isoforms $K_v1.2$, $K_v1.4$, $K_v1.5$ and $K_v1.6$ could be detected in oligodendrocyte lineage cells (Attali et al., 1997; Schmidt et al., 1999). Cs^+-sensitive inward delayed rectifier K^+ currents ($I_{K_{IR}}$) have also been detected on some NG2 glia (Chittajallu et al., 2004; Knutson et al., 1997; Zonouzi et al., 2011). The RNA-seq transcriptome database has shown gene expression of K_vs in a variety of cell types, including NG2 glia (Larson et al., 2016; Zhang et al., 2014).

K_A have an important influence in shaping synaptic input. Treatment with 4-AP in acute hippocampal slices strongly increased the amplitude and half-width of mock post-synaptic potential (PSP) in response to a single glutamate-filled vesicle release in NG2 glia. While blocking Na^+ channels and K_{DR} did not detectably change the duration of mock PSPs (Sun et al., 2016). $I_{K_{DR}}$ play a crucial role during OPC development because their selective blockage of $I_{K_{DR}}$ by TEA decreases cell proliferation and differentiation to mature oligodendrocytes (Attali et al., 1997; Chittajallu et al., 2005; Gallo et al., 1996; Knutson et al., 1997). Moreover, proliferation of NG2 glia can be inhibited by AMPA receptor activation through inhibition of $I_{K_{DR}}$ (Gallo et al., 1996). Additionally, immunohistochemical evidence indicated weak $I_{K_{IR}}$ 4.1 expression in NG2 glia in gray and white matter (Butt and Kalsi, 2006; Tang et al., 2009). $I_{K_{IR}}$ was enhanced during maturation, highlighting its importance in the maturation process of oligodendrocyte lineage cells (Maldonado et al., 2013; Moshrefi-Ravasdjani et al., 2016; Neusch et al., 2001). $I_{K_{IR}}$ are also up-regulated in post-mitotic cells of the oligodendrocyte lineage (Knutson et al., 1997; Sontheimer et al., 1989; Yuan et al., 2002). Expression of $I_{K_{IR}}$ in glial cells has been implicated in several other functions, including stabilization of resting membrane potentials and removal

of extracellular K^+ (Butt and Kalsi, 2006).

1.2 The expression and function of voltage-gated Na^+ channels in NG2 glia

Voltage-gated Na^+ channels (Na_v) can also be detected in NG2 glia in different brain regions of rodents by whole-cell patch clamp recordings (Barres et al., 1990; Chittajallu et al., 2004; Clarke et al., 2012; De Biase et al., 2010; Ge et al., 2009; Karadottir et al., 2008; Schools et al., 2003; Tong et al., 2009; Zhou et al., 2006), but peak current amplitudes detected from NG2 glia were in a range of one or two hundred pico-amperes, which was much smaller compared to that of neurons (Maldonado et al., 2011).

NG2 glia are heterogeneous in respect to Na_v expression and excitablity of membranes in the cerebral cortex and cerebellar white matter (Chittajallu et al., 2004; Karadottir et al., 2008). Voltage-gated Na^+ currents (I_{Na_v}) were observed in all NG2 glia in many brain regions of white matter (corpus callosum and cerebellar white matter) and gray matter (hippocampus and cerebellar molecular layer) at the earlier developmental periods (P5-P8, P12-P15, P20-P26) with no consistent change in I_{Na_v} density in an age-dependent manner (De Biase et al., 2010).

Both amplitude of I_{Na_v} and synaptic current frequency decrease when progenitors undergo differentiation (De Biase et al., 2010; Kukley et al., 2010). The transient NG2 cell-synaptic connectivity is not only spatially, but also temporally regulated in coordination with the active differentiation phase of these progenitors in the second postnatal week (Orduz et al., 2015). These evidence suggests that Na_vs are diversely expressed in NG2 glia during development. It is also very likely that Na_vs play an important role in amplifying synaptic input in NG2 glia at an earlier postnatal period.

1.3 The expression of voltage-gated Ca^{2+} channels in NG2 glia

Ca^{2+} influx into the cytoplasm elevates intracellular [Ca^{2+}], which induces a series of physiological activities through membrane-bound proteins like AMPA/Kainate receptors, P2X purinoceptors, and voltage-gated Ca^{2+} channels (VGCCs) in response to raised extracellular [K^+] (Butt and Kalsi, 2006). Voltage-gated Ca^{2+} currents, present in all excitable cells, are classified into six types based on their physiological properties and pharmacological profiles, namely L, N, R, P/Q, and T types (Nowycky et al., 1985). In response to changes on membrane depolarization, the T-type is termed as low-voltage activated

channel (LVA), while the other types are high-voltage activated (HVA). LVA currents inactivate faster, more completely and at more negative membrane potentials than HVA currents (Bean, 1989a), while HVA channels require larger depolarization and subsequently inactivate slower. L-type channels consist of the subtypes Cav1.1 - Cav1.4. The remaining HVA currents, P/Q-, N- and R-types are Cav2.1 - Cav2.3, respectively and the T-type are Cav3.1 - Cav3.3 (Tuckwell, 2012).

in vitro and *in situ* studies demonstrated the co-expression of HVA/L-type and LVA/T-type Ca^{2+} channels in somata and processes of NG2 glia in gray and white matter (Berger et al., 1992; Blankenfeld Gv et al., 1992; Coppi et al., 2013; Kirischuk et al., 1995; Paez et al., 2009a,b). Ca^{2+} influx via VGCCs was greatly reduced in response to depolarization with high K^+ after NG2 glia differentiation (Paez et al., 2010). GABA application evoked transient [Ca^{2+}] elevation can be diminished by L-type VGCC blockers in cultured $O1^+$ precursor cells and $Nestin^+/NG2^+$ cells from acute brain slices (Haberlandt et al., 2011; Kirchhoff and Kettenmann, 1992; Tanaka et al., 2009). Immunohistochemistry analysis provided the evidence for L-, N- and R-type Ca^{2+} channel expression in OPCs and oligodendrocytes in the forebrain, spinal cord white matter and cerebellum (Agrawal et al., 2000; Chen et al., 2000; Paez et al., 2012). L-type and T-type Ca^{2+} currents were observed in hippocampal NG2 glia at postnatal days 7 to 15 by whole-cell patch clamp (Haberlandt et al., 2011). Single-cell RT-PCR showed the predominant expression of mRNA encoding L-type VGCCs subunits Cav1.2 and Cav1.3, and T-type VGCCs subunits Cav3.1 and Cav3.2 (Haberlandt et al., 2011). Mock PSPs can also trigger Ca^{2+} signal through VGCC activation in soma and proximal processes which were highly sensitive to a cocktail of VGCC blockers (R-type blocker SNX-482 and T-type blocker TTA-P2) (Sun et al., 2016). Several VGCC isoforms expressed in NG2 glia have also been confirmed in RNA-Seq transcriptome (Larson et al., 2016; Zhang et al., 2014).

1.4 Physiological and pathological functions of VGCCs in NG2 glia

Ca^{2+} currents in NG2 glia are smaller than other voltage-gated ion channels and little is known about VGCCs in NG2 glia under neither physiological nor pathological conditions. We believe that VGCCs contribute to CNS homeostasis during maturation. However, what are the functions of these VGCCs in NG2 glia compared to known functions in other cell types? In cardiomyocytes their function is quite clear. The cytosolic Ca^{2+} influx through VGCC activation results in Ca^{2+} induced Ca^{2+} release (CICR) from the

endoplasmic reticulum (ER) via ryanodine receptors (RyRs), followed by cellular contractions (Budde et al., 2002). This functional coupling between VGCCs and RyRs also exists in neurons (Chavis et al., 1996). Cav2.1 - 2.3 genes are important mediators of depolarization-evoked release of neurotransmitters (Simms and Zamponi, 2014).This functional coupling between L-type Ca^{2+} channels and RyRs seems to be universal, it also exists in NG2 glia. Depolarization induced Ca^{2+} elevations in NG2 glia are due to initial influx of Ca^{2+} through VGCCs followed by CICR (Haberlandt et al., 2011). But what happens after Ca^{2+} induced Ca^{2+} release mediated by VGCCs in NG2 glia?

In vitro studies demonstrated that activation of VGCCs induced by depolarization increased OPC differentiation. It has been proposed that activation of VGCCs in these cells might act as an initiation signal for myelination (Kirischuk et al., 1995). Knockdown of the Cav1.2 subunit by transfection with siRNAs in primary cultures of mouse OPCs reduced the Ca^{2+} influx by $\sim$75% , indicating a strong Cav1.2 involvement in voltage-gated Ca^{2+} entry in OPCs (Cheli et al., 2015). Cav1.2 knockdown induced OPC proliferation, but prolonged the cell cycle. Moreover, the *in vitro* loss of Cav1.2 in NG2 glia affected their axonal contact and in consequence the initial steps of myelination. However, the Cav1.3 knockdown had no effects on NG2 glia development (Cheli et al., 2015). Additionally, Ca^{2+} influx via VGCCs in response to depolarization stimulate NG2 glia migration, and migration speed can be inhibited by VGCC blockers, indicating that VGCCs play critical roles in cell motility (Paez et al., 2009a, 2010). The conditional deletion of Cav1.2 strongly inhibited myelination in the corpus callosum and cortex *In vivo*. Furthermore, ablation of Cav1.2 inhibited cell migration, proliferation and maturation to oligodendrocytes in cortex and corpus callosum. However, no changes could be observed in adult mice (Cheli et al., 2016). These data suggest that L-type VGCCs are crucial for the adequate migration, proliferation, and maturation of NG2 glia, and subsequently for the myelination in the early postnatal mouse brain.

Many studies showed that glial cells are reprogramming themselves after injury including remodeling of ion channel expression. $I_{K_{DR}}$ were significantly inhibited in NG2 glia after spinal cord injury but I_{K_A} were not affected (Lytle et al., 2009). Hippocampal NG2 glia, in controls and after global cerebral ischemia, revealed a typical current pattern for this glial cell population. They exhibit time- and voltage-independent K^+ conductance together with $I_{K_{DR}}$, I_{K_A} and $I_{K_{IR}}$ currents and, in a subset of cells, fast activating Na^+ inward currents (Pivonkova et al., 2010). Both transient I_{K_A} and sustained $I_{K_{DR}}$ decreased remarkably in NG2 glia from the injured brain region after stab wound injury in the cortex without the impact of $I_{K_{IR}}$ (Bai et al., Under review). However, I_{K_v} and I_{Na_v} current densities

were not changed in NG2 glia of the white matter following demyelination (Sahel et al., 2015). These results indicate that K_v channels are involved in proliferation, differentiation and maturation of NG2 glia during development.

1.5 Summary

NG2 glia express a high density of I_{K_A}, $I_{K_{DR}}$ and $I_{K_{IR}}$ which play essential roles in proliferation, differentiation and maturation during CNS development (Fig. 1.2). A developmental increase in the expression of K_{IR}s results in higher current densities, lower rectification indices and lower membrane resistance. Only complex NG2 glia have I_{Na_v}. In this subpopulation, some NG2 glia are able to generate a single spike or several consecutive spikes while failing to elicit real action potentials. While passive NG2 glia mainly express

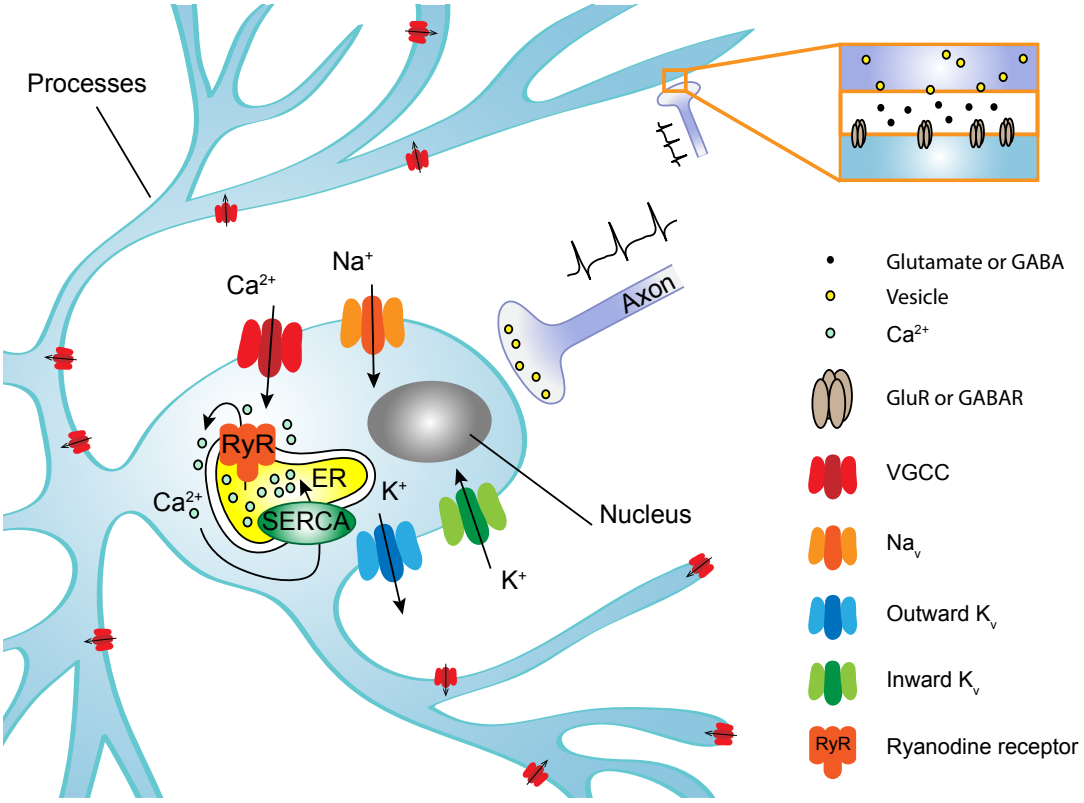

Figure 1.2 Voltage-gated ion channels expression by NG2 glia. NG2 glia express voltage-gated K^+, Na^+ and Ca^{2+} channels in their somata and processes. Ca^{2+} influx into the cytoplasm via VGCCs results in Ca^{2+}-induced Ca^{2+} release via Ryanodine receptors (RyRs). The sarcoplasmic reticulum Ca^{2+}-ATPase (SERCA) pumps cytoplasmic Ca^{2+} back into the endoplasmic reticulum (ER). Highlighted here, NG2 glia receive synaptic input from axons.

I_{K_A}, $I_{K_{DR}}$ and $I_{K_{IR}}$. L- and T-type Ca^{2+} channels were observed in NG2 glia *in situ* or *in vitro* in gray and white matter during CNS development. L-type Ca^{2+} channels are predominantly expressed in NG2 glia and decreased significantly in the cortex with age. Knockdown of Cav1.2 in cultured OPCs suggested that Cav1.2 is mainly involved in mediating voltage-gated Ca^{2+} entry and cell proliferation. *In vivo* conditional ablation of Cav1.2 in NG2 glia inhibits cell proliferation, maturation of OPCs and myelination in cortex and corpus callosum at an early postnatal stage.

Chapter 2

Aims of the study

NG2 glia express voltage-gated Ca^{2+} channels under physiological and pathological conditions. In this study we are addressing the following questions:

1) What is the functional role of VGCCs in NG2 glia during development *in vivo*?

2) Does the knockout of Cav1.2 (*cacna1c*) and Cav1.3 (*cacna1d*) lead to behavioral abnormalities?

3) How do NG2 glia modulate CNS homeostasis and what are the contributions of Cav1.2 and Cav1.3 proteins?

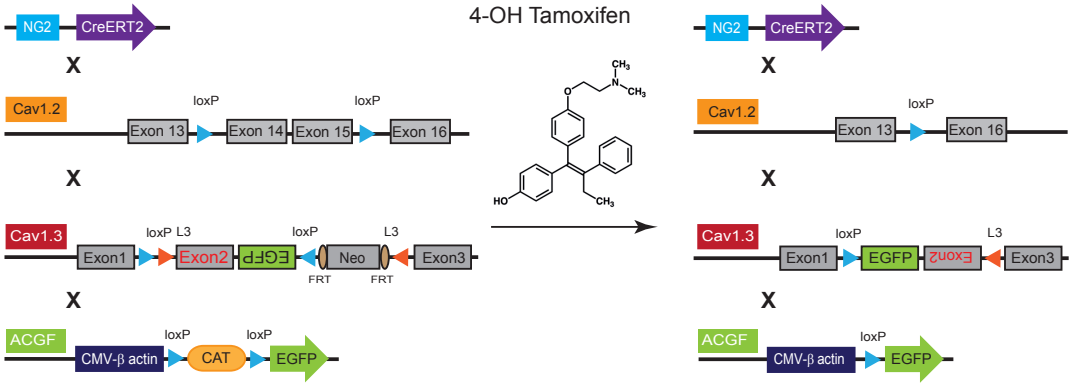

Figure 2.1 Induction of Cav1.2 and Cav1.3 conditional knockout in NG2 glia. Highlighted here are the constructs for generation of the different transgenic mouse strains used for the breed of tamoxifen inducible Cav1.2 and Cav1.3 knockout mice.

We took advantage of homozygous floxed Cav1.2 (Moosmang et al., 2005, 2003) and flexed Cav1.3 (Satheesh et al., 2012) mice crossbred to NG2-CreERT2 knock-in mice (Huang et al., 2014). Triple transgenic mice were additionally crossbred to CAG-EGFP reporter mice (Nakamura et al., 2006) to label recombined cells (Fig. 2.1). The NG2-CreERT2 knock-in mouse line can circumvent the disadvantages of the non-homologous

Cre-expressing transgenic mice. This mouse line allows reliable gene targeting in NG2-expressing cells in the CNS at different developmental stages *in vivo* (Huang et al., 2014). Therefore, with this approach, Cav1.2 and Cav1.3 genes can be deleted specifically in NG2 glia at any time point during CNS development.

Chapter 3

Materials and Methods

3.1 Materials

3.1.1 Chemicals and reagents

All chemicals were purchased from the following companies: Carl Roth (Karlsruhe, Germany), Applichem Panreac (Heidelberg, Germany), Invitrogen (Karlsruhe, Germany), Merck (Darmstadt, Germany), Acros (New Jersey, USA), Grüssing (Filsum, Germany), Sigma-Aldrich (Deisenhofen, Germany) and Tocris (Bristol, UK).

3.1.2 Drugs

Table 3.1 Drugs used in electrophysiological studies

Name	Chemical name	Concentration (μM)	Manufacture
4-AP	4-Aminopyridine	5000	Sigma
CNQX	6-Cyano-7-nitroquinoxaline-2,3-dione	30	Tocris
DAP5	D-(-)-2-Amino-5-phosphonopentanoic acid	30	Tocris
Midefradil		50	Sigma
Nimodipine		30	Tocris
NMDA	N-Methyl-D-aspartic acid	25	Tocris
Picrotoxin		50	Sigma
TEA	Tetraethylammonium chloride	120,000	Acros
TTX	Tetrodotoxin (citrate)	1	Alomone Labs
Verapamil		50	Tocris

3.1.3 Antibodies

3.1.3.1 Primary Antibodies

Table 3.2 Primary antibodies

Antibodies	Species	Dilution	Company
GFP	rabbit	1:1000 (IHC)	Clontech
GFP	goat	1:1000 (IHC)	Rockland
GFP	mouse	1:500 (IHC)	Abcam
PDGFRα	rat	1:500 (IHC)	BD Pharmingen
PDGFRα	goat	1:500 (IHC)	R&D Systems
NG2	rat	1:50 (IHC)	Gift from Dr. J. Trotter, Mainz
BrdU	rat	1:1500 (IHC)	Abcam
Caspr	rabbit	1:1000 (IHC)	Abcam
CC1	mouse	1:50 (IHC)	Calbiochem
MBP	mouse	1:1000 (IHC, WB)	Biolegend
MOG	goat	1:1000 (WB)	Abcam
PLP	rabbit	1:1000 (WB)	Gift from Dr. K.A. Nave, Göttingen
GFAP	rabbit	1:1000 (WB)	DAKO
α-Tubulin	mouse	1:5000 (WB)	Sigma
β-Actin	mouse	1:5000 (WB)	Sigma
GAPDH	rabbit	1:5000 (WB)	Sigma

3.1.3.2 Secondary Antibodies

3.1.3.2.1 For immunohistochemistry: Donkey anti-mouse, goat, rabbit or rat secondary antibodies (1:1000) conjugated with Alexa488, Alexa555, Alexa633 or Alexa647 were purchased from Invitrogen (Grand Island NY, USA.) Goat anti-rabbit or rat secondary antibodies (1:500) conjugated with Cy5 were purchased from Dianova (Hamburg, Germany).

3.1.3.2.2 For Western blot: Anti-rabbit, goat and mouse secondary antibodies (1:10,000) conjugated with HRP (horseradish peroxidase) were purchased from Dianova.

Table 3.3 Mouse lines

Mouse line	Citation
TgH (NG2-EYFP)	(Karram et al., 2008)
TgH (NG2-CreERT2)	(Huang et al., 2014)
TgH (CACNA1C-flox)	(Moosmang et al., 2005, 2003)
TgH (CACNA1D-EGFP flex)	(Satheesh et al., 2012)
TgN (CAG-CAT-EGFP)	(Nakamura et al., 2006)

3.1.4 Mouse lines

All the mouse lines were maintained in C57BL/6N background. All experiments were carried out at the University of Saarland in strict accordance with the recommendations to European and German guidelines for the welfare of experimental animals. Animal experiments were approved by the Saarland states “Landesamt für Gesundheit und Verbraucherschutz” in Saarbrücken/Germany (animal license number: 72/2010, 65/2013 and Cervical dislocation).

3.2 Methods

3.2.1 Tamoxifen administration

Tamoxifen (T5648, Sigma-Aldrich, St. Louis, USA) was dissolved in corn oil (Sigma-Aldrich, St. Louis, USA) to achieve the concentration of 10 mg/mL. Neonatal mice were intraperitoneally injected with tamoxifen on a dosage of 100 mg/kg body weight, once per day at P7 and P8. Young adult mice were injected by tamoxifen intraperitoneally once per day for three consecutive days from P21 to P23 and additional two injections every two days after three weeks.

In all experiments except behavior tests (only male used), both male and female mice were used, and the number of males and females in each analysis group was balanced.

3.2.2 In situ experiments

3.2.3 Slice preparation

Mice were anesthetized with isofluran (Abbvie, Ludwigshafen, Germany) before decapitation. The brains were removed from the skull and immersed in an ice-cold, oxygenated (5% CO_2/ 95% O_2, pH $\sim$7.4) slice preparation solution containing (in mM) 87 NaCl, 3 KCl,

25 $NaHCO_3$, 1.25 NaH_2PO_4, 3 $MgCl_2$, 0.5 $CaCl_2$, 75 sucrose and 25 glucose. Coronal slices of 300 μm thickness were prepared with a vibratome (Leica VT 1200S, Nussloch, Germany) and transferred to a nylon basket slice holder for incubation in artificial cerebral spinal fluid (ACSF) containing (in mM) 126 NaCl, 3 KCl, 25 $NaHCO_3$, 15 glucose, 1.2 NaH_2PO_4, 2 $CaCl_2$, and 2 $MgCl_2$ at 32°C for 0.5 h. The slices were taken out of the water bath and placed to room temperature (RT) with continuous oxygenation before use.

3.2.4 Electrophysiology

For in situ recording, the slices were transferred to the recording chamber and continuously perfused with oxygenated ACSF containing 1 mM $MgCl_2$ and 2.5 mM $CaCl_2$ at a flow rate of 2-5 mL/min. NG2 glia located in the neocortex were identified using a Zeiss microscope (Axioskop 2 FS mot, Zeiss) with a 40x water immersion objective and filter sets for YFP and GFP. Image were detected with QuantEM 512SC camera (Photometrics, Tucson) and displayed on a monitor. Whole-cell membrane currents were recorded by EPC 10 USB amplifier (HEKA Elektronik Dr. Schulze GmbH, Lambrecht/Pfalz, Germany), low pass filtered at 3 kHz and data acquisition was controlled by Patchmaster software (HEKA). Patch pipettes (resistance, 7∼9 MΩ) were fabricated from borosilicate capillaries (Outside diameter: 1.5 mm, inside diameter: 0.86 mm; Sutter, USA) using a Micropipette Puller (Model P-97, Sutter Instrument Co., CA). Patch pipettes were filled with a solution containing (in mM) 120 KCl, 2 $MgCl_2$, 5 EGTA, 10 HEPES and 5 Na_2ATP (pH∼7.2). The holding potential in voltage clamp mode was -80 mV. Resting membrane potential was measured within 30 s after establishing the whole-cell recording.

For recording L-type Ca^{2+} currents, pipette solutions contained (in mM): 120 CsCl, 1 $MgCl_2$, 0.5 $CaCl_2$, 5 EGTA, 10 HEPES, 5 Na_2ATP and 20 Tetraethylammonium chloride (TEA), its pH value was adjusted to ∼7.2 with CsOH. The extracellular solutions contained (in mM) 120 TEA, 10 HEPES, 5 $CaCl_2$, 5 4-Aminopyridine (4-AP) and 10 Glucose. TTX (1 μM) was added to the bath to block voltage-gated Na^+ channels (VGSC). Whole-cell voltage-clamp was used for membrane currents recording from reporter$^+$ cells in acute brain slices. NG2 glia could be clearly distinguished from pericytes, which are also reporter$^+$, on the basis of their distinct morphologies (Ziskin et al., 2007). In the NG2-CreERT2 mouse line, recombined NG2 glia differentiate into oligodendrocytes which are therefore also reporter$^+$. However, the reporter$^+$ oligodendrocytes are easily distinguished in terms of their much lower membrane resistance and quite different morphologies. Resting membrane potential was measured in whole-cell current-clamp mode with a current injection set to 0.

For the recording of postsynaptic currents, NG2 glia in the layer II/III of the somatosensory cortex were measured while a concentric bipolar microelectrode (MicroProbes, USA) was placed in the layer V close to the border of layer IV, with a stimulus duration of 300 μs (Lalo et al., 2014). Patch pipettes were filled with a solution containing (in mM) 125 K gluconate, 20 KCl, 2 $MgCl_2$, 0.5 EGTA, 5 HEPES and 5 Na_2ATP, its pH value was adjusted to ∼7.2 with KOH. The recordings were in whole-cell voltage-clamp mode. 6-cyano-7-nitroquinoxaline-2, 3-dione (CNQX, 30 μM) and D-(-)-2-Amino-5-phosphonopentanoic acid (D-AP5, 30 μM) were applied via the perfusion system (custom-made).

For the recording of compound action potentials in the corpus callosum, coronal brain slices of 360 μm thickness were prepared. Micropipettes were filled with ACSF which had a resistance of 1-3 MΩ. The stimulating electrode was lowered into corpus callosum (CC) at approximately 1 mm lateral to middle. The recording electrode was placed at the contralateral CC at a distance of 2.0 mm from the stimulating electrode. Negative responses were evoked in current clamp mode by varying the intensity of stimulus pulses in steps from approximately threshold level to an asymptotic maximum (e.g., 0.2-4.0 mA). The stimulus duration was 200 μs. The sample sweeps were acquired every 5 s. CC conduction velocity was estimated by changing the distance between the stimulating electrode and recording electrode with the holding stimulus intensity constant. The stimulating electrode was placed 1 mm away from the midline, while the recording electrode was moving from 2.5 mm away from the stimulating electrode in the contralateral hemisphere to the closest distance of 0.5 mm in 0.5 mm steps (Crawford et al., 2009). To enhance the signal to noise ratio, all quantitative electrophysiological analysis were conducted on waveforms that are the average of at least 15 successive data acquisition sweeps. Waveforms analysis was performed with Igor pro 6.3.7.2 (WaveMetrics, Oregen, USA). The callosal axon conduction velocity was fitted with Graghpad Prism 6.0 (GraphPad Software, Inc., La Jolla, USA).

For the recording of long-term depression (LTD), the field excitatory postsynaptic potentials (fEPSP) were recorded in layer II/III of the medial prefrontal cortex (mPFC) and CA1 of hippocampus by stimulating the axons of layer V in mPFC and CA3 in hippocampus respectively. Picrotoxin (50 μM) was perfused in the bath to inhibit gamma-Aminobutyric acid A-type receptors ($GABA_A$Rs). The stimulus duration was 100 μs in mPFC and 150 μs in hippocampus, current injection was 0.2-0.6 mA. Micropipettes were filled with ACSF which had a resistance of 1-3 MΩ. To elicit LTD, low frequency stimulation (LFS) of presynaptic axons was used at 1 Hz for 15 min (Luscher and Malenka, 2012). Only 20% - 80% of fEPSP slope was analyzed. The recordings generally were lasting

for at least half an hour for the baseline before stimulation and 45 min to induce LTD after stimulation. Waveform analysis was performed by Igor pro 6.3.7.2. The statistical analysis was performed by Graphpad Prism.

All the experiments were conducted at room temperature (RT, 22 – 24 °C).

3.2.5 Ca^{2+} imaging

Reporter^{+} NG2 glia were loaded with 100 μM Fluo-4 potassium salts via patch pipette. Fluo-4 potassium salts (ThermoFisher Scientific Inc.) were prepared into stock solution at a concentration of 2 mM in water and then stored at -20°C. Before every experiment, Fluo-4 was dissolved in pipette solution containing (in mM) 125 potassium gluconate, 20 KCl, 2 $MgCl_2$, 0.05 EGTA, 10 HEPES and 5 Na_2ATP and 0.018 $CaCl_2$, its pH value was adjusted to ∼7.2 with KOH. The dye was allowed to diffuse into fine processes at least for 30 min before imaging. The holding potential in voltage clamp mode was at -80 mV. Zeiss microscope equipped with 63x water immersion objective was used to visualize the regions of interest and the images were captured with a QuantEM 512SC camera. Imaging acquisition was controlled by Imaging Workbench software 5.2.20.6 (INDEC BioSystems, USA) at 20 Hz. To evoke signals, cells were depolarized from -110 mV to 10 mV for 100 ms by 25 pulses. The baseline was recorded for 10 s before that. Photobleaching was corrected by a mono-exponential curve. The equation: $I(t) = Ae^{-t/tau}$, where the intensity I (t) is a function of time t. The mono-exponential approach considers a homogeneous fluorochrome population with the rate of photobleaching and initial intensity A. Changes in $[Ca^{2+}]_i$, measured as changes in fluorescence intensity (ΔF), were calculated by $\Delta F/F_0=(F-F_0)/F_0$, F_0 is the baseline fluorescence. Data analysis was performed with Image J (Schneider et al., 2012) and custom-made scripts with Matlab (MathWorks, USA) and Graphpad Prism 6.0. All data were shown as mean±SEM.

3.2.6 FM1-43 and FM1-43FX staining

Acute brain slices were cut at 180 μm thickness as described above. After a recovery of at least half an hour, slices were firstly loaded with 10 μM FM1-43FX (ThermoFisher Scientific Inc.) in ACSF for 15 min at RT and then loaded with FM1-43FX containing 60 mM KCl for another 5 min (Fuenzalida et al., 2011). Immediately after treatment, slices were fixed in 4% formaldehyde in PBS (pH∼7.4) for 4 hour for later immunohistochemistry.

3.2.7 5-bromo-2-deoxyuridine (BrdU) treatment

BrdU (Sigma-Aldrich, Taufkirchen bei Mnchen, Germany) (1 mg/mL) was dissolved in autoclaved water. To label all the proliferative cells, all mice at P61 were receiving BrdU in drinking water for 10 days and then were analyzed 24h later after stopping drinking BrdU water (Rivers et al., 2008). The BrdU water was changed to fresh one every two days.

3.2.8 Immunohistochemical analysis

3.2.8.1 Preparation of vibratome slices

All the information of analyzed mice (e.g. sex, date of birth, date of sacrifice, parents, genotype, date of tamoxifen injection, etc.) was documented and saved in the Pyrat animal database (Scionics Computer Innovation GmbH, Dresden, Germany). Animals were anesthetized by intraperitoneal injection of a mixed solution of ketamine (Ketavet, Pfizer, Germany) (1.4%) and xylazine (Rumpon, Bayer Healthcare, Germany) (0.05%) (50 μL/ 10 g body weight) and intracardially perfused by 4% formaldehyde in 0.1 M phosphate buffer (pH $\sim$7.4). After perfusion, brains, cervical spinal cords and optic nerves were dissected and post-fixed in the same fixative for 12-16 h at 4°C. For immunostaining of NG2, 2% formaldehyde in sodium acetate (pH=5.6, 4.8 mL 0.2 M acetic acid mixed with 45.2 mL 0.2 M sodium acetate and calibrated to 100 mL with H_2O) was used for perfusion and post-fixation, and the post-fixation time was shortened to 2 h in RT. Brains were immersed with PBS and cut with a vibrotome (Leica VT1000S) to prepare 35 μm thickness free-floating brain slices. Coronal forebrain sections at the hippocampal level (Bregma -1.34 mm to -1.82 mm), and sagittal sections of the cervical spinal cords were collected.

3.2.8.2 Antibody incubation

Tissue slices were treated with blocking solution (0.3% Triton X-100 and 5% horse serum in PBS) for 1 h at RT, and then transferred to primary antibodies to incubate for at least 12 h at 4°C. Brain slices were rinsed three times with PBS after the incubation of primary antibodies. At last, slices were incubated in secondary antibodies for 1 h at RT. DAPI (0.025 μg/mL final concentration) was added to the secondary antibodies to detect the nuclei. Primary and secondary antibodies were diluted in blocking buffer for use. At least 4 mice per group were examined.

The whole optic nerves were treated with modified blocking buffer including 1% Triton

X-100 for at least 4 h at RT and then incubated with primary antibodies for 48 h at 4°C. After that, the tissue was rinsed triple times with PBS after the incubation of primary antibodies and sequentially treated with fluorescent secondary antibodies for 12 h at 4°C. DAPI was added to the secondary antibodies to label the nuclei. Here primary and secondary antibodies were diluted in modified blocking buffer for use.

For BrdU staining, brain slices were treated as previously described (Guo et al., 2010). Briefly, after all the immunostaining steps, brain slices were fixed in 2% formaldehyde for 30 min at RT followed by denaturing in 2 M HCl at 37°C for 45 min. Then slices were rinsed with PBS and treated with anti-BrdU antibody as well as the secondary antibodies in blocking solution sequentially as described above.

3.2.8.3 Imaging acquisition and analysis

Confocal images were taken using a laser-scanning microscope (LSM-710, Zeiss, Oberkochen, Germany) with appropriate excitation and emission filters. Z-stack images were taken at 0.5-2 μm intervals and processed with ZEN software (Zeiss, Oberkochen, Germany). For analysis of cell differentiation and proliferation capacity, 3-4 brain slices per mouse and at least 4 mice per group were examined. The images were scanned in the whole region of the somatosensory cortex and corpus callosum. For measuring the length of paired paranodes and nodes of Ranvier in white matter from different regions, 3-4 brain slices, 5-6 spinal cord slices and all of two optic nerves per mice and at least 4 mice per group were analyzed.

3.2.9 Morphology analysis

Confocal imagines were taken for morphology analysis from cortical NG2 glia in layer II/III with 0.438 μm intervals. Only $P\alpha^+$ and reporter$^+$ cells were used for analysis. To quantify changes on morphology of Cav1.2/1.3 deficient NG2g glia, two approaches were performed, Sholl analysis and binary analysis. Quantitative radial distribution of glial arborization processes can be automatically evaluated by adapting a method first used to investigate the morphology of neurites for neurons (Sholl, 1953). In this study we used the logarithm of the radius and compared it to the logarithm of the ratio between the number of intersections (N) and the area of the corresponding circle (πR^2), the formula is that (log(R) vs log($N/\pi R^2$) calculated by sholl analysis plugin of Fiji software. This method has been shown to have good discrimination value between various neuron types, and even similar types in different regions, primarily to treat neurons with long dendrites that

do not branch much along their length (Milosevic and Ristanovic, 2007). The branching was analyzed by maximum intensity projections of 8-bit confocal images. The threshold of each individual cell was automatically adjusted before log-log analysis performed. The default minimum radius for the soma was set to 5 μm and every 1 μm increased one circle until the farthest point. The normalization was to the area of each corresponding circle. For binary analysis, we were able to properly establish a morphological difference between WT and dKO mice using the Particle Analysis function of Fiji. Using the same threshold isolated images as before we isolated and counted all particles of 0.2 to 4.15 μm^2. In this part, the particles above 4.15 μm^2 were excluded.

3.2.10 SDS-PAGE and Western blotting analysis

3.2.10.1 Tissue preparation and protein isolation

Samples separated from cortex and corpus callosum of mice at 16 weeks old were collected, respectively. Liquid nitrogen was used to freeze the samples rapidly. The samples were preserved at -80°C. They were transferred into a Precellys tube (Peqlab, Erlangen, Germany) filled with 100 - 300 μl freshly prepared homogenization buffer. The tube was placed immediately into the Precellys 24 (Peqlab, Erlangen, Germany) and homogenized twice for 10 s at 5000 rpm with 5 s in between. The homogenate was aliquoted into 3 tubes. Only 10 μl was used for the measurement of the protein concentration and the others were stored at -20°C.

The protein concentration measurement was performed with Pierce BCA Protein Assay Kit according to manufacturers micro plate's procedure protocol.

Proteins were separated by use of discontinuous SDS-polyacrylamide gel electrophoresis (SDS-PAGE) using the Mini-Protein III system (BioRad, Munich, Germany). The SDS-polyacrylamide gel consists of a stacking gel (4 % acrylamide) and a separating gel (8 % acrylamide). Protein samples were heated at 95°C for 5 min in 4x SDS sample buffer and loaded. The gel was run at constant voltage of 80 V for 30 min and then 100 V until the bromophenol blue line migrated to the bottom of the gel. Gels were then used for Western blot.

3.2.10.2 Western blot and immunodetection

Proteins were transferred from SDS-polyacrylamide gel onto a nitrocellulose (NC) membrane (Protran, Nitrocellulose BA 85, Schleicher & Schll, Dassel, Germany) using a Mini

Transblot apparatus (BioRad, Munich, Germany). The protein electrophoretical transfer in blotting buffer lasted more than 16 h at 4°C, at a constant voltage of 30 V.

After electrophoretic transfer, the NC membrane was removed from the blotting sandwich and blocked in 5 % fatty-free milk powder in PBS for 1 h at RT. Sequentially, primary antibodies were diluted in milk solution. The membrane was incubated with diluted antibodies overnight at 4°C on a shaking platform. The NC membrane was washed three times with 1xPBS-T for 10 min, followed by incubation in appropriate HRP conjugated secondary antibodies in milk solution for 1 h at RT, and then washed with 1xPBS-T three times for 10 min. After washing, the membrane was incubated for 60 s in Enhanced Chemiluminescence Detection (ECL) solution (Western Lightning, Western Blot Chemiluminescence Reagent Plus, PerkinElmer Life Sciences, Inc.). The signal on the NC membrane was then detected by X-ray film in a dark room.

For re-probing of the membrane with a second antibody, the membrane was treated with stripping buffer (0.5 M NaCl, 0.5 M acetic acid) for 1 h at RT with rigorous shaking. After washing, the membrane was incubated in blocking buffer for 1 h at RT. Then the membrane was ready to be probed with another primary antibody as described before.

All cortical proteins were normalized to GAPDH of controls, while callosal probes were normalized to Tuj1.

3.2.11 Behavioral tests by the ErasmusLadder

3.2.11.1 Introduction of the ErasmusLadder

Male mice (8 to 12 weeks) were selected for behavior tests on the ErasmusLadder (Fig. 3.1). In this experiment, male littermates without CreERT2 were used as controls. The whole experiments on the ErasmasLadder included eight sessions. Every session was performed per day and carried out continuously for eight days. The first four sessions were training days and called unperturbed sessions. These sessions contained 42 default trials without perturbation (Fig. 3.2). A single crossing of the ErasmusLadder was recorded as a trial. In the first four days, mice were trained to leave the goal box (shelter) and walk across the ladder after any cue.

The last four sessions were called perturbed sessions. In these sessions, mice encountered several challenges, including conditioned stimulus (tone), unconditioned stimulus (obstacle) and paired both when they were running on the ladder (Fig. 3.2). Starting from the 5th session, a trial protocol was determined by the combination of perturbation and tone cue. Three trial protocols were defined: 1) US-only: with perturbation (US, un-

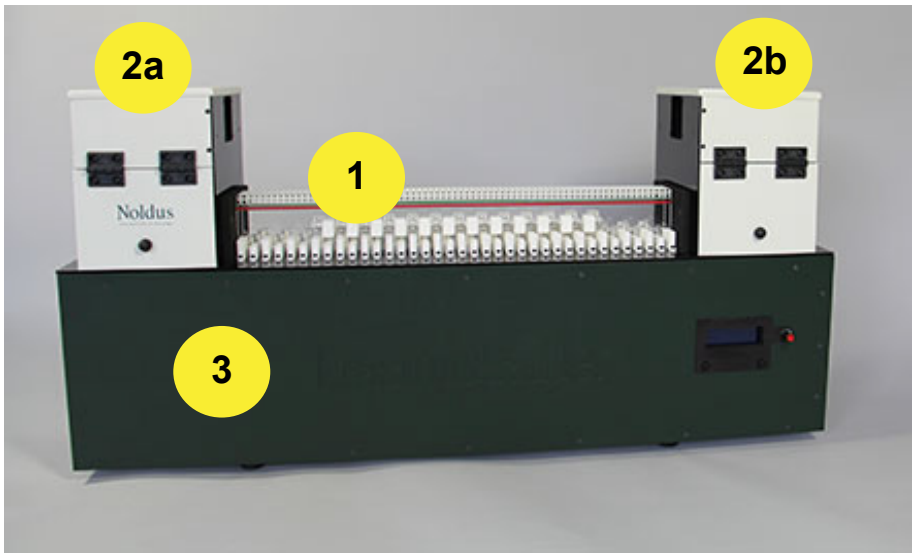

Figure 3.1 The ErasmusLadder used for analysis of motor coordination. The ladder (1) is located between two goal boxes (2a and 2b). The mouse run over the ladder from one goal box to the other one. Underneath the ladder is the base unit with LCD display (3). The figure is from ErasmusLadder 1.1 reference manual (Noldus, 2015).

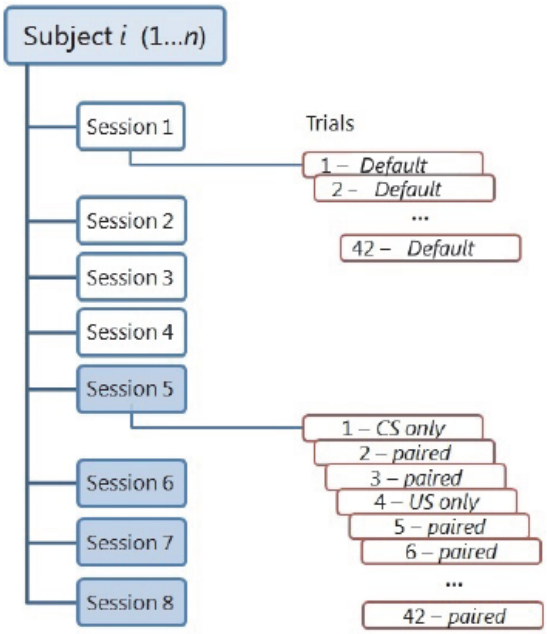

Figure 3.2 The default protocols. Each subject is tested in eight daily sessions. A session includes 42 trials. The figure is from ErasmusLadder 1.1 reference manual (Noldus, 2015).

conditional stimulus) only; 2) CS-only: with tone cue (CS, conditional stimulus) only; 3) Paired: with both tone cue (CS) followed by a perturbation (US) after 250 ms. A perturbation and/or a tone cue was only activated when the software could predict the position of

the mouse with good accuracy. It was not always possible to predict the mouse position and the obstacle to raise during a trial. When the mouse walked with varying speed, a good prediction could not be made and no CS / US/ paired stimulus was given in that trial. Then this trial was classified as undisturbed trial. The sequence was repeated seven times in a session, for a total of 42 trials (Fig. 3.2). When a perturbation (US) was paired with a predictive cue (CS), for example a tone, a learned correction of the walking pattern based on the cue might prevent falling. Control mice typically corrected by increasing their step time immediately after the tone or by making jumps on the ErasmusLadder rungs.

Proper associative conditioning requires precise timing of the CS-US presentation. The default value of the time between CS and US is 250 ms. Because the tone must be activated sufficiently before the perturbation, the software embedded in the ErasmusLadder estimates the position of the mouse on the ErasmusLadder at any time, and determines which obstacle rung has to be raised. In order for the software to make a good prediction of the mouse position, the mouse had to walk at a relatively constant speed and step size. If the mouse made three consecutive steps of constant step size, and with a standard deviation of the time between steps lower than 72 ms, then it was possible to predict the next steps and which obstacle rung is raised, and at what time (Noldus, 2015).

3.2.11.2 Data analysis for the ErasmusLadder

The ErasmusLadder is a fully automated device (Noldus, 2015), which can analyze different aspects of mouse performance on the ladder, such as:

Pre Perturbation (ms): The duration of the last step at the same side as that of the obstacle rung, which ends before the calculated obstacle rung.

Post Perturbation (ms): The duration of the first step at the same side as that of the obstacle rung, which ends after the obstacle rung.

Missteps: The steps from one higher rung to a lower rung (Fig. 3.3).

Short Steps: The step between initial contact of the front paw with one rung and initial contact with the next rung at the same side (Fig. 3.3).

Long Steps: The step between initial contact of the front paw with one rung and initial contact with the second next rung at the same side (Fig. 3.3).

Jump: the step longer than long step (Fig. 3.3).

Resting (Frequency): The number of times the animal is present in the goal box before any cue is given. This number is 1 for a trial if the animal does not enter the ladder before

a cue is given.

Light cue (Frequency): The number of times the light cue is given.

Air cue (Frequency): The number of times the air cue is given.

Leaving after Cue (Frequency): The number of times the animal enters the ladder upon a cue.

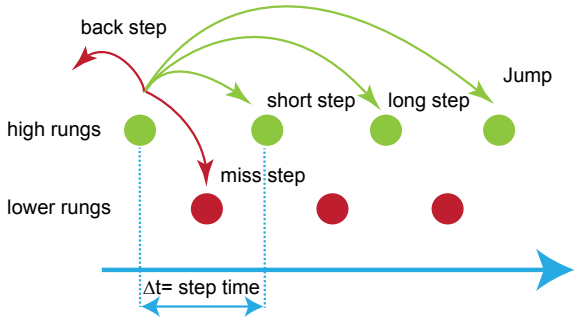

Figure 3.3 The classification of steps. Mice move on the ladder with all kinds of steps, short steps, long steps, jumps and missteps. (from ErasmusLadder 1.1 reference manual).

Additionally, on analyzing the data,

Default, to analyze motor performance;

US-only, to examine the effect of the obstacle as such;

CS-only, to examine the learning effect without the influence of the obstacle;

Paired, to analyze associative motor learning.

3.2.12 Statistical analysis

Statistic differences were analyzed using the unpaired two-tailed student t-test for two-group comparison and one-way ANOVA for multi-group comparison. The levels of significance were set as * $P<0.05$, ** $P<0.01$, *** $P<0.001$. n.s = non-significant. Data are shown as mean$\pm$SEM.

Chapter 4

Results

4.1 NG2 glia: a heterogeneous cell population

Two different subpopulations of NG2 glia, namely complex glial cells and passive glial cells, were described in the stratum radiatum of the hippocampal CA1 sub-region (Steinhauser et al., 1992). Complex glial cells can easily be distinguished from passive NG2 glia due to the expression of voltage-gated ion channels. To examine whether the two distinct subpopulations (complex and passive glial cells) can also be detected in cortical NG2 glia, whole-cell patch clamp recordings were performed in acute brain slices from neonatal and young adult NG2-EYFP (enhanced yellow fluorescent protein) mice, in which EYFP expression is controlled by the NG2 locus. Whole-cell membrane currents were elicited by a voltage step protocol from -140 mV to 80 mV with 10 mV increment, at a holding potential of -80 mV (Fig. 4.1A). NG2 glia showed two different types of membrane currents upon hyper- and depolarization in young mice (P3 to P15). One type was identified by I_{Na_v} with a peak current at -30 mV (Fig. 4.1C) and small inward and large outward K^+ currents (Fig. 4.1B), consistent with hippocampal complex NG2 glia (Steinhauser et al., 1994). The second type was distinguished by leak and outward K^+ currents, while I_{Na_v} could not be detected (Fig. 4.1D), previously described as passive NG2 glia (Kressin et al., 1995; Zhou et al., 2006).

Current-voltage (I-V) relationship curves of complex NG2 glia displayed a non-linear shape, while passive NG2 glia showed a linear curve because of rich I_{Kir} expression (Fig. 4.1E). Compared to passive NG2 glia, complex NG2 glia had higher resting membrane potentials (Complex, -67.4 $\pm$ 4.4 mV n=14 cells; Passive, -78.2 $\pm$ 1.8 mV, *p$<$0.05, P=0.028) and a higher membrane resistance (Complex, 724.4 $\pm$ 147.3 MΩ; Passive, 63.5 $\pm$ 5.9 MΩ, n=15 cells, ***P$<$0.001, P$<$0.0001) (Fig. 4.2A left and right). Both sub-

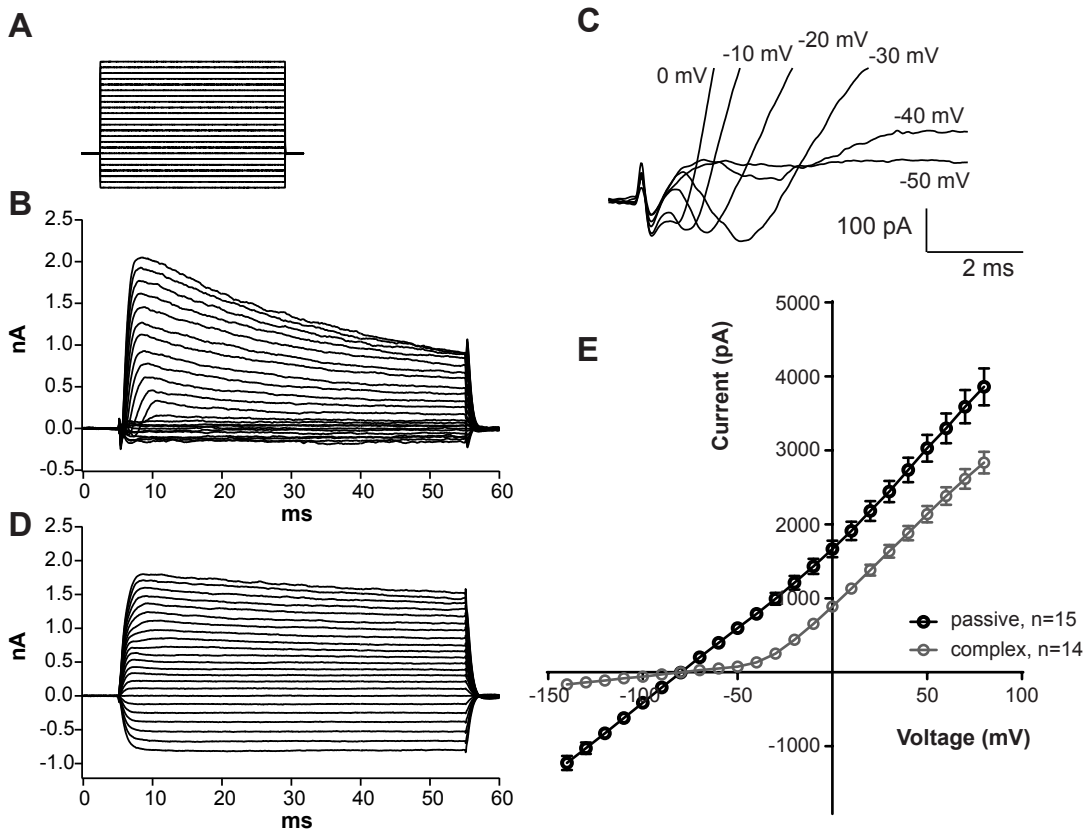

Figure 4.1 Whole-cell membrane current profiles of cortical NG2 glia in young mice (< P16). A, A voltage step protocol was used to elicit the membrane current from -140 mV to +80 mV for 50 ms by 10 mV increment, with a holding potential of -80 mV. B/D, Whole-cell membrane current profiles of complex NG2 glia (B) and passive NG2 glia (D) were identified in the neonatal mice (< P16). C, Magnification of membrane currents of complex NG2 glia demonstrated the successive activation of voltage-gated Na^+ currents. E, Comparison of IV curves in complex (gray) and passive (black) NG2 glia.

populations had no difference in membrane capacitance (Complex, 20.82 $\pm$ 2.95 pF; Passive, 17.51 $\pm$ 2.85 pF) (Fig. 4.2A middle). When either hyperpolarized to -140 mV or depolarized to +80 mV, passive NG2 glia had larger K^+ currents than complex NG2 glia (Passive, -1227 $\pm$ 94 pA; Complex, -164 $\pm$ 38 pA, ***P<0.001, P<0.0001; Passive, 3859 $\pm$ 249 pA; Complex, 2834 $\pm$ 146 pA, **P<0.01, P=0.0017) (Fig. 4.2B).

In adult mice (> P30), these two sub-populations of cortical NG2 glia could still be observed (Fig. 4.3A, C). However, complex NG2 glia no longer expressed Na_vs (Fig. 4.3B). Their current-voltage relationship curves still displayed non-linear shape, with smaller inward K^+ currents than passive NG2 glia (Fig. 4.3D). In adult cortices less complex NG2 glia were observed as compared to neonatal mice, while the number of passive glia was not changed (Fig. 4.2C). These findings suggest the same heterogeneity in cortical NG2

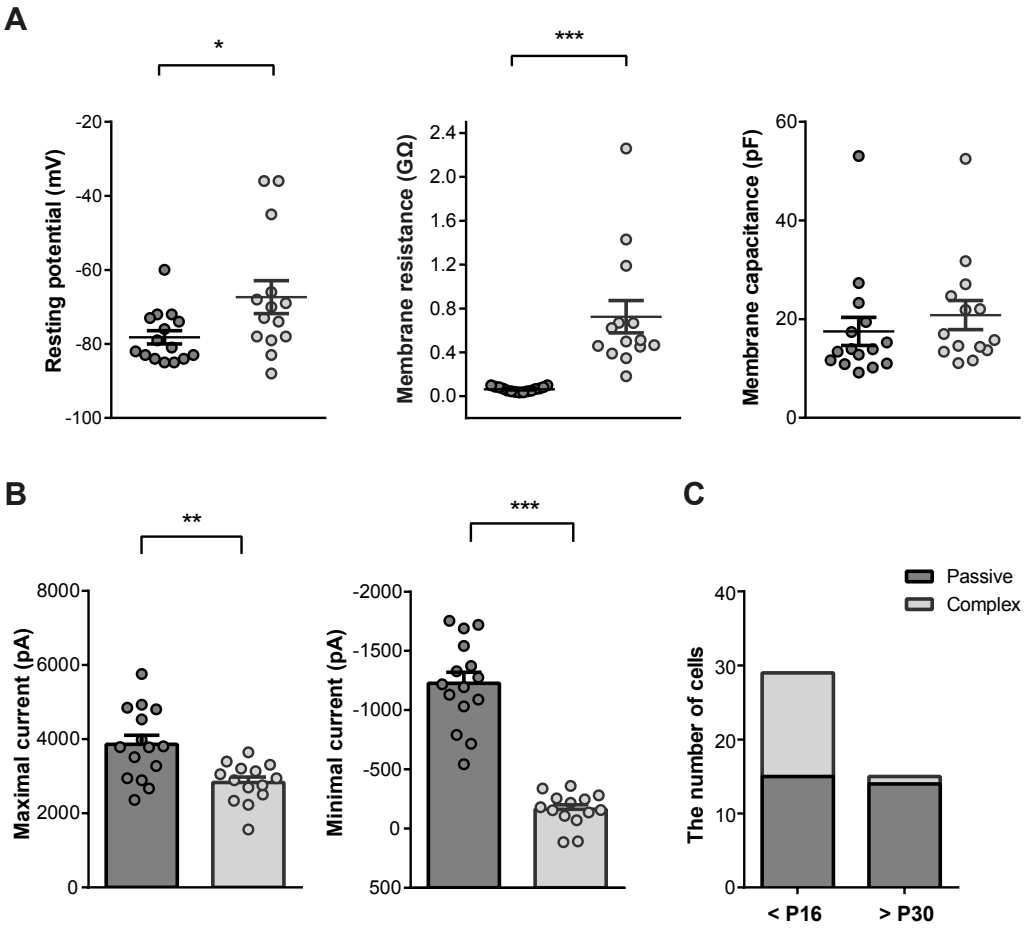

Figure 4.2 Membrane properties of complex and passive NG2 glia in the neonatal cortex. A, Resting membrane potential, membrane resistance and membrane capacitance of complex (light gray) and passive (dark gray) NG2 glia in the cortex prepared from NG2-EYFP mice ($<$ P16). B, Passive NG2 glia had bigger maximal and minimal membrane currents than complex NG2 glia. C, The proportion of complex and passive NG2 glia changed in an age-dependent manner, with a decreased number of complex subpopulation in older mice.

glia as described for hippocampal NG2 glia in terms of K^+ channel expression, especially at the neonatal stage.

4.2 L-type voltage-gated Ca^{2+} channel expression in NG2 glia

To determine the expression of voltage-gated Ca^{2+} channels (VGCCs) in cortical NG2 glia, we patched reporter$^+$ NG2 glia in acute brain slices prepared from NG2-EYFP mice (P7 to P16) in the whole-cell configuration. To isolate Ca^{2+} currents, we used TTX, Cs^+, TEA and 4-AP (Table 3.1) to block voltage-gated Na^+ currents and K^+ currents. Addition-

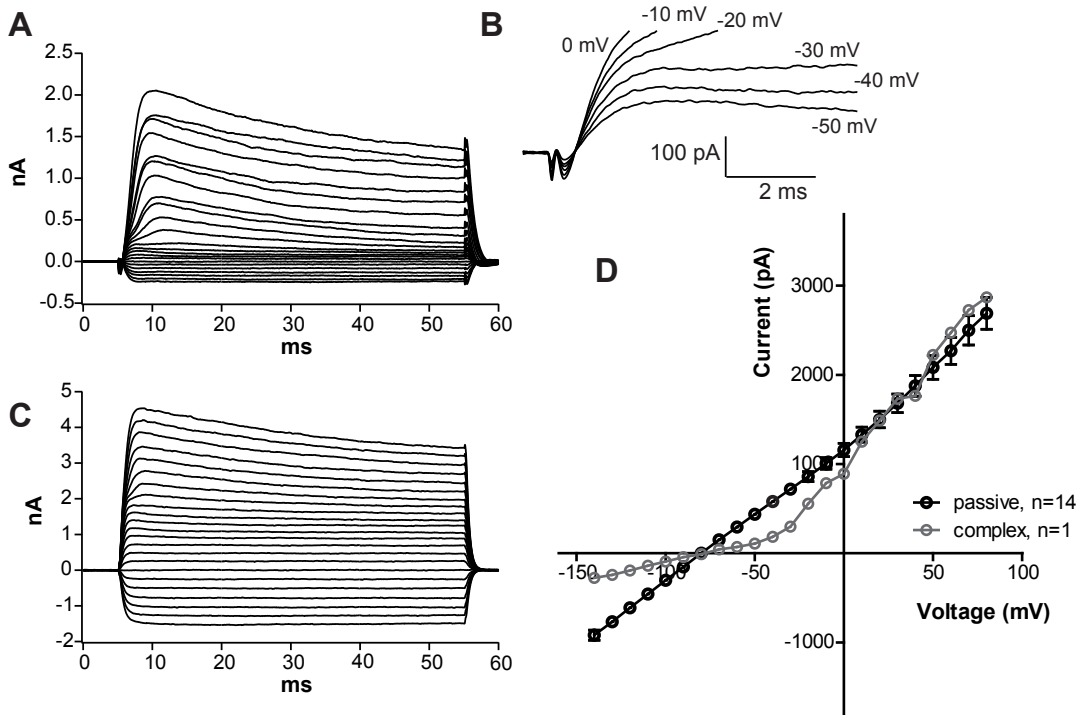

Figure 4.3 Whole-cell membrane current profiles of NG2 glia in the adult cortex. A, Whole-cell membrane current profiles of complex NG2 glia in the adult mice ($>$ P30), showed a combined expression of inward and outward K^+ channels. B, No Na^+ currents were detected in complex NG2 glia at tested age. C, Membrane current profiles of passive NG2 glia displayed big leak K^+ currents. D, Complex subpopulation resulted in multiple rectification in IV curve, while passive NG2 glia yielded a linear IV curve in the adult mice.

ally, $[Ca^{2+}]$ in the extracellular solution was increased to 5 mM (Haberlandt et al., 2011). Prepulse conditioning to -110 mV for 1.5 s was applied before depolarization to remove the inactivation of voltage-gated Ca^{2+} channels (Fig. 4.4A top). By depolarizing from -60 mV to +50 mV, negative responses evoked from -40 mV reached the peak at about 0 mV and then declined with voltage increment. V-shape IV curves revealed that peak inward currents appeared at about 0 mV. The average peak current amplitude was -121.8 $\pm$ 12.54 pA (n=21 cells, Fig. 4.4B). The peak inward currents were vastly blocked by L-type Ca^{2+} channel blocker Nimodipine (n=4, Fig. 4.4C). T-type Ca^{2+} channel blocker Mibefradil only partially diminished the peak inward currents by 11.2 $\pm$ 5.2% (n=4, Fig. 4.4D). These results indicated that cortical NG2 glia express voltage-gated Ca^{2+} channels, predominant by L-type Ca^{2+} channels.

To investigate if VGCCs are expressed in a region- or age-dependent manner, we examined NG2 glia in different brain regions including gray (dorsal cortex and hippocampus) and white matter (corpus callosum) during CNS development using acute brain slices of

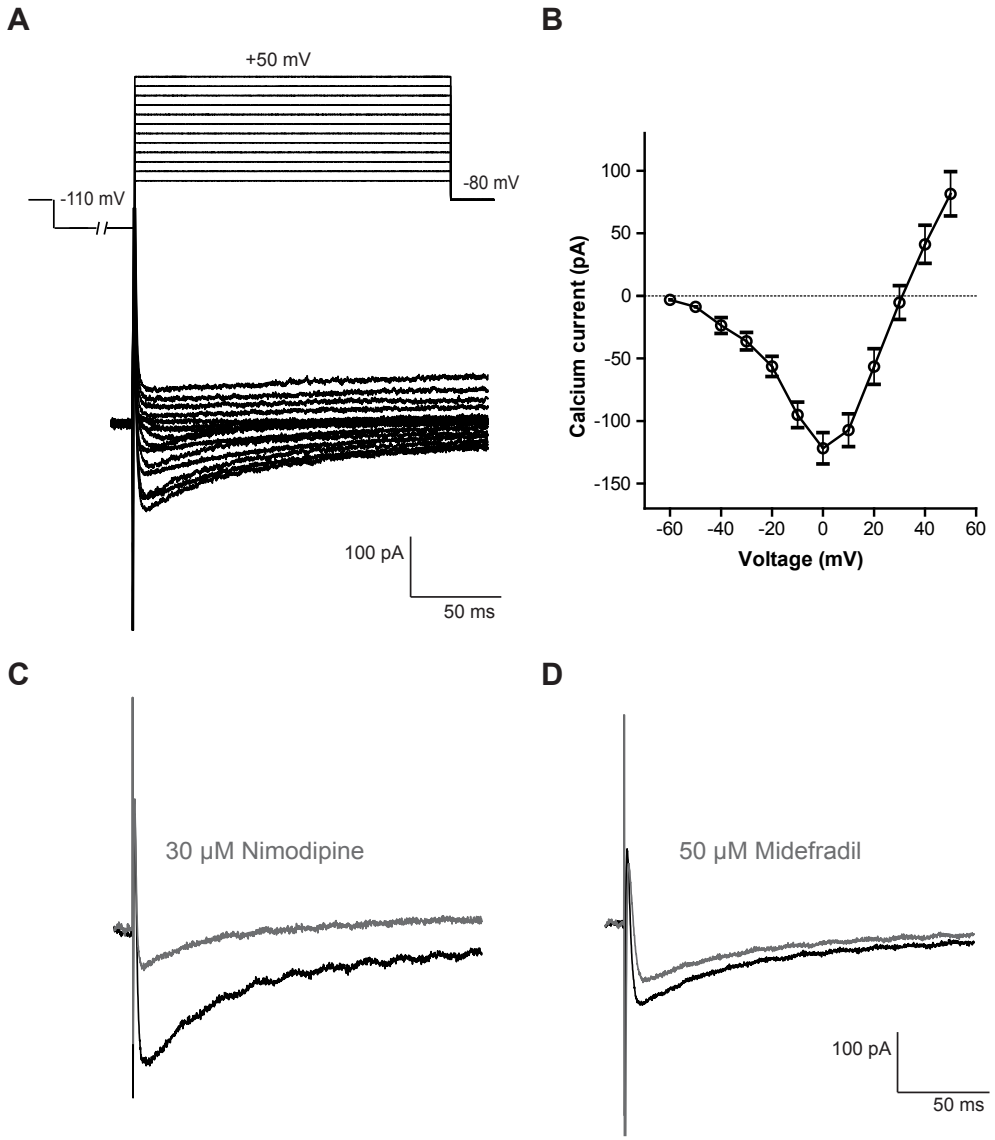

Figure 4.4 The expression of voltage-gated Ca^{2+} channels in cortical NG2 glia. A, Ca^{2+} currents were evoked by voltage steps from -60 mV to +50 mV for 200 ms by 10 mV increment with a conditioning prepulse (1.5 s) to -110 mV, at holding potential of -80 mV. B, The I-V curves of VGCCs (n=21) showed peak inward responses at 0 mV. C, The peak currents could be mostly blocked by the L-type VGCC blocker Nimodipine (gray). D, T-type VGCC blocker Mibefradil only slightly inhibited Ca^{2+} currents (gray).

NG2-EYFP mice from P3 up to 10 weeks. According to their peak current amplitudes at 0 mV, we divided the analyzed NG2 glia into 5 groups ($<$-100 pA, -100 $\sim$ -70 pA, -70 $\sim$ -40 pA, -40 $\sim$ 0 pA, $>$0 pA) in cortex, hippocampus and corpus callosum during development (Fig. 4.5A). We found that not all NG2 glia expressed VGCCs among these three brain regions during the development. About $\sim$75% of cortical NG2 glia (28 of 37

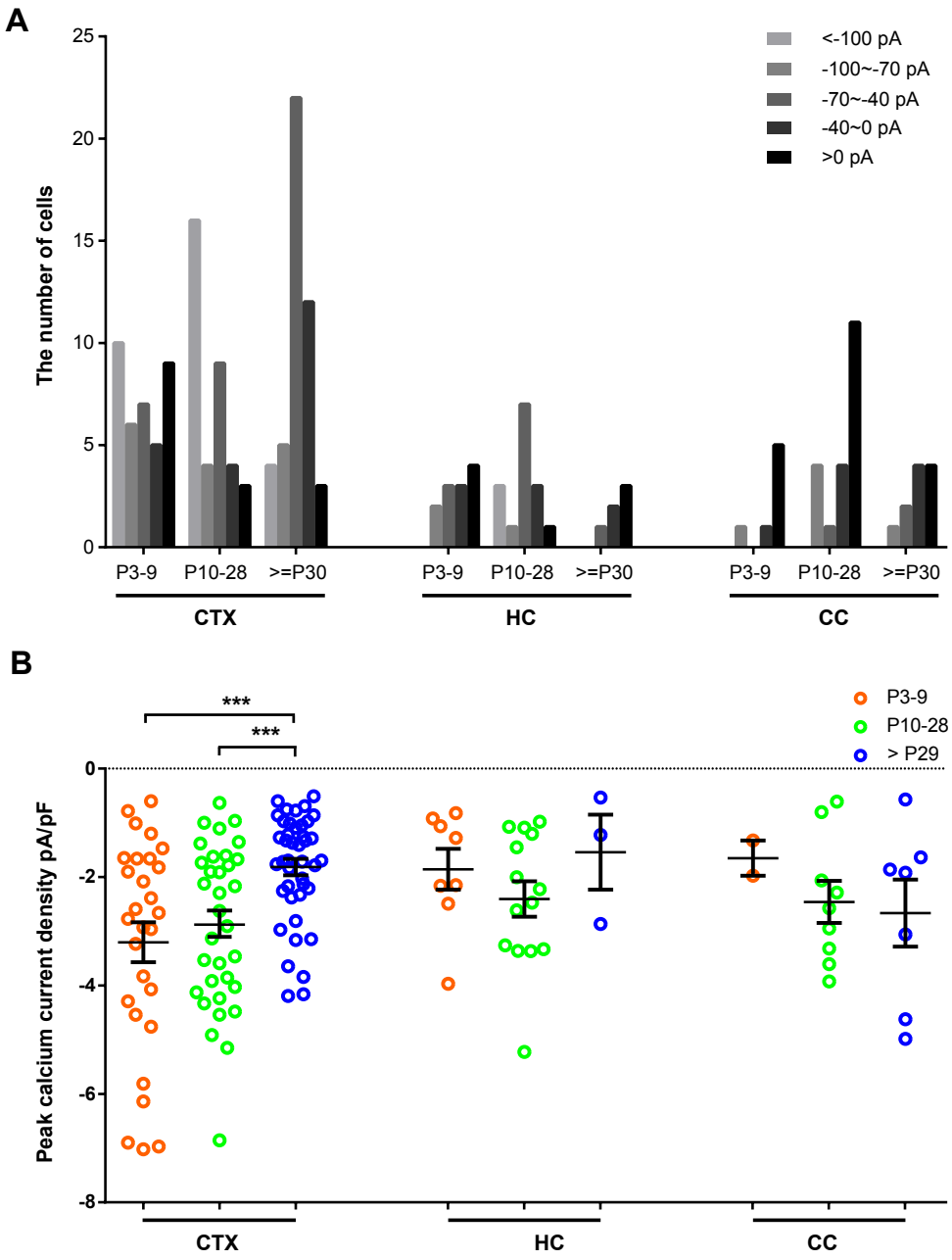

Figure 4.5 Comparison of Ca^{2+} currents in different brain regions during the development. A, NG2 glia examined in different brain regions (CTX, cortex; HC, hippocampus; CC, corpus callosum) during development were divided into five groups according to their peak current amplitudes. B, Peak Ca^{2+} current densities in different brain regions during the development of the CNS showed s significant reduction in the cortex.

cells) displayed Ca^{2+} currents from P3 to P9. The proportion increased to $\sim$ 90% in mice older than 10 days (33 of 36 cells at P10-28, 28 of 30 cells at >=P30). In the dorsal cortex, peak current density decreased significantly with age (P3-9 vs >= P30, -3.20 $\pm$ 0.37

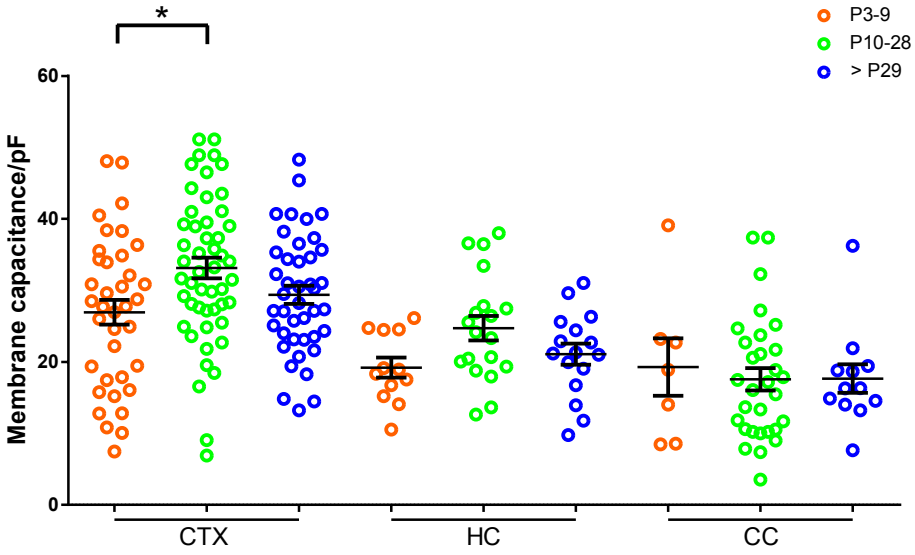

Figure 4.6 NG2 glia retain stable membrane properties in different brain regions during CNS development. Membrane capacitance of NG2 glia in different brain regions remained stable during the maturation of mice.

pA/pF vs -1.82 $\pm$ 0.15 pA/pF, ***P$<$0.001; P10-28 vs $>$= P30, -2.88 $\pm$ 0.26 pA/pF vs -1.82 $\pm$ 0.15 pA/pF, ***P$<$0.001, Fig. 4.5B). The membrane capacitance of NG2 glia in the cortex, hippocampus and corpus callosum did not vary during CNS development, with an average value of 20 to 30 pF (Fig. 4.6). However, the membrane capacitance of cortical NG2 glia from two to four weeks old mice increased remarkably when compared to one week old mice (P3-P9). These data demonstrated that VGCCs are widely expressed in most NG2 glia in all analyzed brain regions, including gray and white matter during CNS maturation. The number of these NG2 glial cells expressing VGCCs increases in the first four postnatal weeks. However, the Ca^{2+} current density is reduced significantly in the cortex during CNS maturation.

4.3 Removal of Cav1.2 and Cav1.3 genes from NG2 glia *in vivo*

To investigate the functional roles of Cav1.2 and Cav1.3 in NG2 glia, we took advantage of the tamoxifen-inducible Cre DNA recombinase to ablate Cav1.2 (*cacna1c*) and Cav1.3 (*cacna1d*) genes specifically in NG2 glia. We crossbred homozygous floxed Cav1.2 and flexed Cav1.3 to NG2-CreERT2 knockin mice. Triple transgenic mice were additionally crossbred to the CAG-EGFP reporter mice to label recombined cells. Our previous data (Fig. 4.5B) revealed a high density of VGCCs in NG2 glia in mice younger than four weeks.

More than 90% NG2 glia were recombined in NG2-CreERT2 x Rosa26-tdTomato mice if mice were treated with tamoxifen at P7 and analyzed at 10 weeks (unpublished data). Here, we applied tamoxifen by injecting mice at P7 and P8, once per day intraperitoneally and recorded voltage-gated Ca^{2+} currents in NG2 glia from P30 to P38 (Fig. 4.7A). Age-matched NG2-EYFP mice were used as controls (CTL). The IV curve of Cav1.2/1.3 deficient NG2 glia in the cortex was shifted to the positive from -60 mV to 40 mV as compared to controls (CTL, black, n=11 cells, dKO, red, n=11 cells) (Fig. 4.7B). Based on their peak current amplitudes at 0 mV, NG2 glia could be divided into 5 groups: $<$-100 pA, -100 $\sim$ -70 pA, -70 $\sim$ -40 pA, -40 $\sim$ 0 pA and $>$0 pA. All NG2 glia from control mice displayed negative currents, namely below -40 pA (n=18 cells), while none of Cav1.2/1.3 deficient NG2 glia showed currents more negative than -100 pA. One quarter (3/12) of NG2 glia from dKO mice did not show detectable negative currents (Fig. 4.7C). The inward peak current density in Cav1.2/1.3 deficient NG2 glia was significantly decreased as compared to controls (CTL -2.50 $\pm$ 0.22 pA/pF, n=18 cells; dKO -1.27 $\pm$ 0.44 pA/pF, n=12 cells, *P$<$0.05, P=0.031) (Fig. 4.7D). These data confirmed that Cav1.2 and Cav1.3 genes have been deleted in NG2 glia three weeks later after tamoxifen administration at P7 and P8.

In addition, we observed that our dKO mice were always smaller than their littermate controls. To quantify the difference, the body weight of dKO mice was normalized to the average of their littermates with the same gender. Both female and male dKO mice displayed a significant reduction by 10% as compared to controls four weeks later after tamoxifen treatment at P7 and P8 (Fig. 4.8). The body weight reduction remained in male dKO mice at 10 weeks, while female dKO mice grew up normally as controls (Fig. 4.8). Therefore, the ablation of Cav1.2 and Cav1.3 might influence the body weight.

Next, we wanted to investigate the function of Cav1.2 and Cav1.3 in NG2 glia in adolescent mice. Tamoxifen was injected intraperitoneally at P21, once per day for three consecutive days and another three times were applied once every two days three weeks later (Fig. 4.9A). Voltage-gated Ca^{2+} currents were analyzed at 10$\sim$11 weeks (Fig. 4.9B). This protocol of tamoxifen administration was designed to allow recombination of new born NG2 glia generated in the subventricular zone. Age-matched NG2-EYFP mice were used as controls. The IV curves of Cav1.2/1.3 deficient NG2 glia in the cortex were also shifted to more positive currents from -30 mV to 40 mV as compared to CTL (CTL, n=15 cells; dKO, n=11 cells) (Fig. 4.9B). Their currents were almost 0 pA at 0 mV. While IV curves of Cav1.2/1.3 deficient NG2 glia showed peak currents elicited at -40 mV which is typical for T-type Ca^{2+} channels (Poetschke et al., 2015) (Fig. 4.9B). According to the

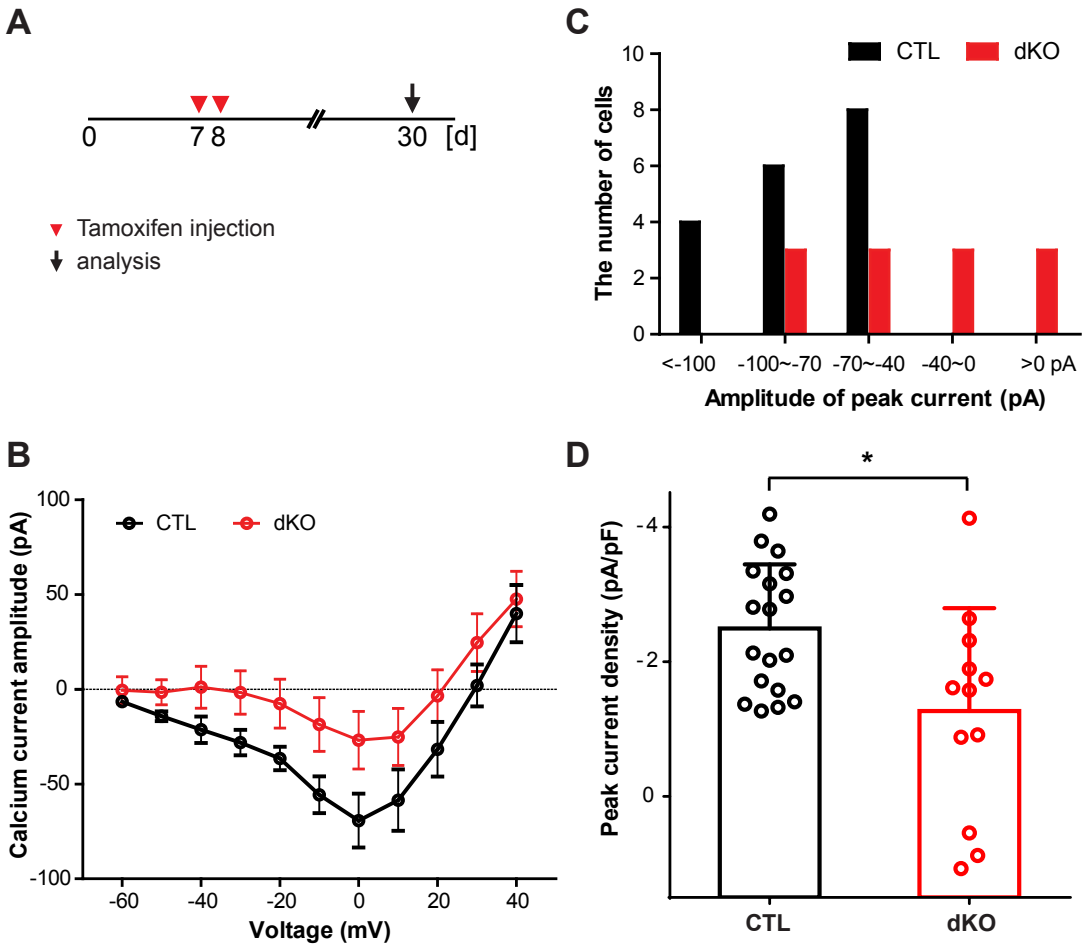

Figure 4.7 Successful knockout of Cav1.2 and Cav1.3 in NG2 glia from neonatal mice. A, Tamoxifen administration and analysis time point. B, IV curves of VGCCs in cortical NG2 glia recorded by whole-cell patch clamp revealed reduction of amplitude in dKO (red, n=11 cells) mice compared to CTL (black, n=11 cells). C, According to size of peak current amplitudes at 0 mV, NG2 glia were divided into five groups between CTL and dKO mice with a shift in dKO mice to more positive currents compared to controls. D, The peak current densities in NG2 glia of dKO mice were smaller than controls (*P$<$0.05, P=0.031).

peak current amplitudes at 0 mV, NG2 glia were divided into four groups: -100 $\sim$ -70 pA, -70 $\sim$ -40 pA, -40 $\sim$ 0 pA and $>$0 pA. Most NG2 glia from controls displayed negative currents, ranging from 0 to -100 pA (n=17 cells), while none of Cav1.2/1.3 deficient NG2 glia showed bigger negative currents than -70 pA. Nearly half of the cells (5/11) did not display negative currents and five cells had inward currents smaller than 40 pA (Fig. 4.9C). The inward peak current density at 0 mV decreased significantly as compared to NG2 glia from controls (CTL -1.63 $\pm$ 0.18 pA/pF, n=15 cells; dKO 0.58 $\pm$ 0.71 pA/pF, n=11 cells, ***P$<$0.001, P=0.0002) (Fig. 4.9D). All these data indicated that Cav1.2 and Cav1.3 genes could be completely deleted in adult NG2 glia with Cre DNA recombination induced

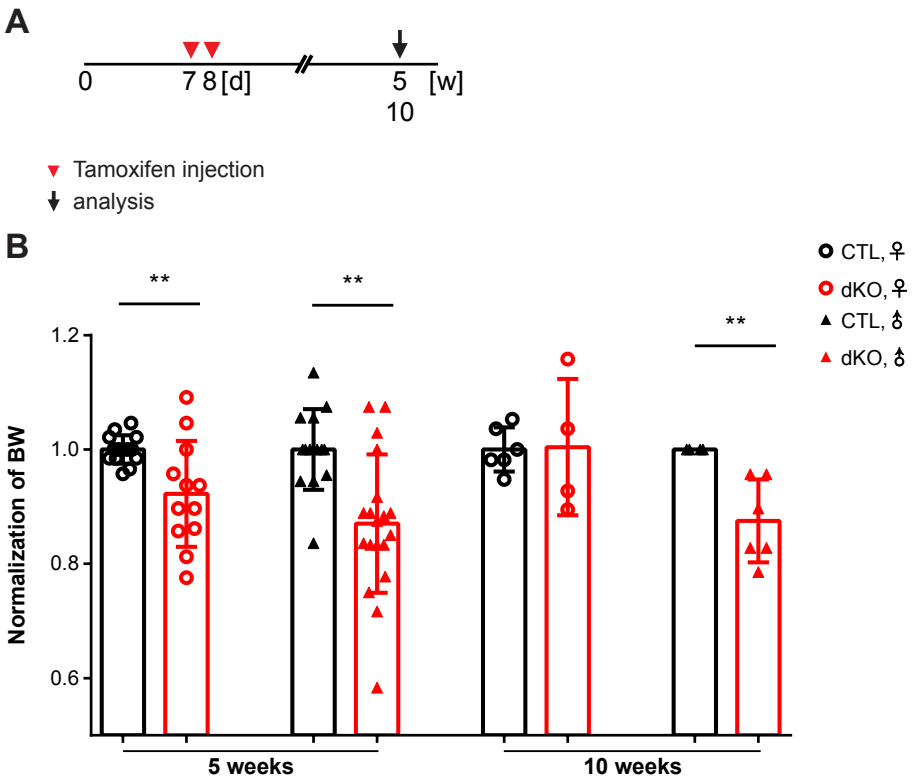

Figure 4.8 dKO mice lost body weight after tamoxifen treatment. A, All mice were treated with tamoxifen at P7 and P8, and then analyzed at 5 weeks and 10 weeks. B, Changes of body weight of two genders from CTL and dKO mice. After tamoxifen treatment, all dKO mice (female and male) lost body weight at 5 weeks age. However, only male dKO mice reduced body weight at 10 weeks age, no alteration was observed in female dKO mice compared to controls. **P$<$0.01.

in 3-week-old mice. In addition, a new peak current appeared at -40 mV suggesting that T-type Ca^{2+} channels might be upregulated due to the ablation of L-type VGCC isoforms Cav1.2 and Cav1.3.

To evaluate if Cav1.2 and Cav1.3 genes can be deleted from NG2 glia in older mice, tamoxifen was injected at 4 or 5 weeks once per day for three consecutive days and two weeks later injected another two times once per day (Fig. 4.10A). Whole-cell patch clamp recordings were carried out in 10 weeks old mice. IV curves of VGCCs in Cav1.2/1.3 deficient NG2 glia displayed a V-like shape (CTL, n=15 cells; dKO, n=6 cells) (Fig. 4.10B), which is similar to controls. Their peak currents were elicited around 0 - 10 mV in control and dKO mice (Fig.4.10B). According to their peak current amplitudes at 0 mV or 10 mV, NG2 glia were divided into four groups: -100 $\sim$ -70 pA, -70 $\sim$ -40 pA, -40 $\sim$ 0 pA and $>$0 pA. There was no difference in their distribution of peak current amplitudes between control and dKO mice (Fig. 4.10C). The current density in Cav1.2/1.3 deficient

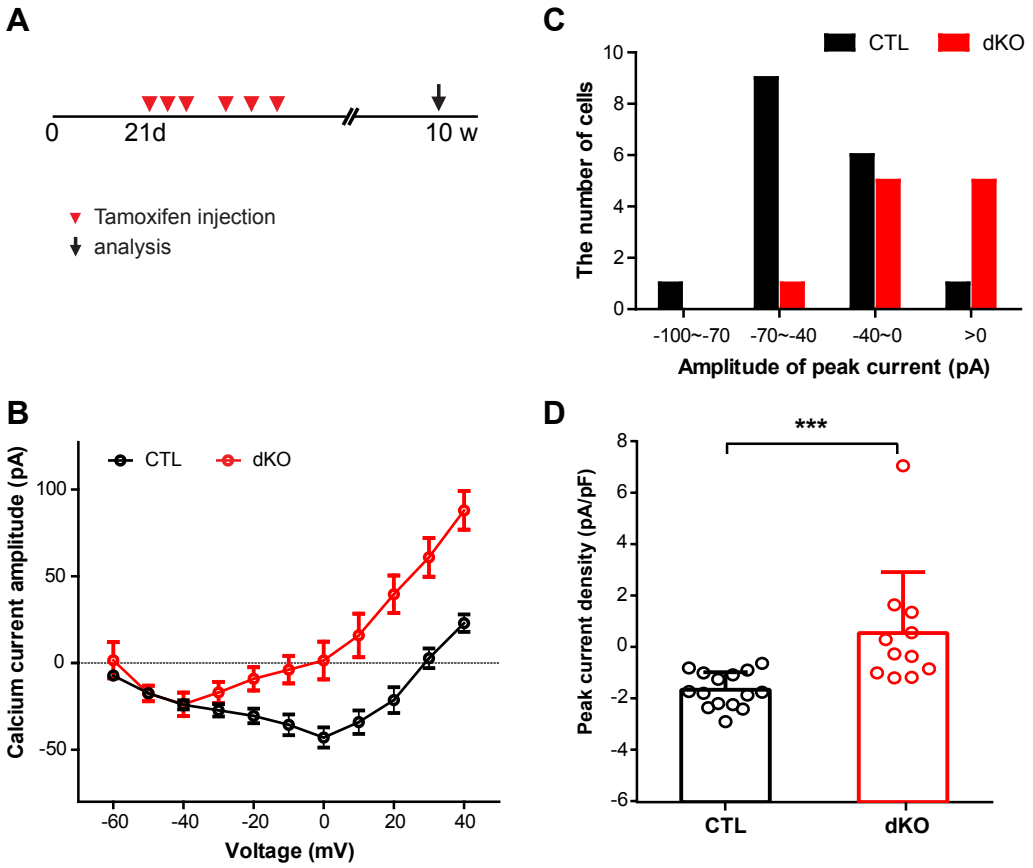

Figure 4.9 Removal of Cav1.2 and Cav1.3 in NG2 glia of adolescent mice. A, Tamoxifen administration and analysis time point. B, IV curves of VGCCs in cortical NG2 glia recorded by whole-cell patch clamp exhibited a Ca^{2+} current decrease in dKO mice compared to controls (CTL, n=15 cells, dKO, n=11 cells). C, According to the size of peak current amplitudes at 0 mV, NG2 glia were divided into four groups between CTL and dKO mice, indicating a shift to more positive currents in dKO mice. D, The peak current densities in dKO mice were significantly reduced compared to controls. ***P$<$0.001.

NG2 glia did not show any reduction as compared to controls (CTL, -1.54 $\pm$ 0.18 pA/pF, n=16 cells; dKO, -1.46 $\pm$ 0.15 pA/pF, n=8 cells; n.s., P=0.769) (Fig.4.10D). To verify the components of inward currents from Cav1.2/1.3 deficient NG2 glia, pharmacological intervention showed peak inward currents were mainly blocked by 30 μM Nimodipine in acute brain slices of dKO mice (Fig. 4.10E), identifying the the inward currents as L-type Ca^{2+} currents. Altogether, these data indicated that Cav1.2/1.3 genes had not been deleted in NG2 glia. Therefore the conditional knockout of Cav1.2/1.3 genes failed in NG2 glia if induced in the four or five weeks old mice.

Taken together, these data demonstrated that L-type VGCC isoforms Cav1.2 and Cav1.3 can be successfully removed from NG2 glia in neonatal and adolescent mice,

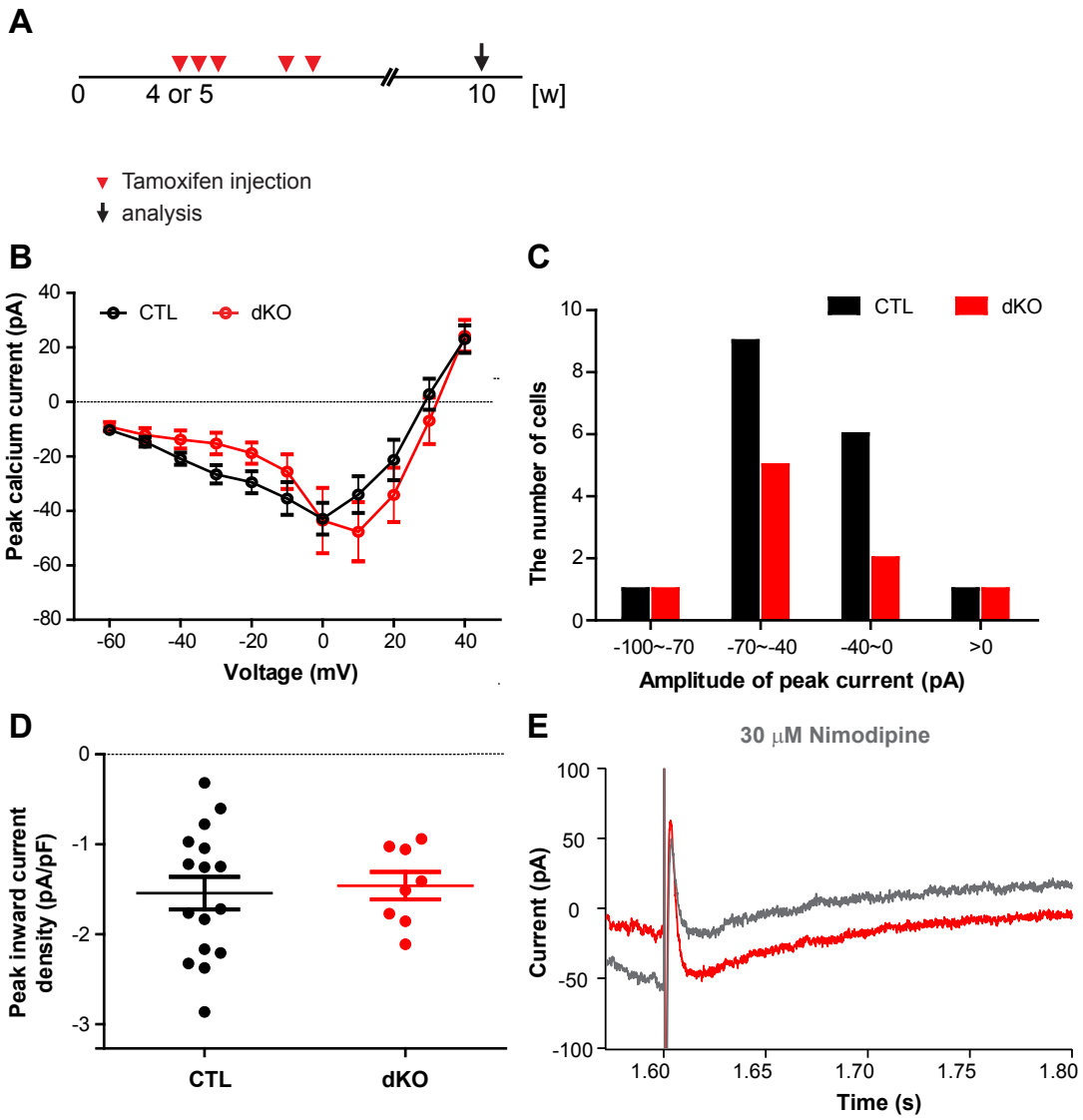

Figure 4.10 Failure to delete Cav1.2 and Cav1.3 in NG2 glia in adult mice. A, Tamoxifen administration and analysis time point. B, IV curves of VGCCs in cortical NG2 glia did not show any difference between CTL (n=15 cells) and dKO (n=6 cells). C, According to the size of peak current amplitudes at 0 mV, NG2 glia were divided into four groups with no shift between CTL and dKO mice. D, The peak current densities of VGCCs in dKO mice were similar to controls. E, Peak currents of VGCCs in NG2 glia from dKO mice were blocked by 30 μM Nimodipine (gray), indicating L-type VGCCs still in NG2 glia.

but not at a later time point. Beside epigenetic changes with maturation, the expression level of CreERT2 controlled by the NG2 locus could be too low for successful DNA recombination in older mice. Therefore, in the following studies, we always applied tamoxifen by intraperitoneal injection at P7 and P8 unless otherwise specified.

4.4 L-type VGCCs as the main contributors to Ca^{2+} influx in NG2 glia

Ca^{2+} influx into the cytoplasm elevates intracellular [Ca^{2+}] through VGCCs, which will induce a series of physiological activities (Butt, 2006). Therefore, we investigated whether the loss of Cav1.2 and Cav1.3 proteins in NG2 glia leads to cellular dysfunction. We performed Ca^{2+} imaging by whole-cell-patching with Fluo-4 potassium salts (100 μM) in pipette solution using acute brain slices from NG2-EYFP and dKO mice. Before Ca^{2+} recording, the resting potential and membrane currents were checked to exclude other types of reporter$^+$ cells, e.g., pre-myelinating oligodendrocytes, mature oligodendrocytes and pericytes. The baseline was recorded for 10 s followed by successive stimulation for

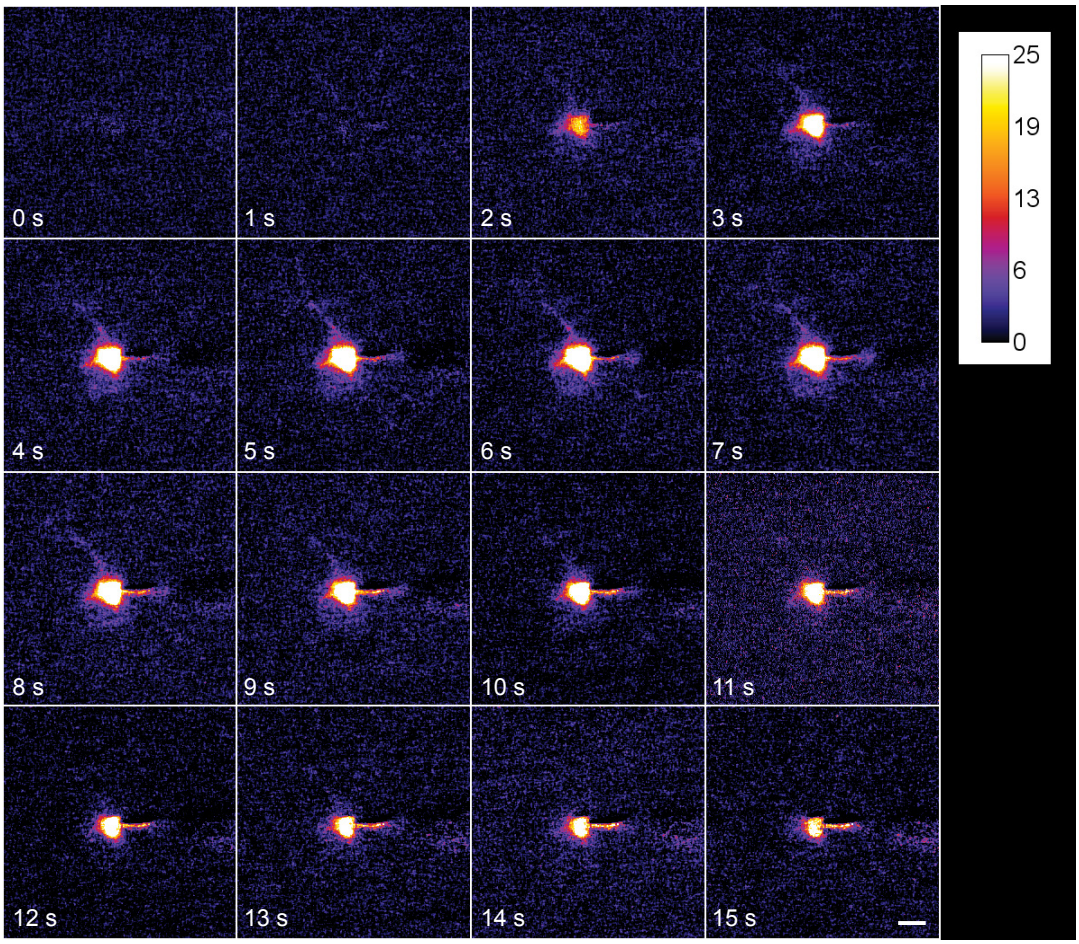

Figure 4.11 Ca^{2+} elevation in cortical NG2 glia upon depolarization. Cortical NG2 glia of control mice were loaded with Fluo 4 potassium slats via whole-cell pipette. At 0 s, successive stimulation by depolarization to 10 mV was applied to patched cells. The basal fluorescence prior to 0s was subtracted from all the images shown here. Scale bar = 5 μm.

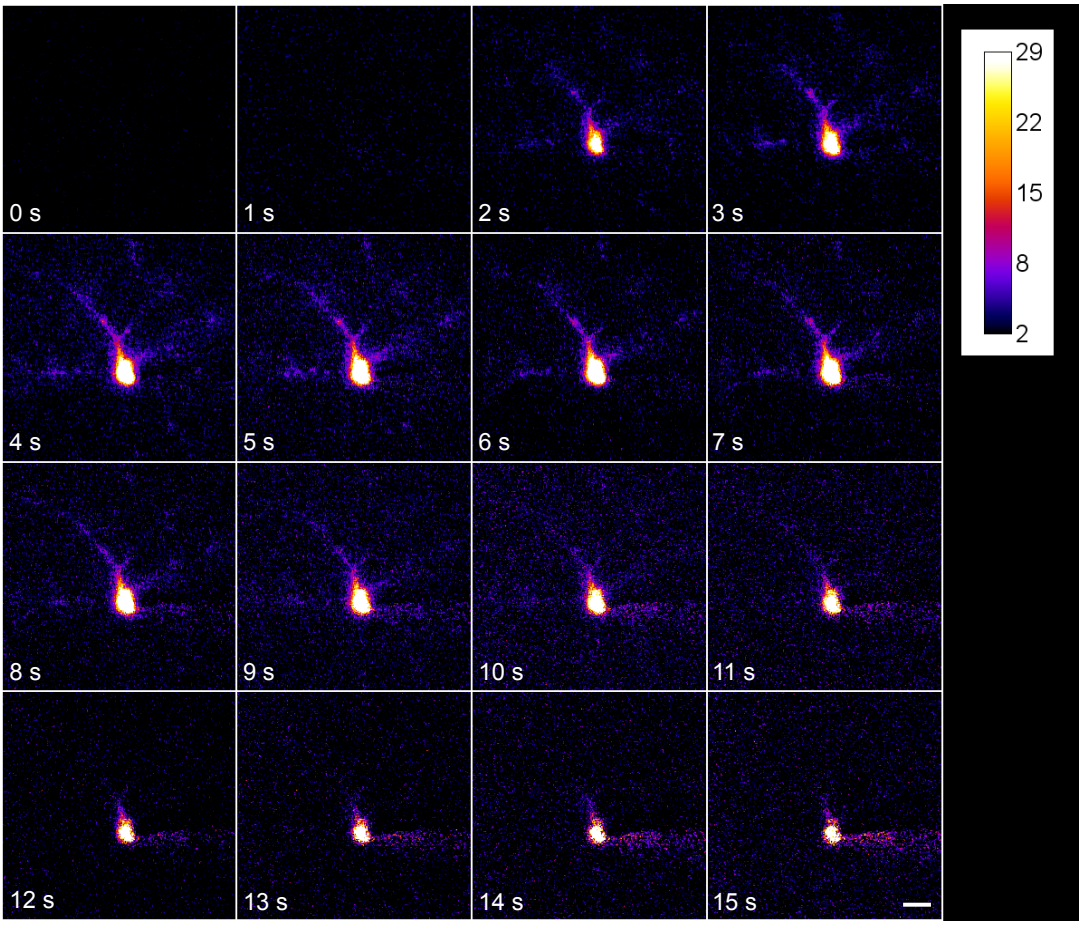

Figure 4.12 Ca^{2+} elevation in Cav1.2/1.3 deficient NG2 glia in the cortex upon depolarization. Cortical NG2 glia of dKO mice were loaded with Fluo 4 potassium slats via whole-cell pipette. At 0 s, successive stimulation by depolarization to 10 mV were applied to patched cells. The basal fluorescence prior to 0s was subtracted from all images. Scale bar = 5 µm.

2.75 s with depolarization to 10 mV for 100 ms repeated 25 times. Typical Ca^{2+} signals in NG2 glia upon depolarization showed a rapid elevation of intracellular Ca^{2+} examples (Fig. 4.11 (CTL) and Fig. 4.12 (dKO)). The peak somatic $[Ca^{2+}]_i$ elevation evoked at about 5 s in control and dKO mice, but was lower in dKOs (Fig. 4.13A). The average somatic fluorescent intensity from Cav1.2/1.3 deficient NG2 glia upon depolarization decreased significantly as compared to controls (CTL, 0.45 $\pm$ 0.03, n=9 cells; dKO, 0.31 $\pm$ 0.05, n=8 cells, *P$<$0.05, P=0.036) (Fig. 4.13B).

Notably, Ca^{2+} elevations could also be found in the processes of control and Cav1.2/1.3 deficient NG2 glia (Fig. 4.14). Signals in the processes were analyzed by a modified Sholl analysis. The first region of interest (ROI) was measured in a one fold distance from the soma. The second ROI was set at two fold distance from the soma. This was done

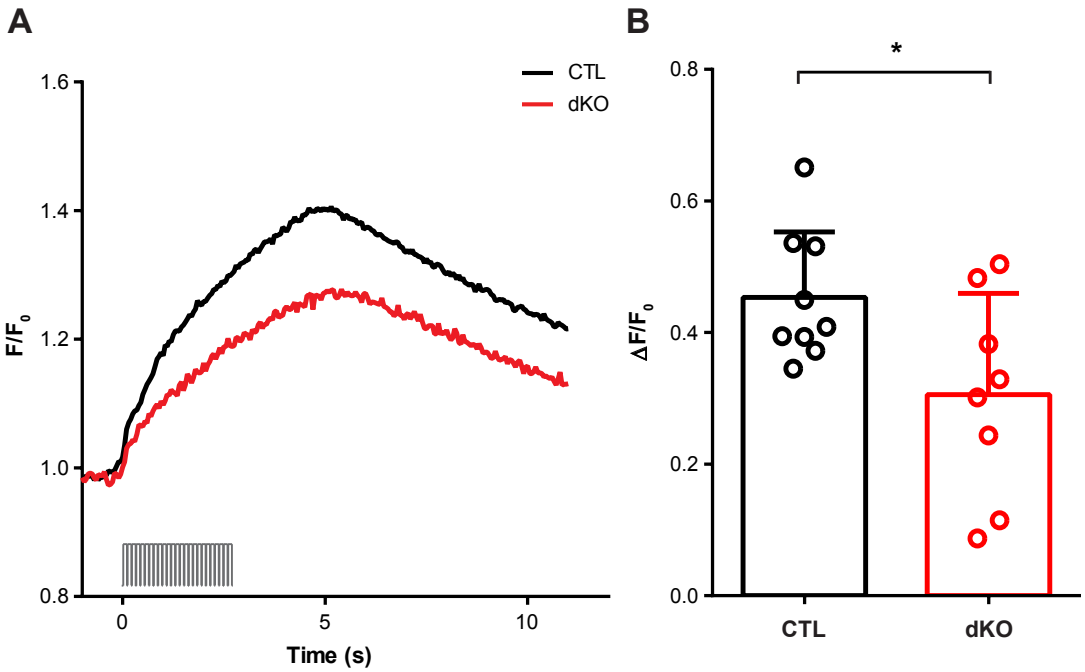

Figure 4.13 Somatic Ca^{2+} elevations were decreased in Cav1.2/1.3 deficient NG2 glia. A, Average of fluorescent intensities in somata of NG2 glia from dKO (8 cells) mice were lower than controls (9 cells) upon depolarization. The gray traces indicate the stimulation protocol applied to the patched cells by depolarizing from -100 to 10 mV for 100 ms with 25 times repetition. The cells were recorded in voltage-clamp mode with a holding potential of -80 mV. B, Peak fluorescent intensities in somata of NG2 glia were significantly reduced compared to control mice. *P$<$0.05, P=0.036.

repetitively until all the processes were reached (Fig. 4.14A). We found that peak Ca^{2+} signals in processes of Cav1.2 and 1.3 deficient NG2 glia were similar to somatic signals, but also lower than in controls (Fig. 4.14B-D). In addition, the $[Ca^{2+}]_i$ elevation almost reached the peak at all analyzed regions (from the first to the farthest ROIs) simultaneously (Fig. 4.14B-D). These data suggest that membrane depolarization rapidly spreads throughout the processes and activates local VGCCs in the processes. The rapid rise of Ca^{2+} signals in the processes of NG2 glia is comparable to the fast dendritic Ca^{2+} responses of cortical neurons under the same stimulus conditions (Fig. 4.15), suggesting that NG2 glia are capable of similar fast signal processing.

However, somatic $[Ca^{2+}]_i$ elevations in Cav1.2/1.3 deficient NG2 glia can still be observed (Fig. 4.13A). To determine whether the Ca^{2+} influx is via L-type VGCCs or other types upon depolarization, we applied the L-type VGCC blocker Verapamil by bath perfusion. The somatic Ca^{2+} signal from NG2 glia upon depolarization in controls (Fig. 4.16A) reduced significantly after 50 μM Verapamil application (0.54 $\pm$ 0.04 vs 0.23 $\pm$ 0.07; n=4

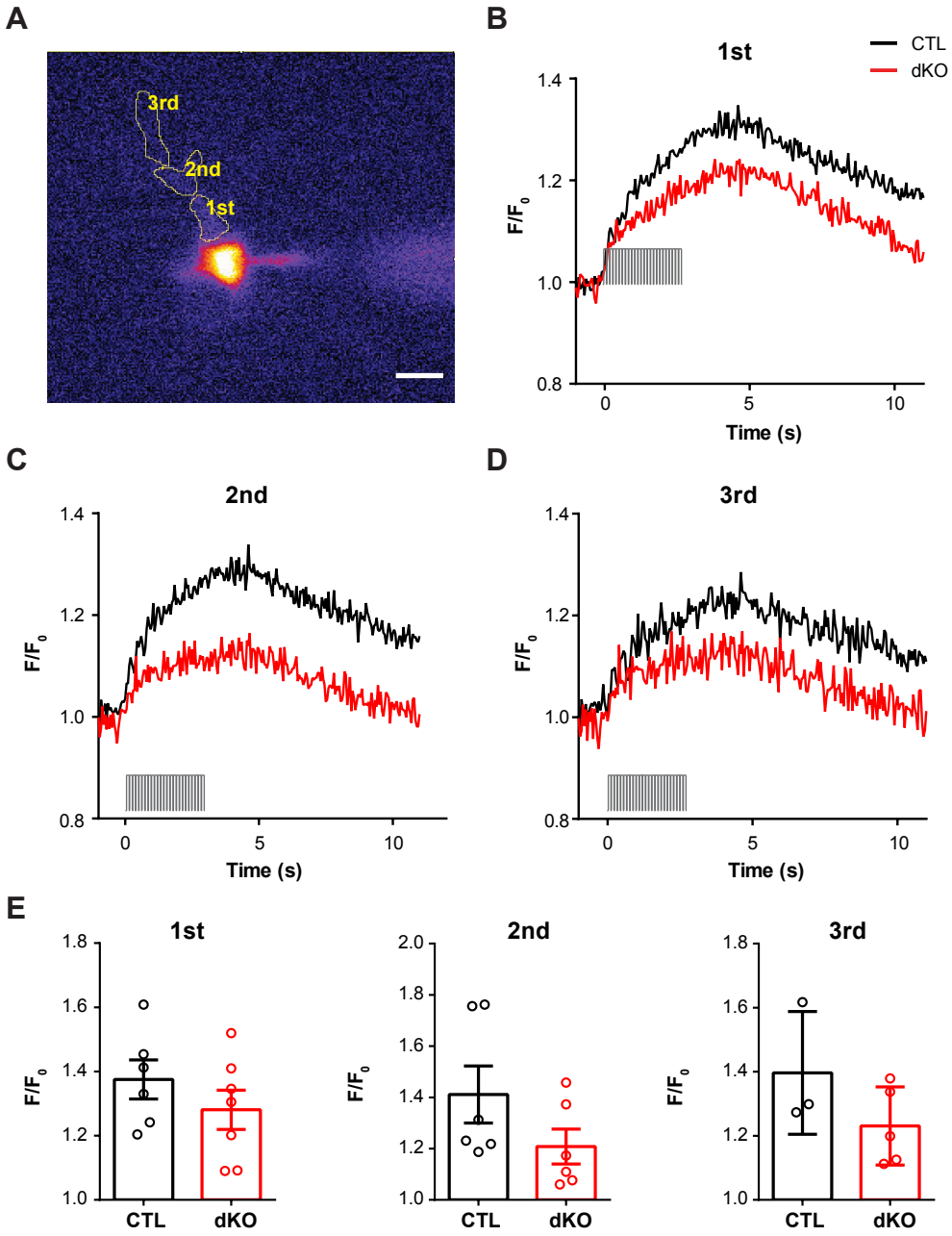

Figure 4.14 Ca^{2+} elevations were reduced in the processes of cortical NG2 glia. A, ROIs were defined in one-fold, two-fold and three-fold distance from the soma. Scale bar = 5 µm. B-D, ROI transients showing primary processes (B), secondary processes (C) and processes with three-fold distance (D), respectively, with a decrease of peak fluorescent intensities in all analyzed regions. The stimulation protocol that was applied to patched cells by depolarizing from -100 to 10 mV for 100 ms with 25 times repetition (gray traces). The cells were recorded in voltage-clamp mode with holding potential of -80 mV. E, Fluorescent intensities in Cav1.2/1.3 deficient NG2 glia were lower than controls in all examined ROIs.

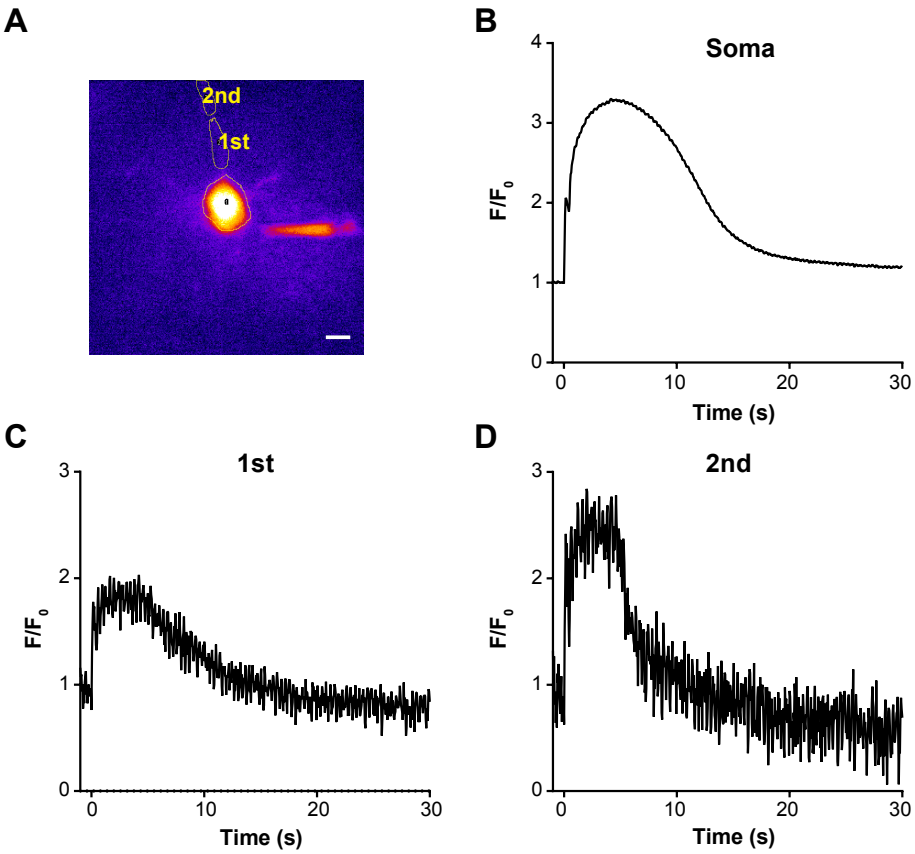

Figure 4.15 Ca^{2+} elevations in neurons. A, ROIs shown in B, C and D. Scale bar = 5 μm. B, Ca^{2+} elevation in the soma of a neuron by depolarization from -100 to 10 mV for 100 ms with 25 times repetition. C-D, The Ca^{2+} signals in primary (C) and secondary (D) dendrites of neuron were rapidly raised up upon depolarization. The cells were recorded in voltage-clamp mode with holding potential of -80 mV.

cells, **P<0.01, P=0.008; Fig. 4.16C), while the somatic Ca^{2+} signal in Cav1.2/1.3 deficient NG2 glia was not influenced (0.43 ± 0.06 vs 0.37 ± 0.06; n=3 cells, n.s., P=0.507; Fig. 4.16B, C). The same phenomenon was observed in processes (Fig. 4.17). Verapamil can abolish large Ca^{2+} signals in primary processes of controls (1.39 ± 0.08, n=4 cells vs 1.14 ± 0.03, n=4 cells, *P<0.05, P=0.034), but had no effect on Cav1.2/1.3 deficient NG2 glial processes (1.37 ± 0.08, n=3 cells vs 1.34 ± 0.06, n=3 cells, n.s., P=0.823, Fig. 4.17C). Altogether, $[Ca^{2+}]_i$ elevations in NG2 glia upon depolarization are initiated by the activation of L-type VGCCs. VGCC activation is synchronized by membrane depolarization at the soma and processes. After ablation of L-type VGCC isoforms Cav1.2 and Cav1.3, Ca^{2+} influx upon depolarization is reduced significantly but not diminished completely and still triggers cellular activities which were probably mediated by other subtypes of VGCCs, e.g., T-type VGCCs.

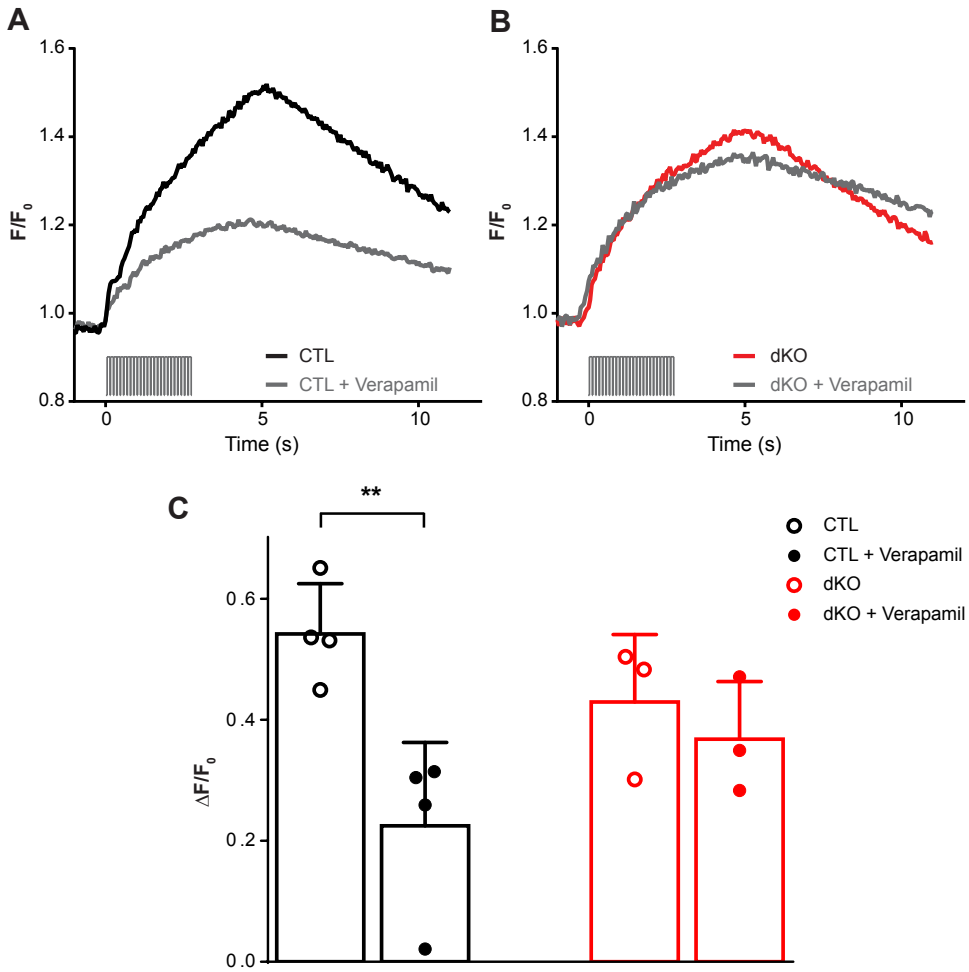

Figure 4.16 Somatic Ca^{2+} elevations in cortical NG2 glia is mediated by activation of L-type VGCCs. A, The average fluorescent intensity in the somata of cortical NG2 glia from controls upon depolarization were inhibited by 50 μM Verapamil (gray). B, 50 μM Verapamil (gray) had no impact on the average fluorescent intensity in somata of cortical NG2 glia from dKO mice upon depolarization. C, After Verapamil treatment, peak $[Ca^{2+}]_i$ elevations in somatic NG2 glia from controls were significantly reduced (**P<0.01, P=0.008), while no difference was detected in dKO mice.

4.5 Normal membrane properties of Cav1.2/1.3 deficient NG2 glia

To investigate whether the deletion of Cav1.2 and Cav1.3 could result in changes on membrane properties, NG2 glia were recorded in the cortex of Cav1.2/1.3 deficient mice (P30-38). Whole-cell membrane currents revealed that two different subpopulations (passive and complex NG2 glia, Fig. 4.18B) were still detected in Cav1.2/1.3 deficient NG2 glia, consistent with the observation in controls (Fig. 4.18A). I_{Na_v} was not observed in

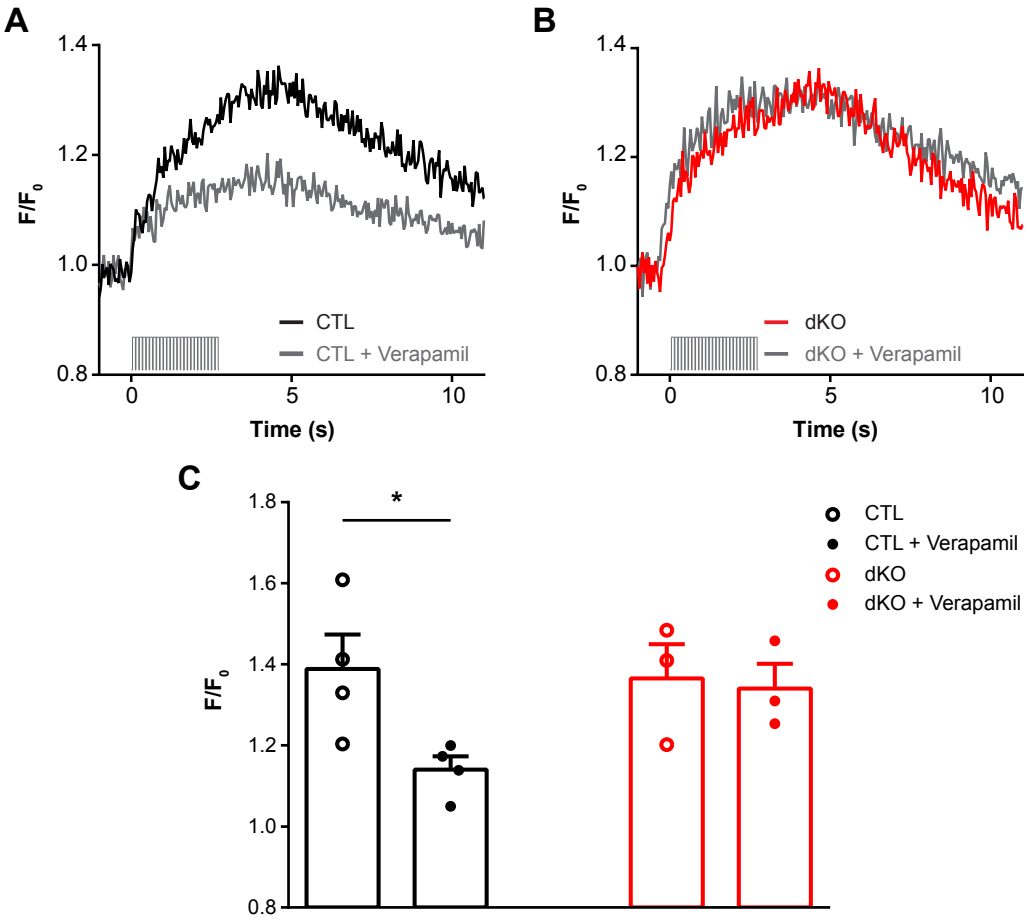

Figure 4.17 Ca^{2+} elevations in the processes of NG2 glia is also mediated by the activation of L-type VGCCs. A, The average fluorescent intensities in the primary processes of cortical NG2 glia from control mice upon depolarization were inhibited by 50 μM Verapamil (gray). B, 50 μM Verapamil (gray) had no impact on the average fluorescent intensity in the primary processes of cortical NG2 glia from dKO mice upon depolarization. C, After Verapamil treatment, peak $[Ca^{2+}]_i$ elevations in primary processes of NG2 glia from control mice were significantly decreased (*$P<0.05$, P=0.034), while no change in dKO mice .

controls and dKO mice at the examined age, compared to younger mice (Fig. 4.1C). In CTL and dKO mice, passive NG2 glia were the major subpopulation at this age, highlighted by the number of patched cells. Complex NG2 glia was barely detectable (1/15 cells from controls, 2/14 cells from dKO mice). The deletion of Cav1.2 and Cav1.3 did not alter the IV curves (Fig. 4.18C-D). In dKO mice, IV curves of complex NG2 glia still was non-linear and passive NG2 glia yielded linear IV curves (Fig. 4.18D).

Cav1.2/1.3 deficient NG2 glia had similar membrane capacitance values (CTL, 29.02 ± 1.31 pF, n=41 cells; dKO, 28.31 ± 2.16 pF, n=19 cells, n.s., P=0.75) and resting membrane potentials (CTL, -81.69 ± 1.33 mV, n=16 cells; KO, -78.13 ± 1.99 mV, n=16 cells,

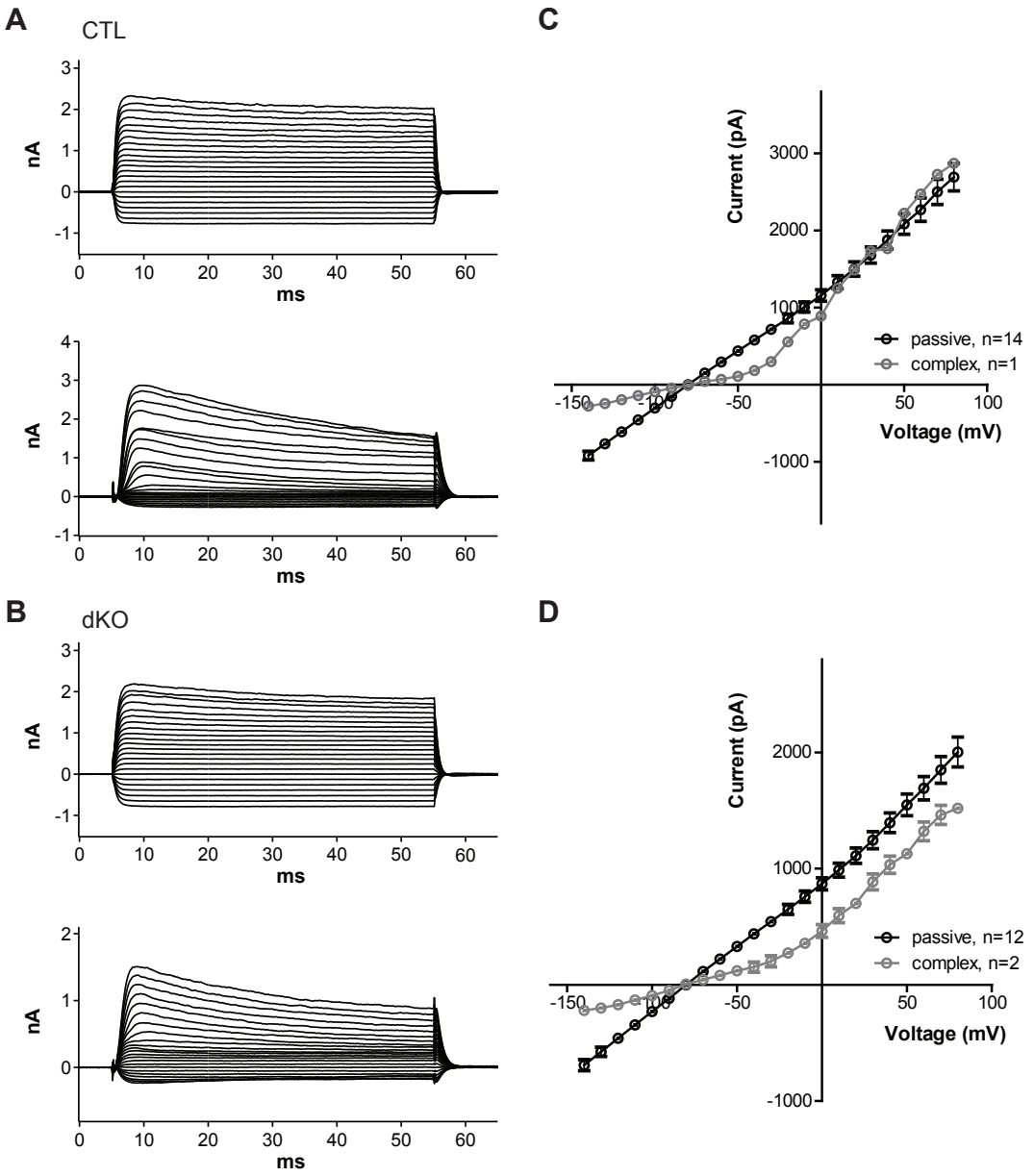

Figure 4.18 Membrane currents of Cav1.2/1.3 deficient NG2 glia. A-B, In control mice cortical NG2 glia displayed two different subpopulations (passive and complex NG2 glia) upon hyper- and depolarization in controls (passive, A top; complex, A bottom) and dKO (passive, B top; complex, B bottom) mice. C-D, The IV curves of these two different subpopulations showed no difference in their curve shapes between CTL (C) and dKO (D) mice.

n.s., P=0.094) as controls (Fig. 4.19A left and middle). But the membrane resistance of Cav1.2/1.3 deficient NG2 glia was higher than in controls (CTL, 86.4 $\pm$ 17.7 MΩ, n=16 cells; dKO, 126.1 $\pm$ 22.9 MΩ, n=15 cells, **P$<$0.01, P=0.0032; Fig. 4.19A right). Passive NG2 glia from dKO mice displayed smaller maximal (CTL, 2691 $\pm$ 178.7 pA, n=14 cells;

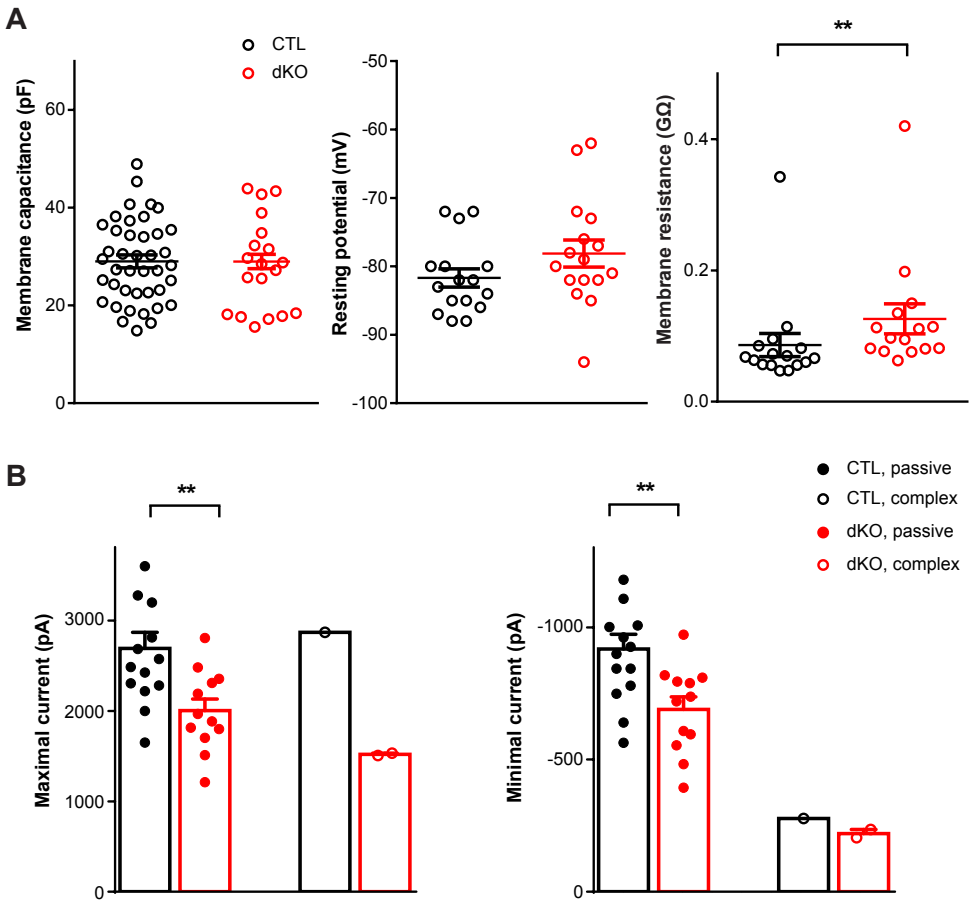

Figure 4.19 Membrane properties of Cav1.2/1.3 deficient NG2 glia. A, Cav1.2/1.3 deficient NG2 glia displayed similar membrane capacitance (left) and resting potential (middle) to controls, while their membrane resistance (right) were higher than controls. B. Maximal and minimal currents of two different subpopulations in CTL and dKO mice.

dKO, 2003 ± 128.5 pA, n=12 cells; **P<0.01, P=0.0064) and minimal (CTL, -919.2 ± 56.0 pA, n=14 cells; dKO, -690.7 ± 47.7 pA, n=12 cells; **P<0.01, P=0.0054) currents compared to controls (Fig. 4.19B). Taken together, these data indicated that Cav1.2 and Cav1.3 proteins do not play a prominent role in regulating the membrane properties of NG2 glia.

4.6 No changes of oligodendroglial differentiation in Cav1.2/1.3 deficient NG2 glia

The primary function of NG2 glia in gray and white matter is the differentiation into oligodendrocytes during CNS development (Huang et al., 2014; Zhu et al., 2008a). To inves-

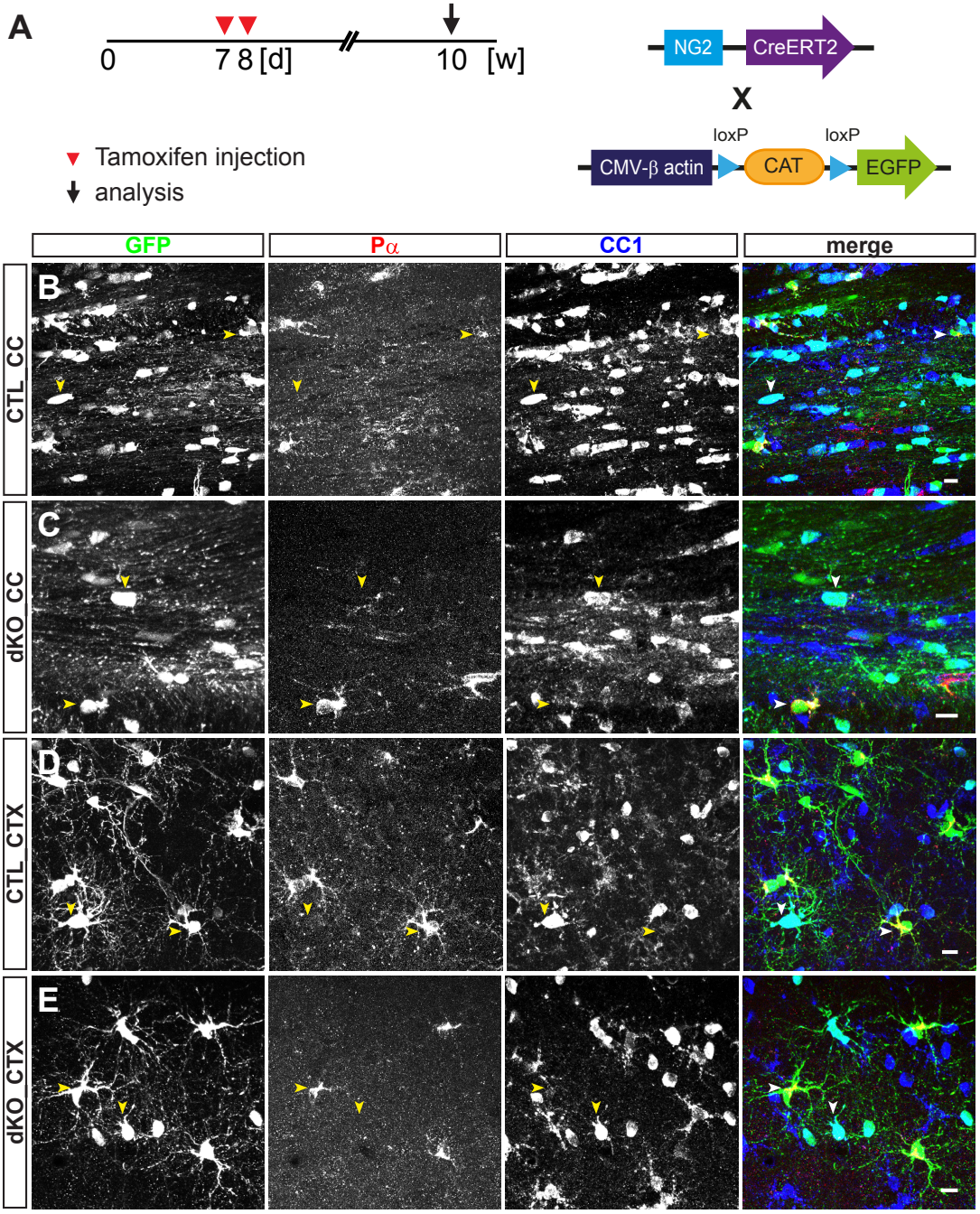

Figure 4.20 NG2 glia retain the ability to differentiate into oligodendrocytes in dKO mice. A, Tamoxifen administration and analysis time point (left) as well as transgenic mice (right). B-E, Recombined cells in the corpus callosum (CC) and cortex (CTX) of CTL and dKO mice in coronal forebrain sections after tamoxifen administration. Confocal images showing GFP$^+$ cells exhibited immunoreactivity to Pα or CC1 in these two regions of CTL and dKO mice. Scale bars = 10 μm.

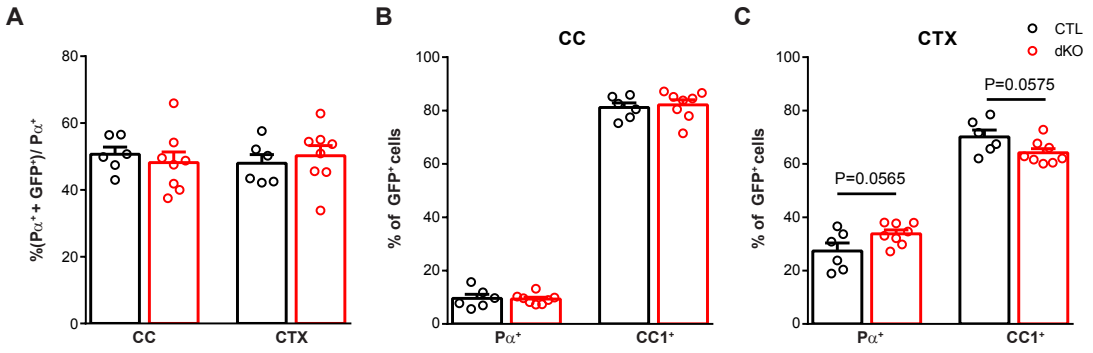

Figure 4.21 Percentages of GFP$^+$ cells in dKO mice using EGFP reporter. A, The percentage of reporter efficiency of ACGF reporter line (CTL, n=6 mice, dKO, n=8 mice). B. The percentage of Pα^+ GFP$^+$ and CC1$^+$ GFP$^+$ cells were in the corpus callsum between CTL and dKO mice. C, The percentage of Pα^+ GFP$^+$ and CC1$^+$ GFP$^+$ cells were in the cortex between CTL and dKO mice.

tigate whether the loss of Cav1.2 and Cav1.3 proteins would impair cell differentiation, we performed immunohistochemistry in 10 weeks old mice after tamoxifen administration at P7 and P8 (Fig. 4.20A). Heterozygous NG2-CreERT2 knock-in mice crossbred with ACGF reporter mice were used as controls. PDGFRα (Pα) as another widely accepted marker for NG2 glia was used to identify NG2 glia (Nishiyama et al., 1996). Adenomatous polyposis coli (APC) CC1 was used to detect mature myelinating oligodendrocytes (Zhu et al., 2012). In corpus callosum (Fig. 4.20A) and cortex (Fig. 4.20C) of controls, GFP$^+$ cells were Pα^+ and CC1$^-$ (horizontal arrowhead) and therefore identified as NG2 glia. The remaining GFP$^+$ cells were Pα^- and CC1$^+$ (vertical arrowhead), which were determined as mature oligodendrocytes, consistent with previous work (Huang et al., 2014). In dKO mice, both cell types, Pα^+ CC1$^-$ NG2 glia and Pα^- CC1$^+$ oligodendrocytes can be detected in corpus callosum (Fig. 4.20C) and cortex (Fig. 4.20E).

To quantify the number of each cell type, we counted Pα^+ NG2 glia and CC1$^+$ oligodendrocytes, as well as GFP$^+$ cells in corpus callosum and cortex. The reporter efficiency of the ACGF reporter line was about 50% in both white and gray matter (CTL CC, 50.66 $\pm$ 2.14%; dKO CC, 48.17 $\pm$ 3.21%, n.s., P=0.561; CTL CTX, 48.00 $\pm$ 2.58%; dKO CTX, 50.21 $\pm$ 3.07%, n.s., P=0.609. CTL, n=6 mice, dKO, n=8 mice) (Fig. 4.21A). In the corpus callosum of dKO mice, only 9.36 $\pm$ 0.68% of GFP$^+$ cells were Pα^+, similar to controls (9.62$\pm$1.51%, n.s., P=0.865) (Fig. 4.21B). More than 80% of GFP$^+$ cells were detected by immunoactivity to the oligodendrocyte specific marker CC1 in both CTL and dKO mice (CTL, 81.15 $\pm$ 1.72%; dKO, 82.14 $\pm$ 1.87%, n.s., P=0.713) (Fig. 4.21B). In the cortex, 33.82 $\pm$ 1.43% of GFP$^+$ in dKO mice were Pα^+, which showed a tendency of in-

creased cell numbers compared to controls (27.36±3.00%; n.s., P=0.0565) (Fig. 4.21C). Accordingly, the number of $CC1^+$ GFP^+ cells in dKO mice (64.20 ± 1.55%) displayed a reduction compared to controls (70.14 ± 2.55%), while a non-significant difference can be detected in the cortex between CTL and dKO mice (n.s., P=0.0575) (Fig. 4.21C). These data indicate that the capability of NG2 glia to differentiate into oligodendrocytes was not influenced by deleting of Cav1.2 and Cav1.3 proteins in white and gray matter.

4.7 Inhibited proliferation of cortical NG2 glia in Cav1.2/1.3 deficient mice

In the mature CNS, uniformly distributed NG2 glia are the major proliferating cell population outside of neurogenic regions like subventricular zone and hippocampus (Dawson et al., 2003; Huang et al., 2014). Cumulative BrdU labeling of NG2 glia in corpus callosum reached a plateau at ∼ 55% in 7-10 days (Rivers et al., 2008), while in the cortex, the labeling increased linearly for 21 days until ∼ 40% of NG2 glia were $BrdU^+$ (Rivers et al., 2008). To investigate whether Cav1.2 and Cav1.3 ablation would impact the self-renewal of NG2 glia, we performed immunohistochemichal analysis in 10 weeks old mice treated with tamoxifen at P7 and P8, receiving BrdU water for 10 days (Fig. 4.22A). CreERT2 negative littermates were used as controls. Confocal images showed some $P\alpha^+$ cells were $BdrU^+$ in corpus callosum (Fig. 4.22B) and cortex (Fig. 4.22D) of controls (horizontal arrowhead), indicating proliferating NG2 glia. The other $P\alpha^+$ cells were non-proliferating $BdrU^-$ cells (vertical arrowhead) in both analyzed regions. In dKO mice, both $P\alpha^+$ $BdrU^+$ and $P\alpha^+$ $BdrU^-$ cells could be found in corpus callosum (Fig. 4.22C) and cortex (Fig. 4.22E). These data suggest that Cav1.2/1.3 deficient NG2 glia still retained self-renewal ability in both brain regions.

However, a further analysis showed that the number of proliferating NG2 glia in the cortex of dKO mice was lower than in controls (CTL, 44.83 ± 1.20%, n=4 mice; dKO, 24.03 ± 1.86%, n=5 mice, *P<0.05, P=0.0159) (Fig. 4.23A), while callosal numbers of proliferating NG2 glia were similar to controls (CTL, 60.78 ± 3.78%; dKO 66.15 ± 2.13%, n.s., P=0.232). To rule out that the decreasing number of NG2 glia is due to cell death or inhibition of proliferation, we quantified the cell density of NG2 glia in different brain regions. However, we did not find altered numbers of $P\alpha^+$ cells in gray and white matter in dKO mice compared to controls (CTL CC, 349.8 ± 11.4 cells/ mm^2; dKO CC, 342.3 ± 20.6 cells/ mm^2, n.s., P=0.778; CTL CTX, 231.8 ± 4.0 cells/ mm^2; dKO CTX, 229.4 ± 7.5 cells/ mm^2, n.s., P=0.803) (Fig. 4.23B). We performed Caspase 3 staining to

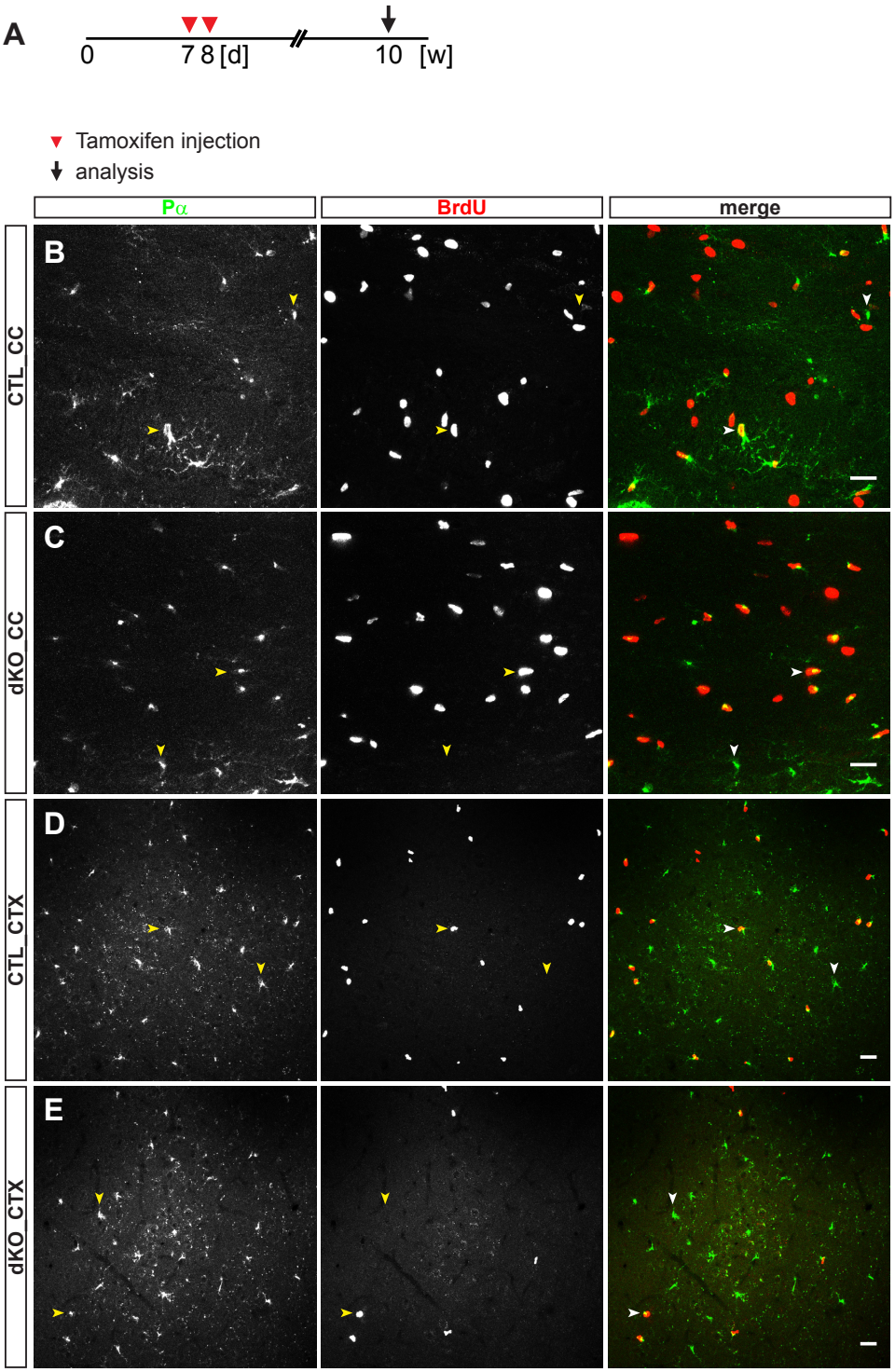

Figure 4.22 Cav1.2/1.3 deficient NG2 glia kept proliferating in the corpus callosum and cortex. A, Tamoxifen administration and analysis time point. B-E, Confocal images showing some cells immunoreactive to BrdU and/or Pα in the corpus callosum and cortex of CTL and dKO mice. Scale bars = 20 μm.

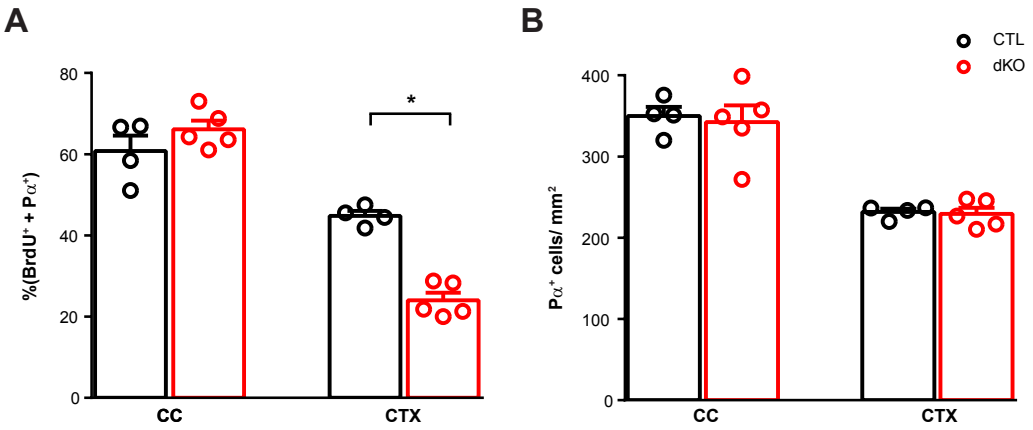

Figure 4.23 Inhibition of cortical NG2 glia proliferation in Cav1.2/1.3 deficient mice. A, The percentages of Pα^+ BrdU$^+$ cells were in the corpus callosum and cortex from CTL and dKO mice, showing less proliferating NG2 glia in the cortex (CTL, n=4 mice, dKO, n=5 mice). B, The number of Pα^+ cells did not change in gray and white matter of CTL and dKO mice.

identify potential increased cellular apoptosis. No difference was detected in the forebrain between CTL and dKO mice (data not shown). This implies that deletion of Cav1.2 and Cav1.3 proteins did not induce cell death in corpus callosum and cortex. Taken together, Cav1.2 and Cav1.3 proteins are playing an important role in mediating proliferation of NG2 glia, but do not affect their survival.

4.8 No requirement of Cav1.2 and Cav1.3 proteins for myelination

Although the differentiation of NG2 glia was not affected by removal of Cav1.2 and Cav1.3, we investigated whether this removal from NG2 glia would induce dysfunctional myelination. We collected samples from cerebral cortex and corpus callosum of dKO mice as well as their CreERT2 negative littermates and performed Western blot analysis to evaluate myelin proteins (Myelin basic protein, MBP; Proteolipid protein, PLP; and Myelin oligodendrocyte glycoprotein, MOG) (4.24A). Here, 16 weeks old mice treated with tamoxifen at P7 and P8 were used. The expression level of MBP (CTL, 1.18 $\pm$ 0.24, n=5 mice; dKO, 0.66 $\pm$ 0.21, n=5 mice, n.s., P=0.140) and MOG (CTL, 0.92 $\pm$ 0.28; dKO, 0.62 $\pm$ 0.11, n.s., P=0.352) from dKO mice showed a decreasing tendency, although no significant difference between them could be detected (Fig. 4.24A). The PLP expression level in dKO mice was similar to controls (CTL, 0.69 $\pm$ 0.15; dKO, 0.57 $\pm$ 0.13, n.s., P=0.563).

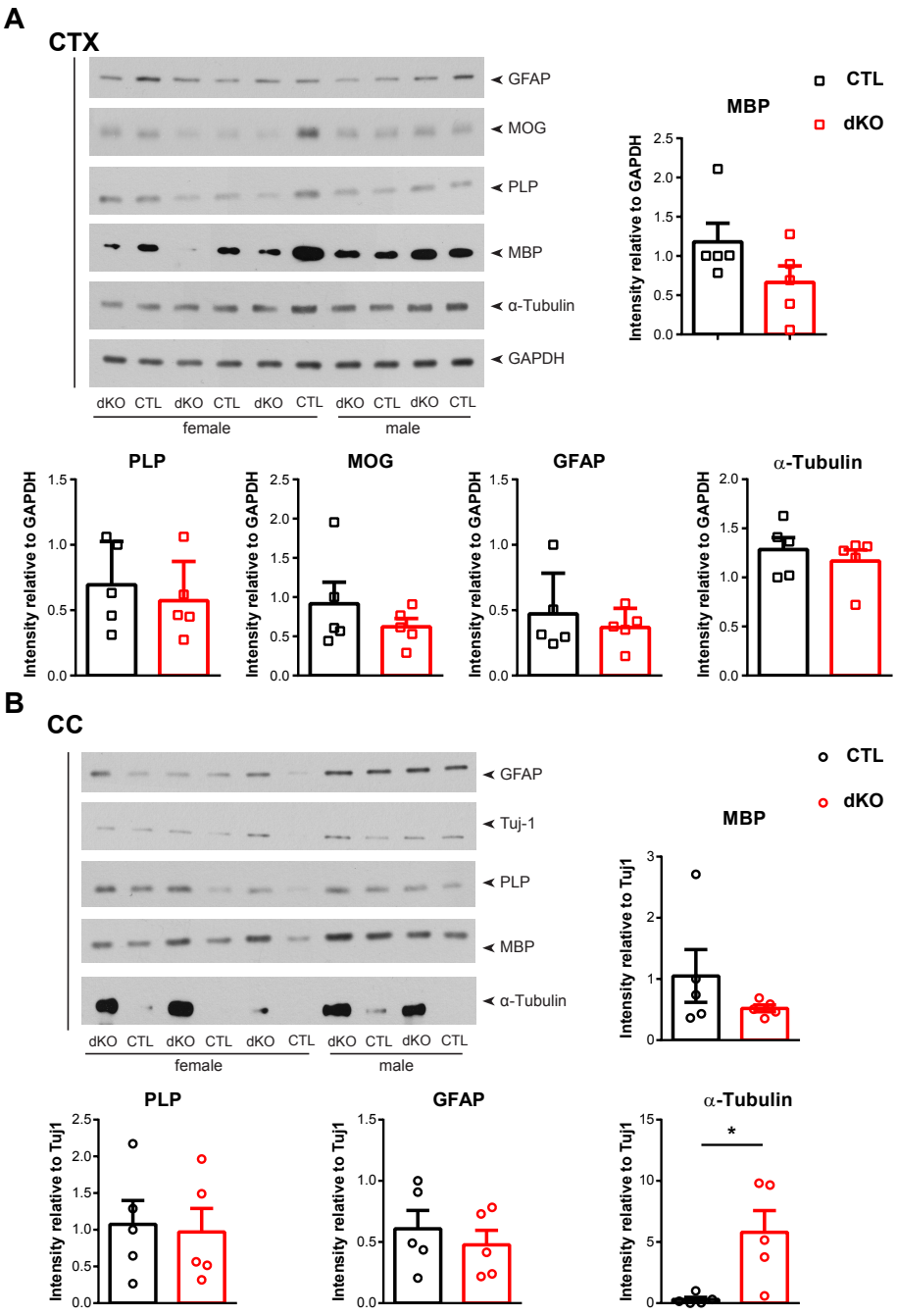

Figure 4.24 Knockout of Cav1.2 and Cav1.3 in NG2 glia did not alter myelin protein expression. A-B, Total protein samples from cerebral cortex (A) and corpus callosum (B) of dKO mice and their littermate controls were analyzed by Western blot to assess the expression of MBP, PLP, MOG, GFAP and α-Tubulin. GAPDH was used as the internal standard control in cortex and Tuj1 in corpus callosum. All quantitative data were summarized based on the relative spot intensities and plotted as percentage. CTL, n=5 mice; dKO, n=5 mice.

Deletion of Cav1.2 and Cav1.3 genes from NG2 glia did not influence astrocytes (CTL,

0.47 ± 0.14; dKO, 0.37 ± 0.06, n.s., P=0.521) and the microtubule cytoskeleton (CTL, 1.29 ± 0.12; dKO, 1.17 ± 0.11, n.s., P=0.498) in the cortex (Fig. 4.24A).

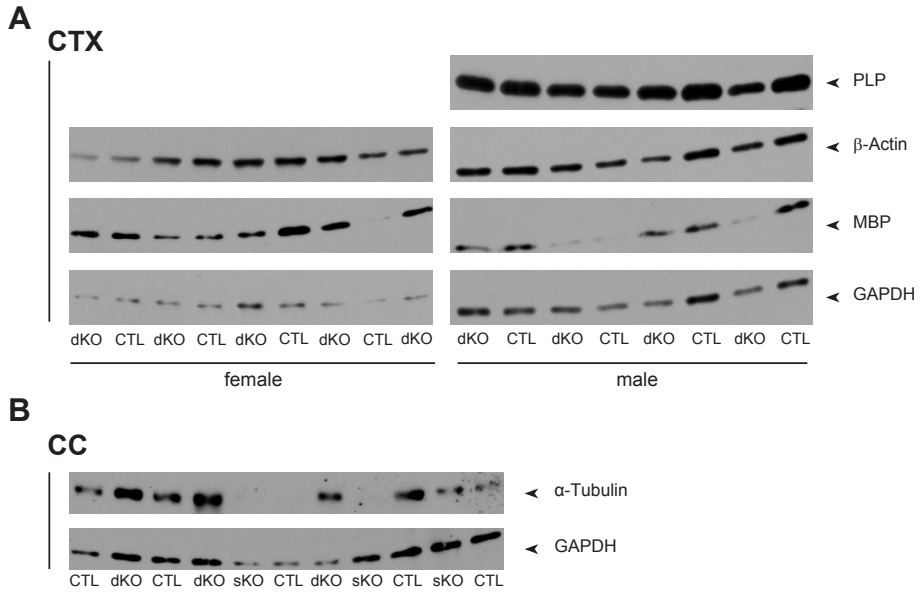

Figure 4.25 Knockout of Cav1.2 and Cav1.3 in NG2 glia disturbed microtubule cytoskeleton in the corpus callosum. A-B, Total protein samples from cerebral cortex (A) and corpus callosum (B) of dKO mice and their littermate controls from another cohort were analyzed to assess the expression of myelin proteins MBP and PLP, β-Actin, GAPDH and α-Tubulin. In corpus callosum, the samples from Cav1.2-/- and Cav1.3+/- mice (sKO) were also collected.

Comparing CTL and dKO mice in corpus callosum, no changes of myelin proteins MBP (CTL, 1.05 ± 0.43, n=5 mice; dKO, 0.52 ± 0.06, m=5 mice, n.s., P=0.257) and PLP (CTL, 1.07 ± 0.32; dKO, 0.97 ± 0.32, n.s., P=0.825) were detected (Fig. 4.24B). Astrocytes were also not affected by removal of Cav1.2 and Cav1.3 protein from NG2 glia in the corpus callosum (CTL, 0.61 ± 0.15; dKO, 0.48 ± 0.12, n.s., P=0.514). By investigating the expression level of the microtubule cytoskeleton in dKO mice compared to controls, α-Tubulin increased significantly in the corpus callosum contrary to cortical data (CTL, 0.30 ± 0.18; dKO, 5.79 ± 1.77, *P<0.05, P=0.015) (Fig. 4.24B). Tuj-1 (used for normalization) is a neuron-specific class III β-Tubulin (von Bohlen und Halbach, 2007), implying that neuronal tubulin expression was not affected by deletion of Cav1.2 and Cav1.3 from NG2 glia. Additionally, corpus callosum is the white matter in the brain where NG2 glia and oligodendrocytes are enriched. Therefore, the microtubule cytoskeleton of NG2 glia and oligodendrocyte lineage cells might be disturbed by ablation of Cav1.2 and Cav1.3 from NG2 glia due to the upregulation of α-Tubulin.

To confirm the findings on α-Tubulin expression changes in the corpus callosum, we

collected more samples from another cohort to repeat the experiment. In the cerebral cortex, no significant differences were detected on myelin proteins (MBP and PLP) as well as cytoskeletal protein either from female or male animals (Fig. 4.25A). In corpus callosum, the expression level of α-Tubulin from dKO mice enhanced as compared to controls (Fig. 4.25B). Here, we also collected the samples from homozygous floxed Cav1.2 and heterozygous flexed Cav1.3 mice which exhibited the same level of α-Tubulin as controls (Fig. 4.25B). These data suggests that only the double knockout of Cav1.2 and Cav1.3 can disturb the homeostasis of the microtubule cytoskeleton network. Taken together, these data demonstrate that Cav1.2 and Cav1.3 genes are not required for myelination during the development but play crucial roles for the microtubule cytoskeleton. Removal of Cav1.2 and Cav1.3 genes from NG2 glia does not affect neighboring cells in the brain, like astrocytes. In the cortex, a potential upregulation of α-Tubulin might be concealed by the other cell types (including neurons) due to the analysis of whole cortical homogenates.

4.9 Partial loss of fine processes in Cav1.2/1.3 deficient NG2 glia

Western blot analysis showed changes in the cytoskeletal network due to the knockout of Cav1.2 and Cav1.3 genes from NG2 glia. Thus, we investigated the morphology of NG2 glia in the absence of Cav1.2 and Cav1.3. Because NG2 glia in the corpus callosum have a special compacted structure, we focused on cortical NG2 glia, hypothesizing that an effect was concealed due to other neural cells in the biochemical analysis, as NG2 glia are not the main subpopulation in the cortex. To confirm our hypothesis, Sholl and binary analysis were performed to analyze the morphology of NG2 glia in layer II/III of the cerebral cortex.

NG2 glia exhibit numerous, highly branched processes (Fig.4.26A). The Sholl analysis (Fig.4.26B) showed that the logarithm (inters/area) from Cav1.2/1.3 deficient NG2 glia was significantly smaller than normal NG2 glia from CTL in the range of 32 to 41 μm far away from the soma (Fig.4.26C). These data suggested that Cav1.2/1.3 deficient NG2 glia had less branches in their fine processes.

Besides this, we observed that Cav1.2/1.3 deficient NG2 glia had less GFP particles in their fine processes than controls (Fig.4.26A). To further quantify the differences in these fine processes, binary analysis was applied. Larger than 1-20 pixel^2 particles were ruled out. Cav1.2/1.3 deficient NG2 glia had significantly less (1-20 pix^2) particles (CTL,

542.1 ± 35.3, n=35 cells; dKO, 326.5 ± 25.6, dKO, n=28 cells; ***P<0.001, P<0.0001) and the total area of these particles was smaller (CTL, 83.90 ± 6.28 μm^2; dKO, 46.48 ± 3.98 μm^2, ***P<0.001, P<0.0001) (Fig.4.26D left and middle). No difference in the average size of these particles could be found (CTL, 0.15 ± 0.01 μm^2; dKO, 0.14 ± 0.01 μm^2, n.s., P=0.127) (Fig.4.26D right). These data implied Cav1.2/1.3 deficient NG2 glia occupied less space and their processes were not so long with a less complex morphology compared to controls. These data implies that NG2 glia from dKO mice might have less contacts with axons.

4.10 Shortened paranodes in Cav1.2/1.3 deficient mice in the corpus callosum

To further investigate whether the ablation of Cav1.2 and Cav1.3 from NG2 glia have an impact on myelination, Caspr and MBP co-staining was performed in 10 weeks old mice after tamoxifen administration at P7 and P8. Caspr expression is restricted to the paranodes of mature myelinated axons in the peripheral and CNS (Einheber et al., 1997). Therefore we estimated the paranodal length by measuring Caspr staining. MBP was used to visualize myelinated axons (Fig. 4.27). We only analyzed the complete pair of paranodes (Fig. 4.28A) and did not consider the single ones. The blank region between two paranodes is the node of Ranvier (Fig. 4.28A). Caspr staining was concentrated in the paranodal regions of the small myelinated fibers of the corpus callosum in CTL and dKO mice (Fig. 4.27).

In the corpus callosum of dKO mice, the paranodal length was significantly shortened as compared to controls (CTL, n=7 mice; dKO, n=7 mice, **p<0.01, P=0.005; Table 4.1). In addition, the callosal node of Ranvier in dKO mice seemed to be shorter than controls, but no significant difference was found (n.s., P=0.057) (Table 4.1; Fig. 4.28A). The distribution of the paranodal length displayed leftward shift (Fig. 4.28B), especially the portion of callosal paranodes of 3.0-4.0 μm in dKO mice significantly increased from 8.7

Table 4.1 Paranodal length in white matter

Brain region	Paranodes (μm) CTL vs dKO	Node of Ranvier (μm) CTL vs dKO
Corpus callosum	5.10 ± 0.05 vs 4.56 ± 0.15	1.42 ± 0.26 vs 0.85 ± 0.07
Spinal cord	5.06 ± 0.14 vs 4.94 ± 0.14	0.46 ± 0.07 vs 0.36 ± 0.06
Optic nerve	4.67 ± 0.10 vs 4.58 ± 0.07	0.41 ± 0.02 vs 0.38 ± 0.03

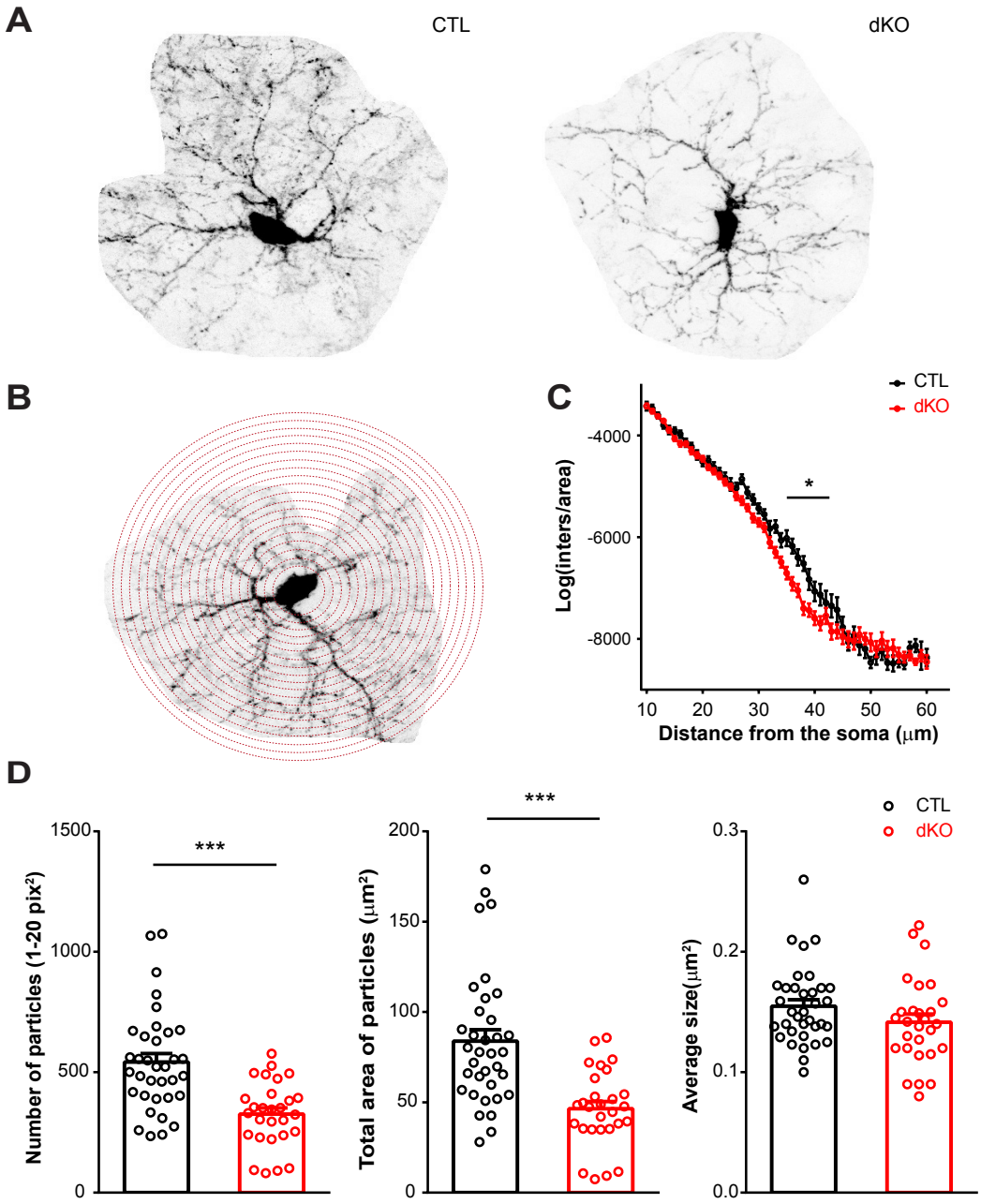

Figure 4.26 Ca1.2/1.3 deficient NG2 glia exhibited less complex morphology. A, The typical NG2 glia in layer II/III of cortex from CTL and dKO mice. B, Diagram of classic Sholl analysis, where process intersections were counted every 1 μm. C, In the range of 32 to 41 μm far away from the soma, Cav1.2/1.3 deficient NG2 glia displayed less processes than normal cells (CTL, n=18 cells, dKO, n=62 cells). D, The processes quantification on binary analysis showed that Cav1.2/1.3 deficient NG2 glia had less 1-20 pix^2 particles (left), smaller size (middle) than normal NG2 glia, but there was no difference on average size between these two groups (right), indicating NG2 glia in dKO mice lost some fine processes.

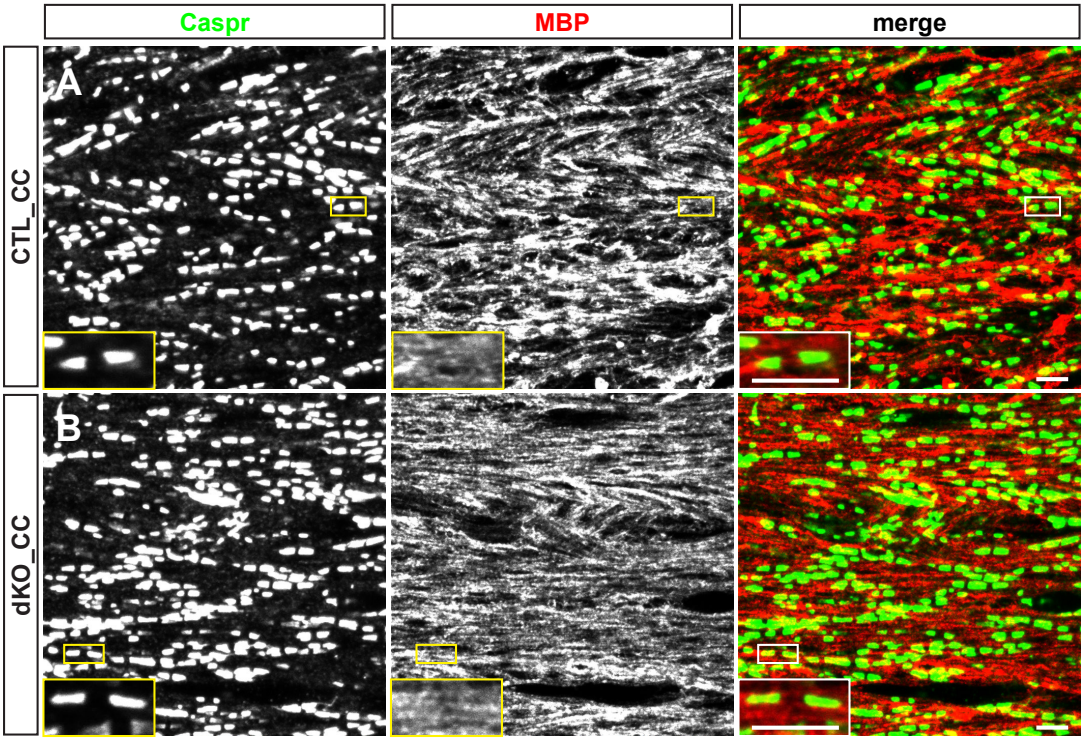

Figure 4.27 Paranodes in corpus callosum of CTL and dKO mice. A-B, Co-immunolabeling of Caspr and MBP in corpus callosum from CTL (A) and dKO (B) mice. Left, Caspr; middle, MBP; right, merge. Maximum intensity projection for each staining are shown here. The yellow box showed the magnification of a pair of paranodes in corpus callosum. Scale bar = 5 μm.

± 1.6% (CTL, n=7 mice) to 22.7 ± 5.1% (dKO, n=7 mice; *P<0.05, P=0.023), and in the portion of 4.0-5.0 μm, the number was raised from 34.9 ± 2.4% (CTL) to 45.6 ± 1.6% (dKO) (**P<0.01, P=0.003). Accordingly, in the range of 5.0-6.0 μm, the number of callosal paranodes in dKO mice was significantly reduced from 38.3 ± 3.5% (CTL) to 24.7 ± 4.7% (dKO; *P<0.05, P=0.040) as well as the portion of 6.0-7.0 μm was remarkably decreased from 11.6 ± 2.0% (CTL) to 3.5 ± 1.1% (dKO; **P<0.01, P=0.004). Therefore, these data indicates that the deletion of Cav1.2 and Cav1.3 proteins from NG2 glia resulted in the shortening of paranodal lengths in the corpus callosum.

To determine if the alteration of paranodal length is region specific, we also performed the immunostaining against Caspr and MBP in the spinal cord in 10 weeks old mice. The confocal analysis showed that Caspr staining was restricted to the paranodal regions of the myelinated fibers of the spinal cord in CTL and dKO mice (Fig. 4.29). No changes in the length of paired paranodes (CTL, n=7 mice, dKO, n=7 mice; n.s., P=0.557) and nodes of Ranvier (n.s., P=0.299) as well as the distribution of paranodal lengths in the

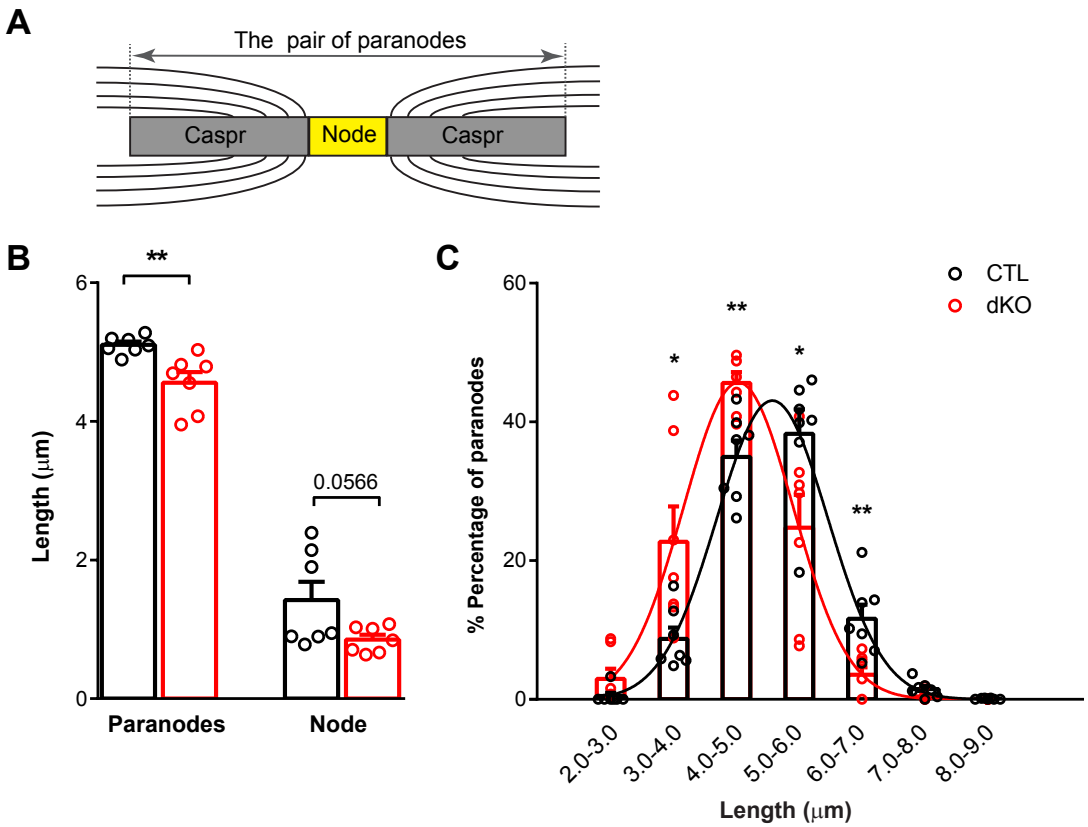

Figure 4.28 The length of paired paranodes in corpus callosum from Cav1.2/1.3 deficient mice were shortened. A, The diagram of paired paranodes. B, The length of paired paranodes and nodes of Ranvier in the corpus callosum between CTL (n=7 mice) and dKO (n=7 mice) mice. C, The distribution of paranodal length in dKO shifted to the smaller range compared control mice.

spinal cord between CTL and dKO mice were found (Table 4.1; Fig. 4.30). So these data suggests that the deletion of Cav1.2 and Cav1.3 proteins did not alter the myelinated structure in the spinal cord.

The optic nerve is an ideal location to quantify CNS myelination, since the axons are aligned, myelination is relatively uniform, and the geometry and timing of myelin wrapping is well described (Snaidero et al., 2014; Zuchero et al., 2015). We performed immunohistochemistry in the optic nerve whole mounts against Caspr and MBP. Confocal analysis showed that Caspr staining was also concentrated in the paranodal regions of the myelinated fibers of the optic nerve in CTL and dKO mice (Fig. 4.31). However, no significant differences in the length of paired paranodes (CTL, n=4 mice; dKO, n=5 mice, n.s., P=0.515) and nodes of Ranvier (n.s., P=0.436) as well as the distribution of paranodal length in the optic nerve between CTL and dKO mice were observed (Table 4.1; Fig. 4.32). These data were consistent to the previous results in the spinal cord. Similarly,

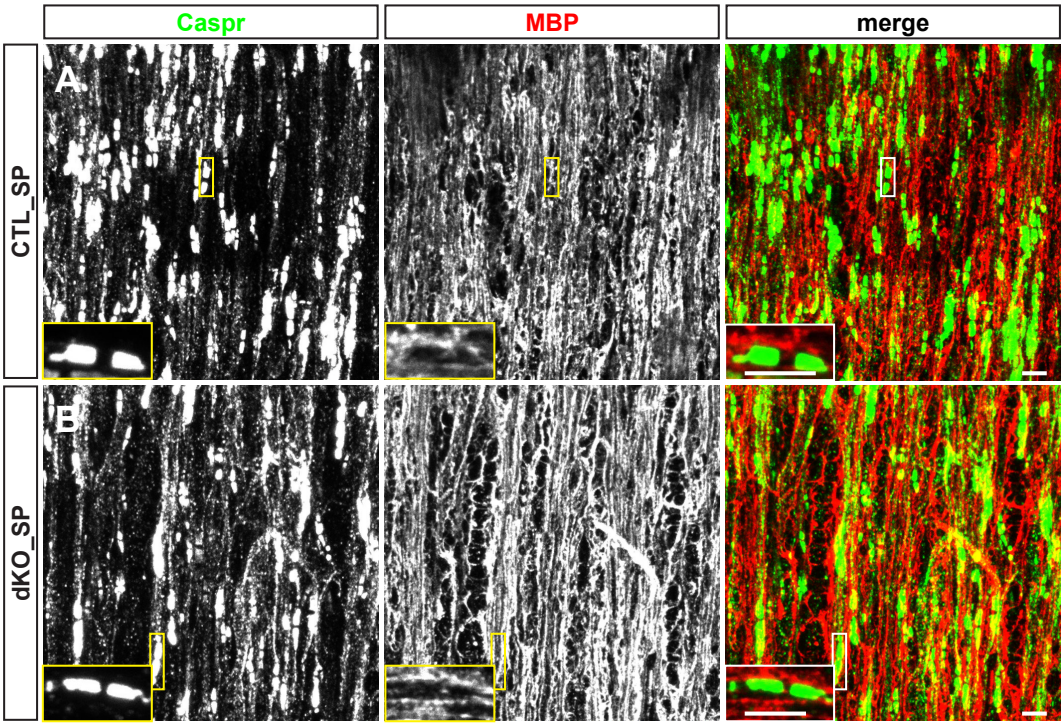

Figure 4.29 Paranodes in the spinal cord of CTL and dKO mice. A-B, Co-immunolabeling of Caspr and MBP in the spinal cord of CTL (A) and dKO (B) mice. Left, Caspr; middle, MBP; right, merge. Maximum intensity projection for each staining are shown here. The yellow box showed the magnification of a pair of paranodes in the spinal cord. Scale bar = 5 μm.

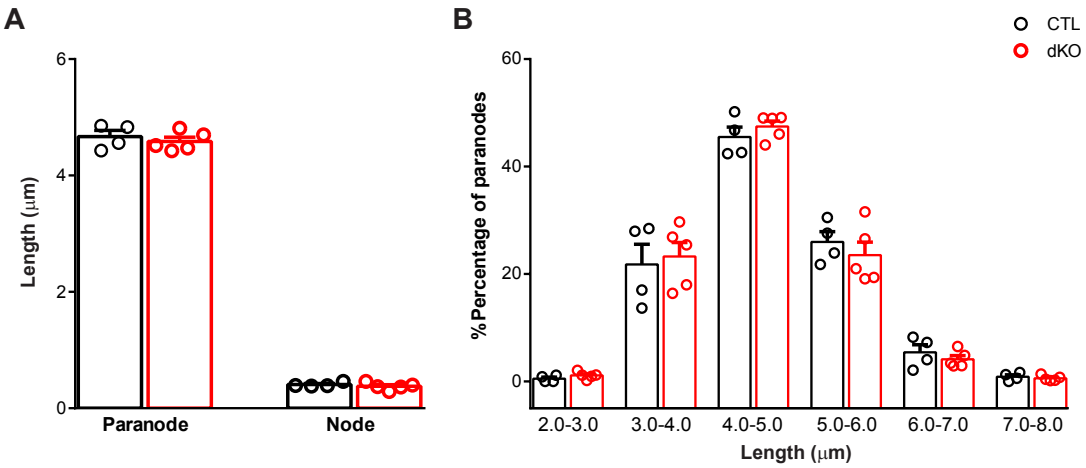

Figure 4.30 Deletion of Cav1.2 and Cav1.3 did not alter the length of paired paranodes and nodes of Ranvier in the spinal cord. A, The length of paranodes and nodes of Ranvier in the spinal cord between CTL and dKO mice. B, The distribution of paranodal length in dKO and CTL mice.

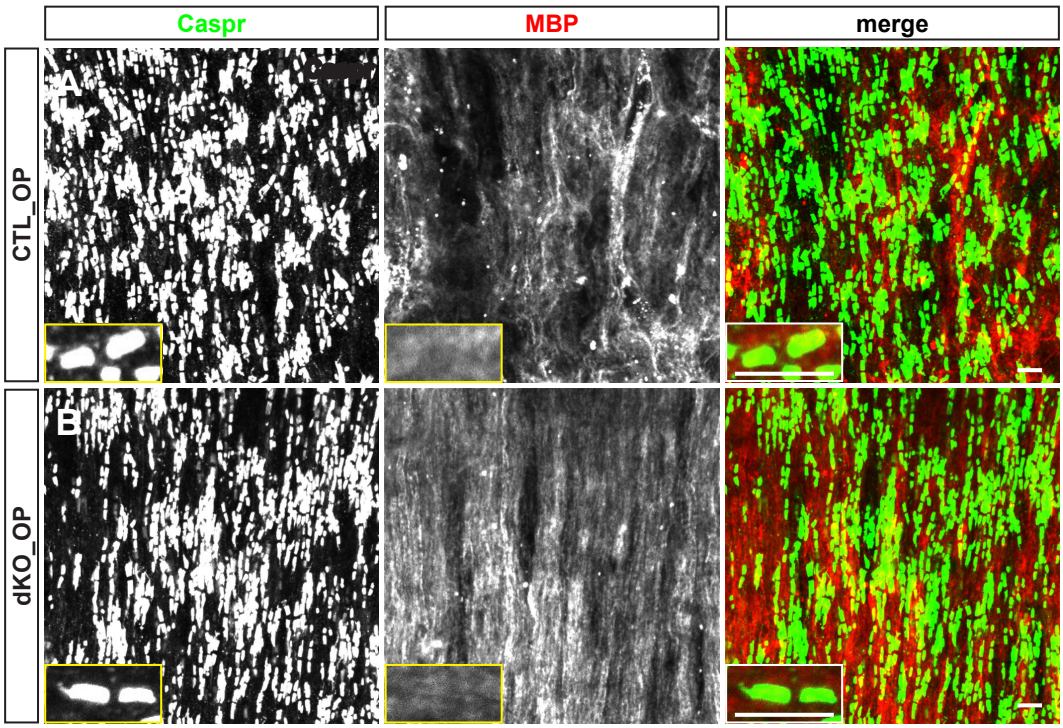

Figure 4.31 Paranodes in the optic nerve of CTL and dKO mice. A-B, Co-immunolabeling of Caspr and MBP in the optic nerve of CTL (A) and dKO (B) mice. Left, Caspr; middle, MBP; right, merge. Maximum intensity projection for each staining are shown here. The yellow box showed the magnification of paired paranodes in the optic nerve. Scale bar = 5 μm.

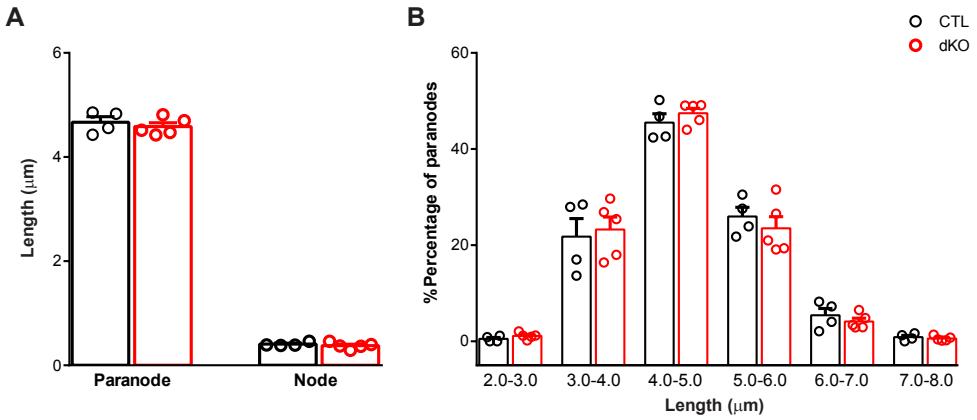

Figure 4.32 Deletion of Cav1.2 and Cav1.3 did not alter the length of paired paranodes and nodes of Ranvier in optic nerve. A. The length of paired paranodes and nodes of Ranvier in optic nerve between CTL and dKO mice. B, The distribution of paranodal length in dKO mice was the same as control mice.

the myelinated structure in the optic nerve was not influenced by removal of Cav1.2 and Cav1.3 from NG2 glia.

4.11 No alteration of conduction velocity in callosal axon after ablation of Cav1.2 and Cav1.3 in NG2 glia

The callosal paranodal pair was shortened by deletion of Cav1.2 and Cav1.3 from NG2 glia. Therefore conduction velocity of axons in the corpus callosum might be altered accordingly. To characterize the functional consequences of Cav1.2 and Cav1.3 in NG2 glia, compound action potential (CAP) measurements of callosal axons were performed. Acute brain slices prepared from the dKO mice and their littermate controls at 10 weeks after tamoxifen injection at P7 and P8 were analyzed. After stimulus artifact, two inward waves were elicited (Fig. 4.33). Previously, the callosal CAP has been described about their characteristics of biphasic waves with an early component evoked by fast conducting myelinated axons (N1) and a later occurring component mainly from slower unmyelinated axons (N2) (Crawford et al., 2009). Here we analyzed the CAP amplitudes of N1 and N2 waves from peak to peak as indicated with the dashed lines in Fig. 4.33B.

Callosal CAP recordings at five different distances between stimulus and recording electrodes from CTL and dKO mice were measured (Fig. 4.34A). Conduction velocity of myelinated callosal axons was calculated by linear regression with a value of 0.847 $\pm$ 0.046 ms^{-1} (n=21 slices from 5 mice) in controls and 0.853 $\pm$ 0.042 ms^{-1} in dKO mice (n=13 slices from 3 mice), whereas conduction velocity of unmyelinated axons were 0.311 $\pm$ 0.095 ms^{-1} in controls and 0.314 $\pm$ 0.093 ms^{-1} in dKO mice (Fig. 4.34B). No signifi-

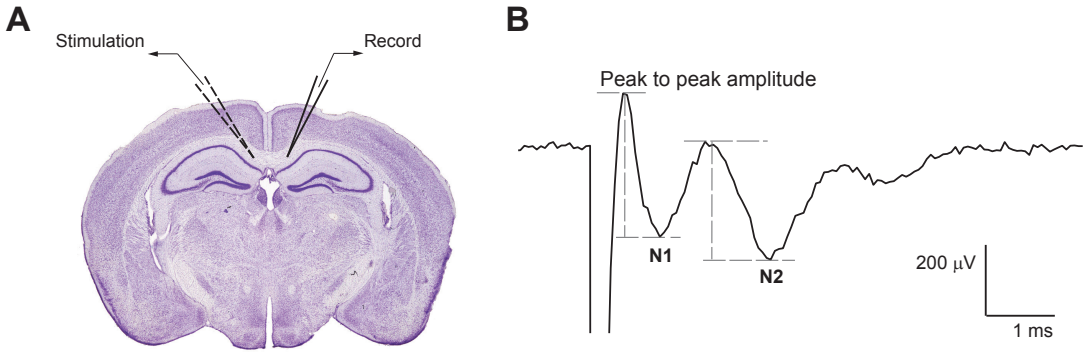

Figure 4.33 Strategy of callosal compound action potential recordings. A, Coronal forebrain sections at hippocampal level (Bregma -0.94mm to -2.46 mm). A bipolar electrode was used for stimulation in the corpus callosum of one hemisphere and another glass electrode filled with ACSF was placed at the contralateral hemisphere for recoding. B, A typical CAP recording. Following the artifacts of stimulation, there are two waves appearing. The first wave is called N1 wave which generated from myelinated axons, the second wave is termed as N2 wave which generated from unmyelinated axons. The CAP amplitude is measured as the vertical distance from peak to peak of N1 and N2 waves.

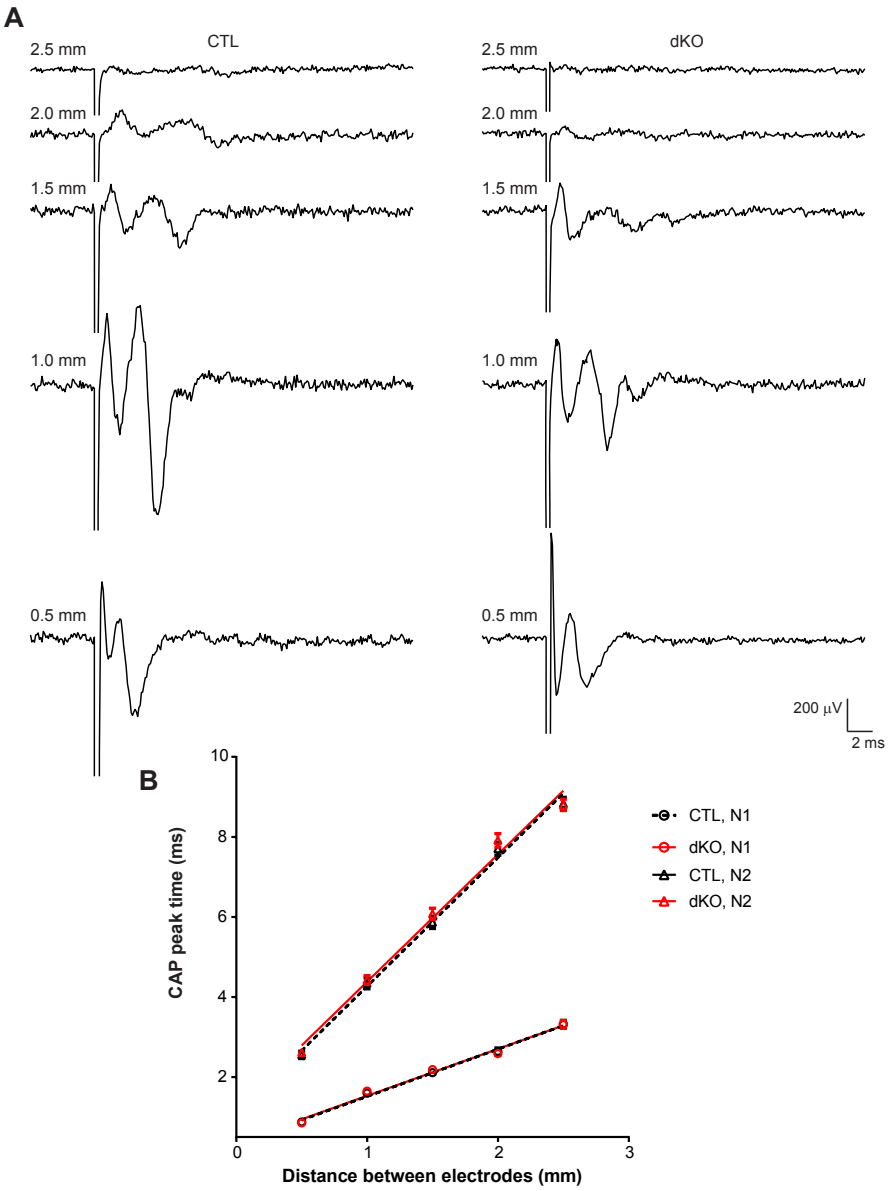

Figure 4.34 Callosal conduction velocity was not influenced by the deletion of Cav1.2 and Cav1.3 in NG2 glia. A, Representative CAP recordings were shown at the different distances between stimulus and recording electrodes (from 0.5-2.5 mm) in corpus callosum from CTL (left panel) and dKO (right panel) mice. B, The measurements of peak latency at the different distances allow an estimation of the conduction velocity for both N1 and N2 waves. No differences were detected in conduction velocity of these two waves between CTL and dKO mice (CTL, n=21 slices from 5 mice; dKO, n=13 slices from 3 mice).

cant difference was detected in the conduction velocity of axons in the corpus callosum, despite different paranodal length between controls and dKO mice.

The callosal CAP responses of both waves N1 and N2 increased proportionally upon the increment of stimulus currents in CTL and dKO mice (Fig. 4.35). The peak amplitude

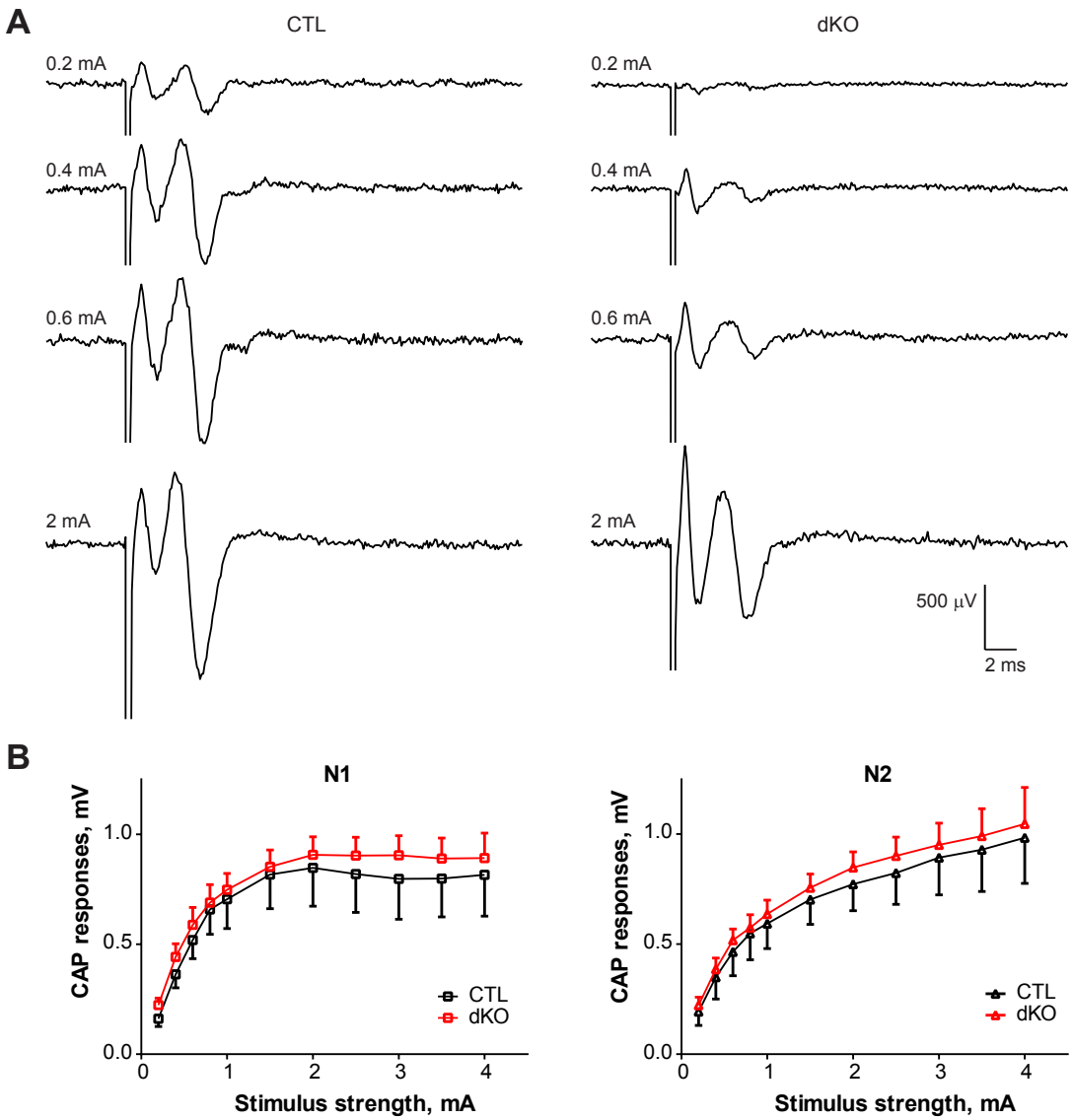

Figure 4.35 The stimulus-response upon current injection in corpus callosum from CTL and dKO mice. A, Typical CAP recordings upon the increment of current injection were shown in corpus callosum from CTL (the left panel) and dKO (the right panel) mice. B, The average stimulus-response amplitudes of N1 and N2 waves in CTL and dKO mice (CTL, n=12 slices from 4 mice; dKO, n=11 slices from 3 mice).

of N1 at 4 mA of current injection was 0.82 $\pm$ 0.19 mV in controls (n=12 slices from 4 mice) and 0.89 $\pm$ 0.11 mV in dKO mice (n=11 slices from 3 mice), while the peak amplitude of N2 at 4 mA of current injection was 0.98 $\pm$ 0.21 mV in controls and 1.05 $\pm$ 0.17 mV in dKO mice with no significant difference. These data suggests that ablation of Cav1.2 and Cav1.3 from NG2 glia did not influence conduction velocity of callosal axons, despite shortened callosal paranodes.

4.12 No changes of synaptic input in the somatosensory cortex after removal of Cav1.2 and Cav1.3

It has been reported that NG2 glia can receive synaptic input from axons (Dimou and Gallo, 2015). To determine whether knockout of Cav1.2 and Cav1.3 would influence the function of Neuron-NG2 glia synapses, we recorded excitatory postsynaptic currents (EPSCs) of cortical NG2 glia in layer II/III by stimulating presynaptic axons in layer V in the presence of the $GABA_AR$ antagonist picrotoxin (Fig. 4.36B). Acute brain slices were prepared from 10 weeks old mice after tamoxifen administration at P7 and P8 (Fig. 4.36A). Age-matched NG2-EYFP mice were used as controls. The EPSC amplitude of Cav1.2/1.3 deficient NG2 glia was -70.34 $\pm$ 17.94 pA (n=7 cells). No significant difference was calculated as compared to control mice (-105.30 $\pm$ 11.92 pA, n=20 cells; n.s., P=0.138) (Fig. 4.36D). Pharmacological inhibition showed that EPSCs of cortical NG2 glia were mediated by AMPARs and NMDARs in the presence of AMPAR antagonist CNQX and NMDAR antagonist DAP5. These data showed that the deletion of Cav1.2 and Cav1.3 did not alter the components of EPSCs in cortical NG2 glia (Fig. 4.36E). Taken together, it implicates that the ablation of L-type VGCC isoforms Cav1.2 and Cav1.3 in NG2 glia did not affect the synaptic connectivities.

4.13 NMDA-dependent long-term depression deficit in Cav1.2 and Cav1.3 knockout mice

NG2 glia are playing an important role in neuronal synaptic signaling. As a hallmark of neuronal plasticity, neuron-glia synapses undergo activity dependent modifications analogous to long-term potentiation (LTP) at excitatory synapses. (Ge et al., 2006). Pharmacological inhibition of NG2 or genetic ablation of NG2 protein results in striking reduction in NMDA receptor dependent LTP in pyramidal neurons of the somatosensory cortex (Sakry et al., 2014). Ablation of NG2 glia causes deficits in the excitatory glutamatergic synaptic transmission in the prefrontal cortex (PFC) of adult brain (Birey et al., 2015). In addition, morphological and physiological interactions between NG2 glia, astrocytes and neurons, such as extension of glutamatergic synapses onto NG2 glia in the hippocampus (Bergles et al., 2000), have been well described (Wigley et al., 2007). Based on the previous findings of morphological changes in NG2 glia of dKO mice, especially with the significant difference on the fine processes of NG2 glia, we suspected that NG2 glia had loss contact with neurons. Therefore, to determine whether the knockout of Cav1.2/1.3

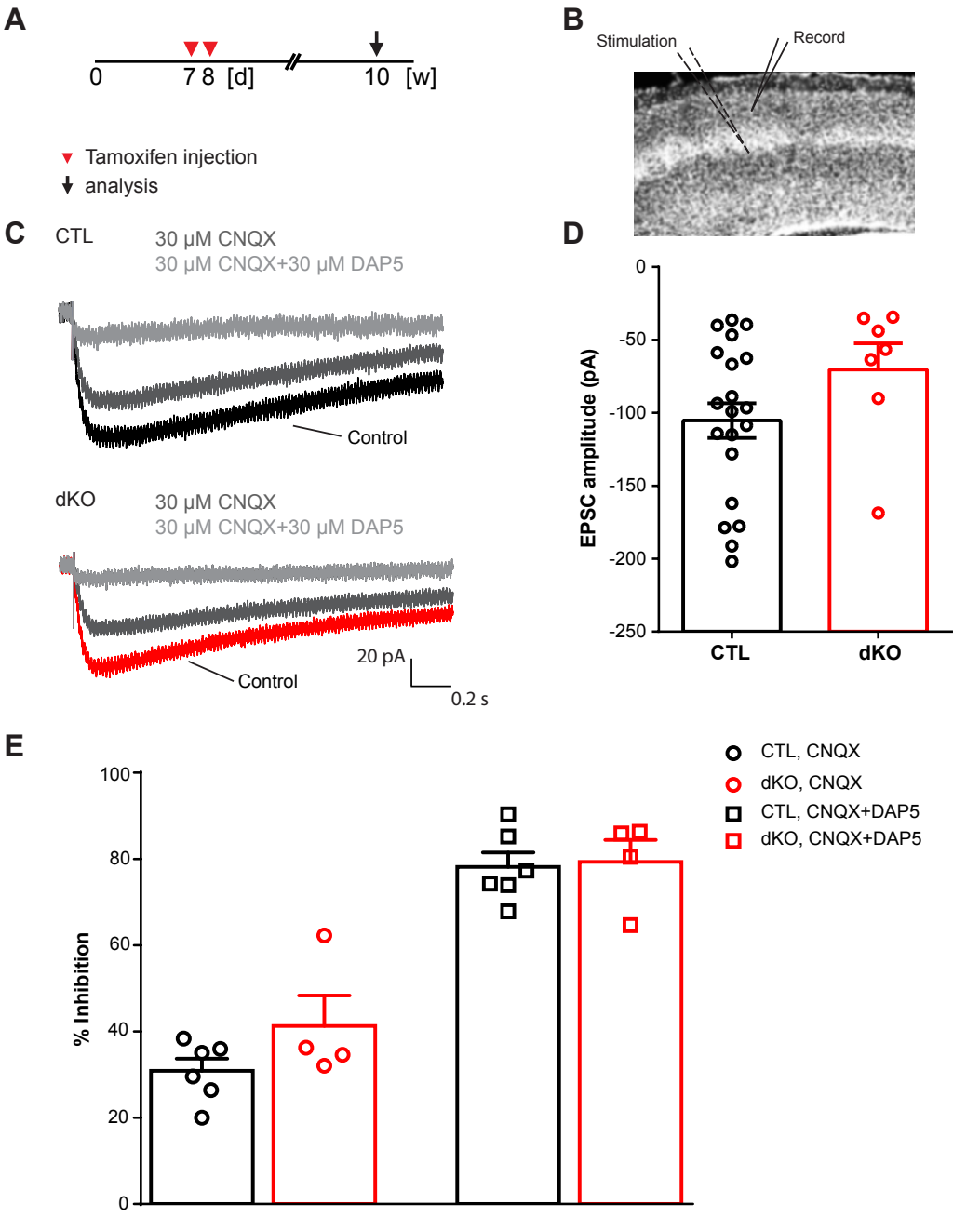

Figure 4.36 Removal of Cav1.2/1.3 did not affect neuron-glia synapses in the somatosensory cortex. A, Tamoxifen administration and analysis time point. B, Reporter$^+$ NG2 glia were recorded in layer II/III by stimulating the presynaptic axons of layer V. C, The EPSC profiles from CTL and dKO mice in the absence and presence of cocktail blockers (AMPA receptor antagonist CNQX and NMDA receptor antagonist DAP5). D, EPSC amplitudes of CTL and dKO mice. E, The inhibition of EPSC in CTL and dKO mice by antagonists of AMPARs and NMDARs.

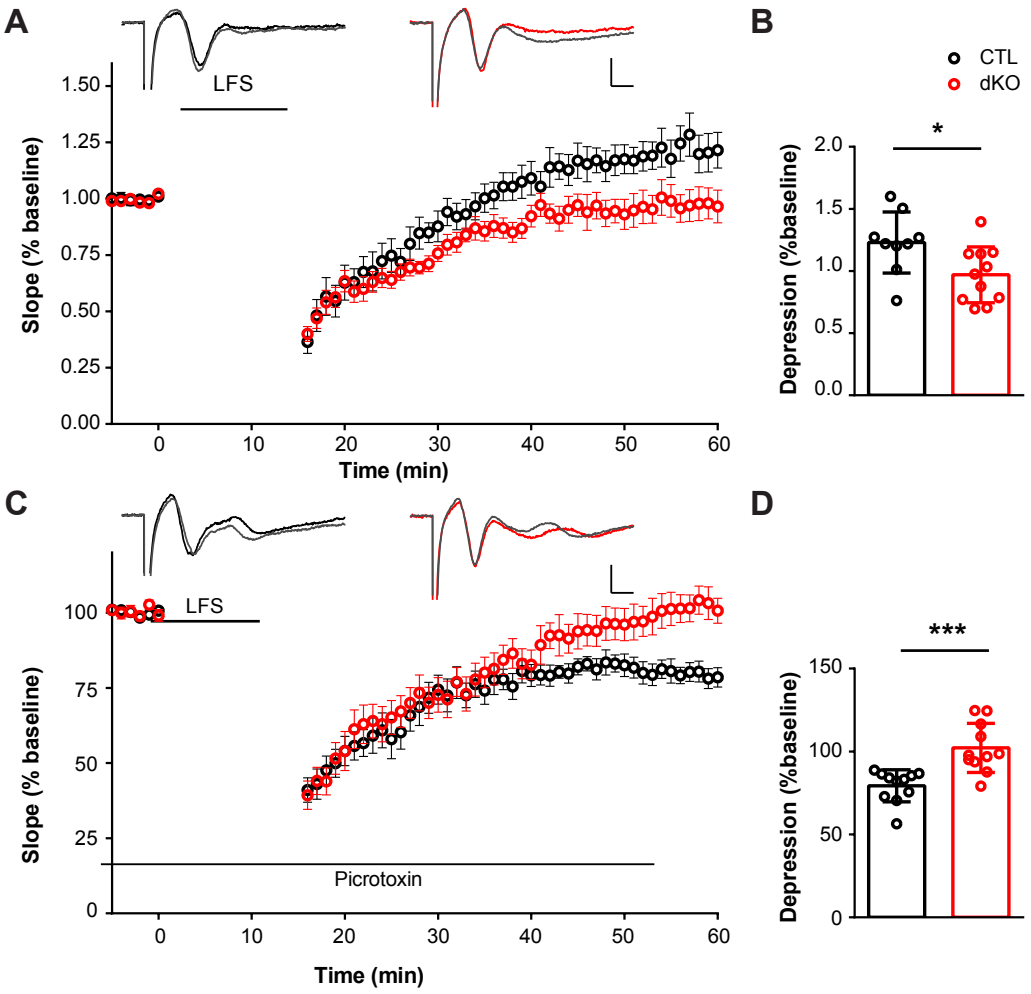

Figure 4.37 LTD induced by low frequency stimulation in hippocampus. A, Data from all slices of CTL (black) and dKO (red) showed changes in fEPSP slope as percentage of baseline before and after LFS (1Hz for 15 min) in normal ACSF. The typical EPSP traces were from CTL (left) and dKO mice (right) before and after (gray) stimulation. Scale bar, x=2 ms, y=0.5 mV. B, The slope fraction of the last five minutes of recording in CTL and dKO mice. C, Data from all slices of CTL and dKO showed changes in fEPSP slope before and after LFS in the presence of picrotoxin. The small top figures show the fEPSP in CTL and dKO mice before and after stimulation. D, The percentage of depression induced by LFS showed that LTD were elicited in control mice but not in dKO mice.

from NG2 glia would influence neuronal network, we performed a series of recording of field excitatory postsynaptic potentials (fEPSP) in the hippocampal CA1 of by stimulating the CA3 region. Brain slices were prepared from dKO mice and their CTL littermates at 8 - 12 weeks. The classic low frequency stimulation (LFS) was used to evoke long term depression (LTD) which was recorded for 45 min. After LFS, LTD failed to be elicited in control mice in the absence of the $GABA_AR$ antagonist picrotoxin (Fig. 4.37A). The

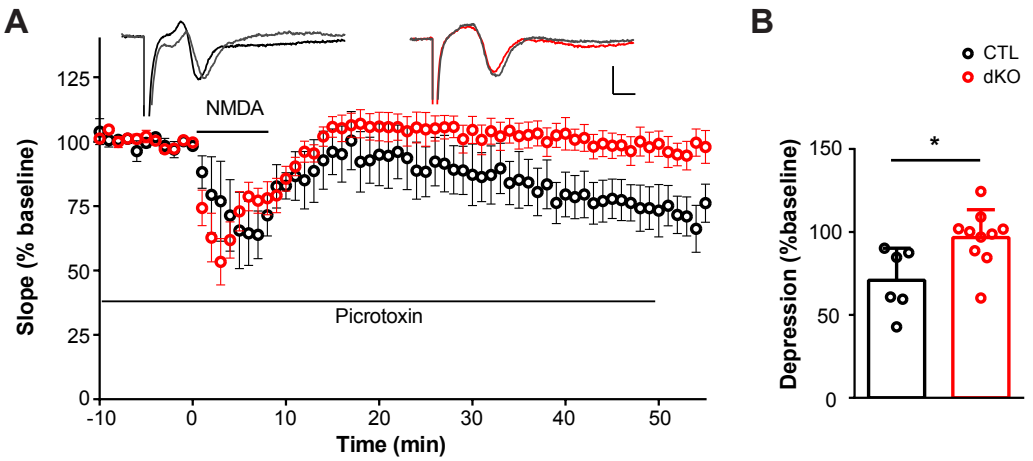

Figure 4.38 LTD induced by NMDA perfusion in hippocampus. A, Data from all slices from CTL and dKO mice showed changes in fEPSP slope before and after 25 μM NMDA perfusion for 7 min. The two inlet figures showed the responses from CTL (left) and dKO (right) mice before and after treatment. B, The percentages of depression showed that LTD was induced by NMDA perfusion in control mice but not in dKO mice.

slope fraction of the last five minutes of recordings from control mice (122.9 ± 8.2%, n=9 slices from 6 mice) was higher than in dKO mice (97.0 ± 6.8%, n=11 slices from 5 mice; *P<0.05, P=0.024) (Fig. 4.37B). Thereby, to elicit a robust depression, picrotoxin was employed in the bath, leading to a stable depression in controls after LFS(79.3 ± 2.9%, n=11 slices from 8 mice) (Fig. 4.37C). However, dKO mice were induced LTD after LFS (102.2 ± 4.5%, n=11 slices from 6 mice), significant different from controls (***P<0.001, P=0.0004) (Fig. 4.37D).

Another form of LTD was induced by NMDA perfusion, leading to a robust LTD lasting 50 min in controls (70.9 ± 7.9%, n=6 slices from 4 mice) (Fig. 4.38A). However, dKO mice failed to induce LTD after NMDA perfusion (96.6 ± 5.3%, n=10 slices from 4 mice), which was significantly different from controls (*P<0.05, P=0.014) (Fig. 4.38B). These data demonstrated that LTD can be successfully induced in controls by LFS and NMDA perfusion in the presence of picrotoxin. However, LFS- and NMDA-induced LTD was completely eliminated in dKO mice. This suggests that the neuronal network was disturbed after deleting Cav1.2 and Cav1.3 from NG2 glia.

To determine whether the LTD deficit from dKO mice was regional specific, we performed fEPSP recordings in layer II/III of the medial prefrontal cortex by stimulating the presynaptic axons in layer V in the presence of picrotoxin (Fig. 4.39A-B). LTD was also elicited in the mPFC of controls, which displayed a robust depression (77.2 ± 3.5%, n=12 slices from 7 mice) (Fig. 4.39C, D). The fEPSP slope of dKO mice declined immediately

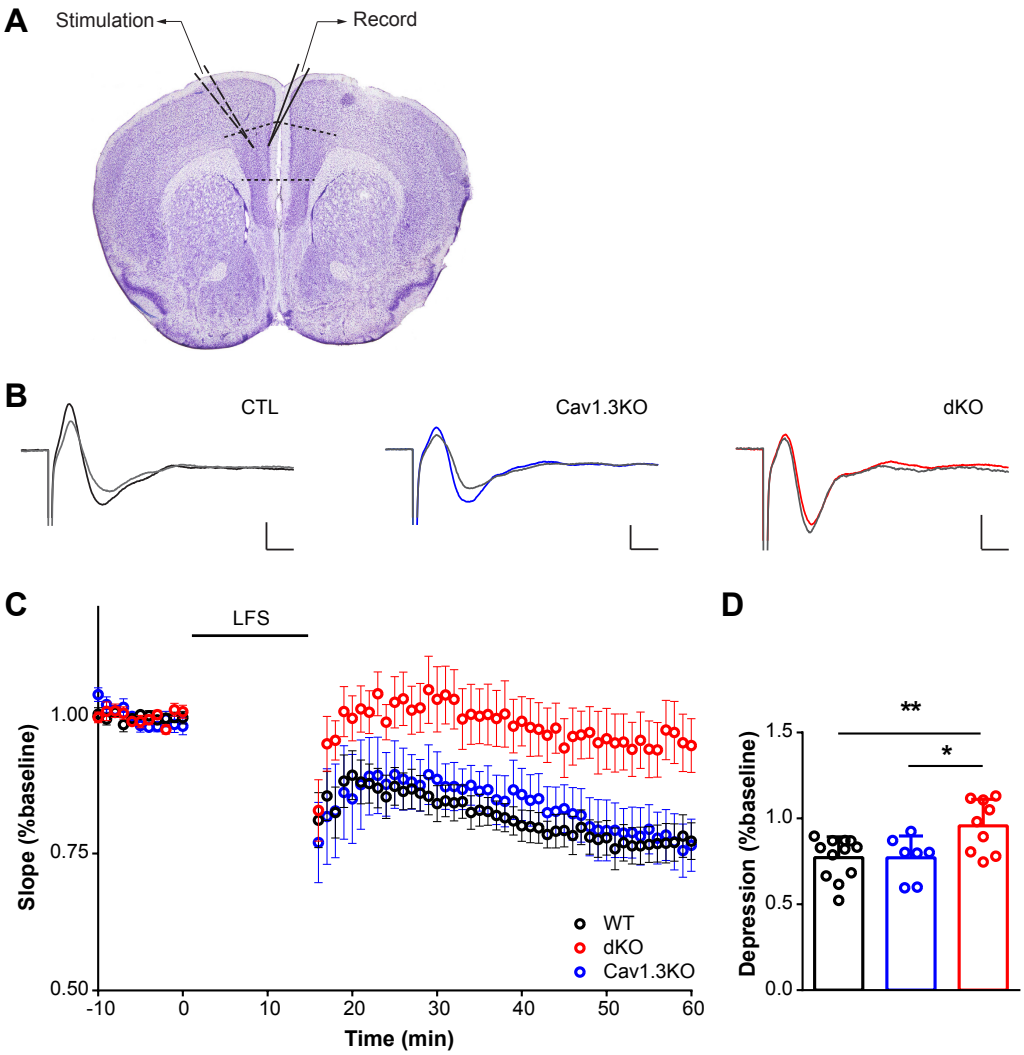

Figure 4.39 LTD induced by LFS in the medial prefrontal cortex. A, The postsynaptic responses were recorded in layer II/III of the medial prefrontal cortex by stimulating the presynaptic axons in layer V in the presence of picrotoxin. The slices with mPFC were collected from Bregma 2.34-1.78. B, Typical EPSPs from CTL (black), Cav1.3KO (blue) and dKO mice (red) before and after (gray) stimulation. Scale bar, x=2 ms, y=1 mV. C, Data from all slices among CTL (black, n=12 slices from 7 mice), Cav1.3 (blue, n=6 slices from 2 mice) and dKO (red, n=9 slices from 5 mice) showed changes in fEPSP slope as percentage of baseline before and after low frequency stimulation (1Hz for 15 min). D, The depression fraction of the tested three groups revealed that LTD was induced in the mPFC of CTL and Cav1.3 single knockout mice but not in dKO mice.

after LFS and then ascended to the baseline, with the average slope of the last five minutes of 95.7 $\pm$ 5.1% (n=9 slices from 5 mice), significant larger than controls (**P$<$0.01, P=0.006) (Fig. 4.39D). To further test the impact of Cav1.3 to the LTD deficit, we performed LTD recordings in Cav1.3 single knockout mice. We found that LTD could also

be elicited in Cav1.3 single knockout mice, which showed a stable depression (74.5 ± 4.8%, n=6 slices from 2 mice) after stimulation, consistent to controls (Fig. 4.39C, D), but different from dKO mice (*P<0.05, P=0.014) (Fig. 4.39D). Therefore, these data demonstrated that a robust depression could be elicited after LFS application in the mPFC of controls, while LTD failed to be elicited not only in the hippocampus but also in the medial prefrontal cortex of dKO mice. Further studies showed that conditional sinngle knockout of Cav1.3 in NG2 glia had no impact on the neuronal network. Taken together, these data suggest that the knockout of Cav1.2 and Cav1.3 in NG2 glia led to a disturbance in the neuronal network in a non-region dependent manner.

4.14 Vesicular release of NG2 glia

Recent transcriptome profiling studies have revealed that NG2 glia express a number of genes previously considered as neuron-specific genes (Nishiyama et al., 2016). A small portion of SNAP25$^+$ and synaptophysin$^+$ puncta were found in contact with NG2 glia membranes in the white matter (Kukley et al., 2007). Synaptophysin was also detected in NG2 glia, indicating they might be capable of releasing neurotransmitters and communicating with astrocytes and/or neurons (Hamilton et al., 2010). To confirm this observation, we performed FM1-43FX dye staining in acute brain slices, fixed the slices after depolarization with high K$^+$, and then stained them with NG2 antibody (Fuenzalida

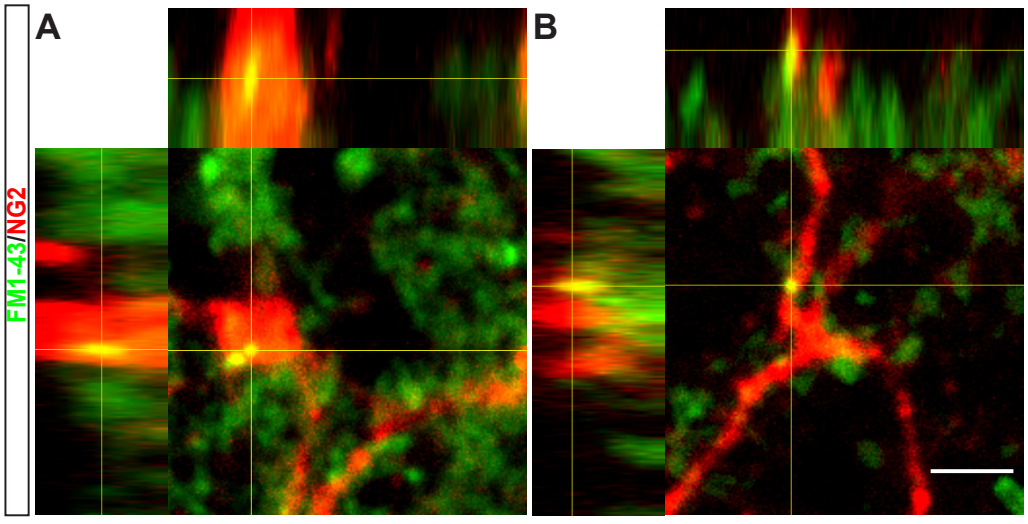

Figure 4.40 FM1-43 dye staining in NG2 glia. A-B, Orthogonal views of the co-localization between NG2 protein staining and FM1-43 dye in the processes of NG2 glia from wild type mice. Scale bar = 2 μm.

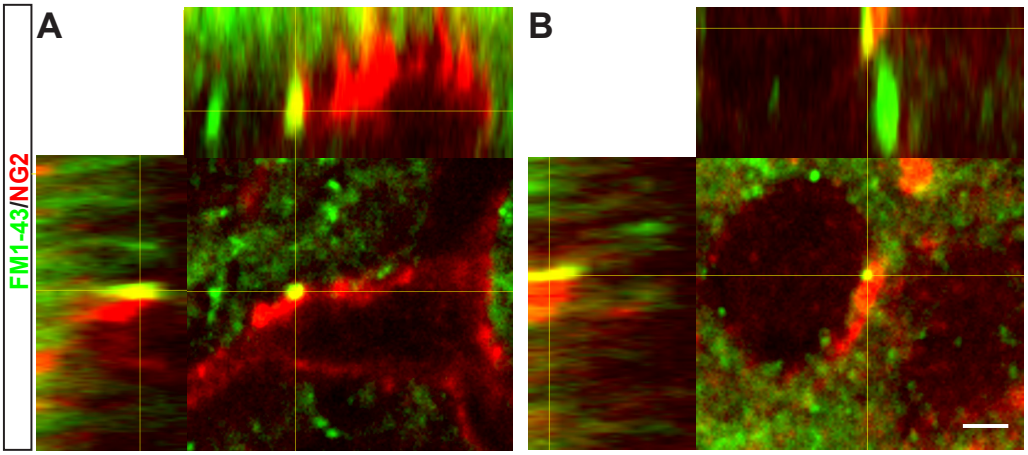

Figure 4.41 FM1-43 dye staining in Cav1.2/1.3 deficient NG2 glia . A, Orthogonal views of co-localization between NG2 protein staining and FM1-43 dye in the soma of Cav1.2/1.3 deficient NG2 glia. B, Orthogonal views in the process. Scale bar = 2 μm.

et al., 2011; Hirrlinger et al., 2004). The styryl dye FM1-43 is a powerful tool to track exocytosis, endocytosis and recycling of secretory granules or vesicles (Amaral et al., 2011). FM1-43$^+$ puncta were found in somata and processes of NG2 glia in control mice (Fig. 4.40), suggesting that NG2 glia have vesicles which could be released via the activation of VGCCs. In Cav1.2/1.3 deficient mice, FM1-43$^+$ puncta can still be seen in somata and processes of NG2 glia after the loss of L-type VGCCs in response to high extracellular K^+ (Fig. 4.41). No obvious difference in the quantity of FM1-43$^+$ vesicles could be found, however, the vesicle release from NG2 glia might be impaired. To further determine if transmitter release is impaired, live imaging has to be performed in acute brain slices with FM1-43 dye.

4.15 Cav1.2/1.3 knockout mice with anxiety-like behavioral abnormalities

Our previous data exhibited an inhibited NG2 glia proliferation in the cortex and shortened paired paranodes in the corpus callosum of Cav1.2/1.3 deficient mice. These evidence was also reported in chronically stressed mice with the onset of major depression disorder (MDD) (Czeh et al., 2007; Miyata et al., 2016). In addition, the complete ablation of NG2 glia in the PFC induces depressive-like behaviors in mice (Birey et al., 2015). All these evidence suggests that NG2 glia modulate the behavior of mice but the mechanism is still unknown. Previous studies showed that NMDAR-dependent LTD is required

for behavioral flexibility and might act by weakening previously encoded memory traces when new information is processed (Nicholls et al., 2008). Based on the LTP deficit, inhibited proliferation of NG2 glia and shortened paranodes in Cav1.2/1.3 knockout mice, we suspected that Cav1.2/1.3 knockout mice might show behavioral abnormalities.

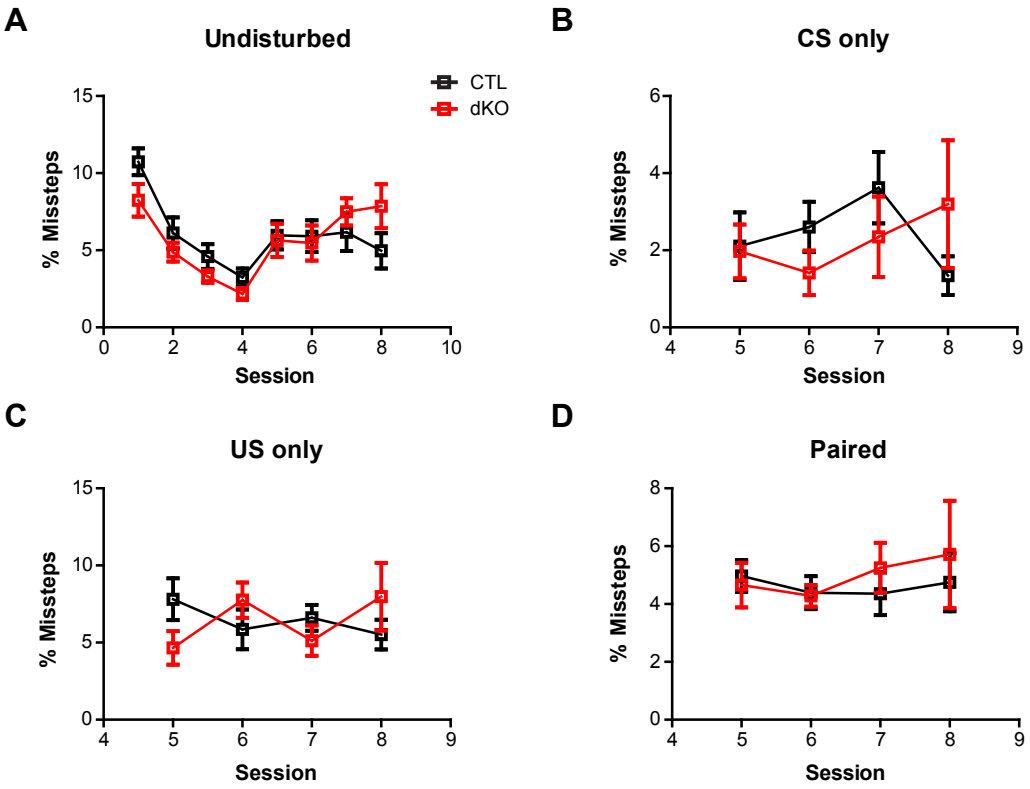

Figure 4.42 Cav1.2/1.3 deficient mice showed unaltered motor learning on the ladder. A-D, CTL and dKO mice generated similar percentage of missteps in undisturbed (A), CS only (B), US only (C) and paired (D) trials in each session. CTL, n=14 mice; dKO, n=10 mice.

We performed behavioral tests on the ErasmusLadder with male dKO mice and their littermate controls at 8∼12 weeks. On the ladder, if mice move their paws from one higher rung to a lower rung, one misstep is counted. Along with the training, both control and dKO mice learnt to walk on the ladder, therefore reduced the percentage of missteps (Fig. 4.42A). Hence, misstep is an important indicator for motor learning. During the training sessions, control and dKO mice did not show any difference of the percentage of missteps (Fig. 4.42A). After four days of training, tone (conditional stimuli, CS) and perturbation (unconditional stimuli, US) stimuli were introduced into the trials. When perturbation sessions started, both CTL and dKO mice increased the percentages of missteps due to the introduced stimuli. However, no difference was detected in all tested trials (undisturbed

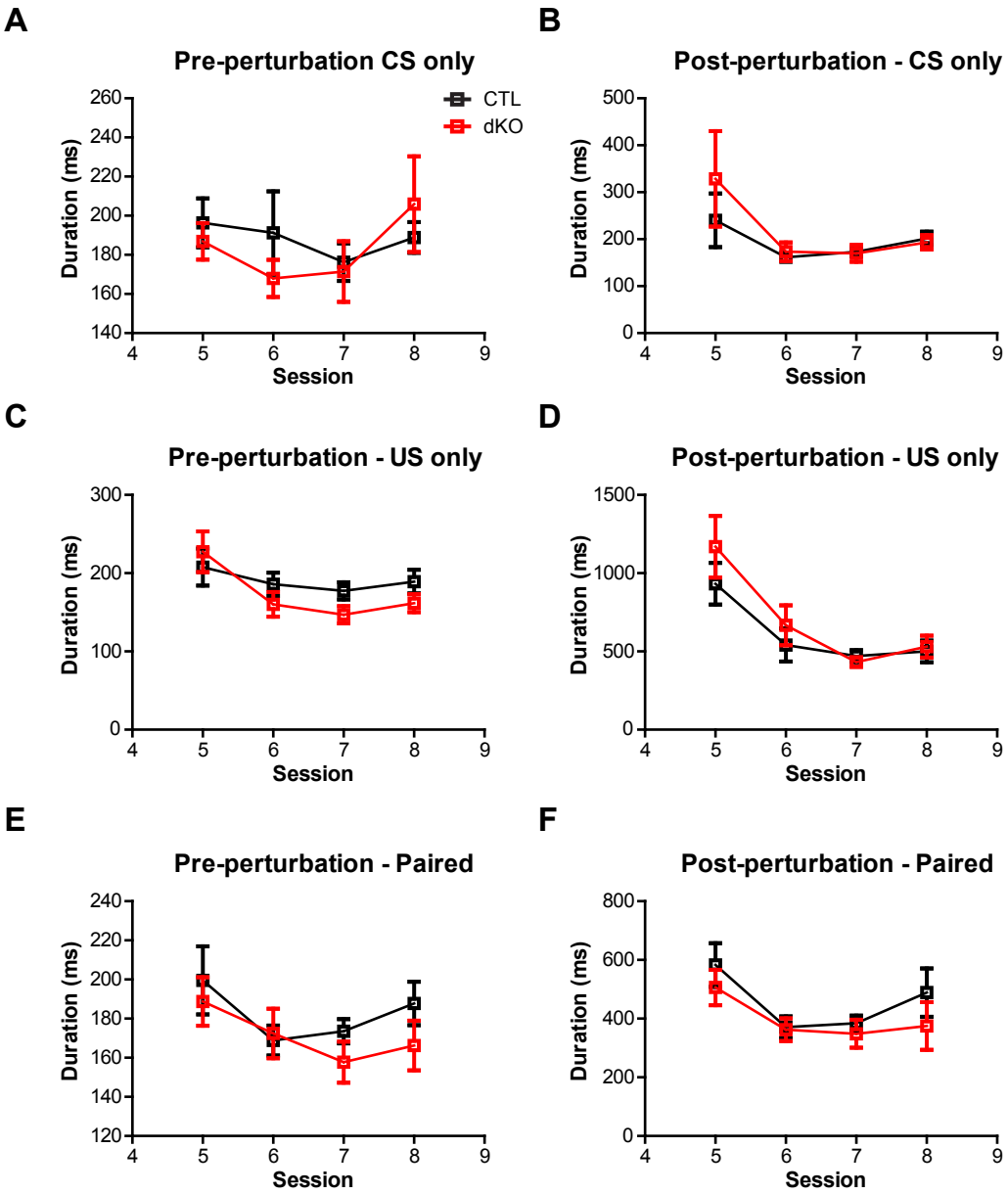

Figure 4.43 Cav1.2/1.3 deficient mice showed unaltered motor coordination. A-F, The duration of pre-perturbation and post-perturbation of CTL (black) and dKO (red) mice was recorded in trials of CS only (A, B), US only (C, D) and paired (E, F) with no significant difference. dKO mice reacted as fast as control mice when they encountered stimuli. CTL, n=14 mice; dKO, n=10 mice.

(Fig. 4.42A), CS only (Fig. 4.42B), US only (Fig. 4.42C) and paired (Fig. 4.42D)). These results demonstrated that motor learning of dKO mice was not affected by Cav1.2 and Cav1.3 deletion in NG2 glia.

When mice encountered stimuli, the duration of pre-perturbation and post-perturbation were both calculated by the system, indicating the time of the last step ends before (pre-

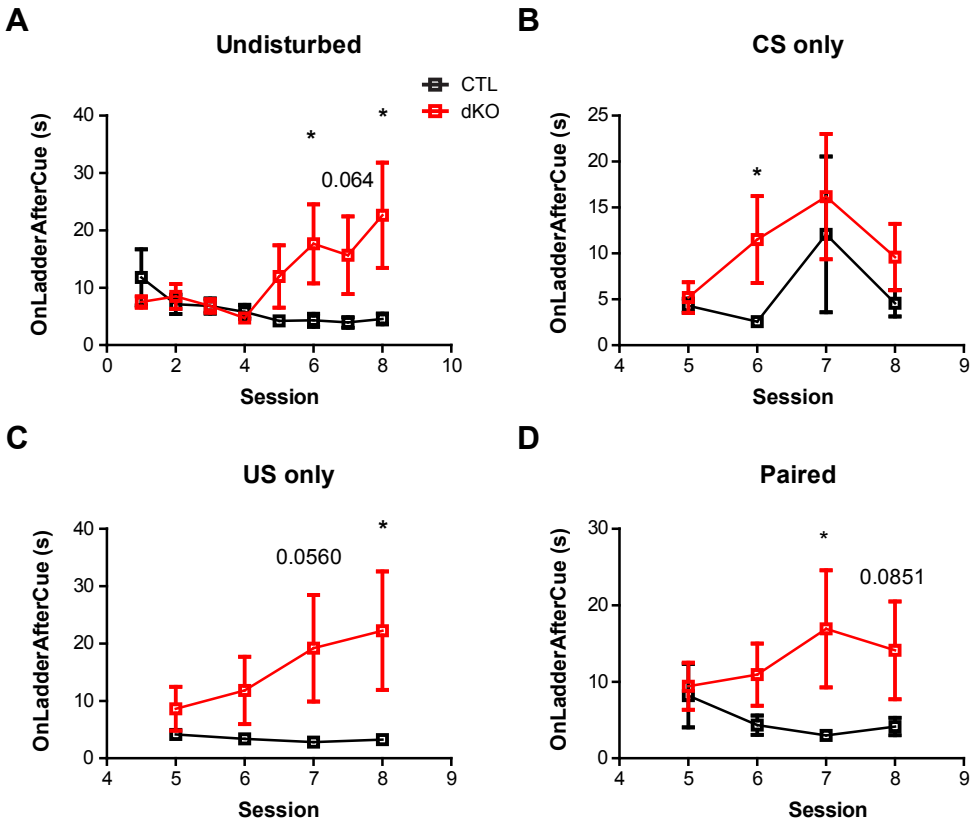

Figure 4.44 Cav1.2/1.3 deficient mice stayed longer on the ladder after cue. A-D, The time that mice spent on the ladder after cue was recorded. dKO mice took longer time on the ladder after cue than controls in undisturbed (A), CS only (B), US only (C) and paired (D) trials in each session. CTL, n=14 mice; dKO, n=10 mice. *P$<$0.05.

perturbation) and after (post-perturbation) the calculated obstacle rung as the same side. These two parameters were used to evaluate motor coordination. The dKO mice displayed similar reaction time as controls, as indicated by durations of pre-perturbation and post-perturbation in trials of CS only (Fig. 4.43A, B), US only (Fig. 4.43C, D) and paired (Fig. 4.43E, F). These results indicated that motor coordination of dKO mice was not affected by Cav1.2 and Cav1.3 deletion in NG2 glia.

However, in this experiment, we noticed that dKO mice showed more stress and anxiety-related behavior compared to control mice in the perturbation sessions. For example, after encountering several stimuli, most dKO mice showed refusal to enter the ladder immediately after cue. Some dKO mice even exhibited freezing behavior on the ladder. They walked slower and irregularly so that the stimuli could not be triggered. Consequently, dKO mice generated more undisturbed trials (appendix Fig. 7.1, 7.2). Therefore, we calculated the total time mice spent on the ladder after cue (detailed step

types on the ladder shown in appendix Fig. 7.3, 7.4, 7.5, 7.6, 7.7). Indeed, dKO mice stayed longer on the ladder after cue in the perturbation sessions than control mice in all trails (undisturbed (Fig. 4.44A), CS only (Fig. 4.44B), US only (Fig. 4.44C) and paired (Fig. 4.44D)). Altogether it implicates that the knockout of Cav1.2 and Cav1.3 in NG2 glia resulted in alterations of anxiety-related behavior after stimuli challenge, rather than motor behavior changes.

Chapter 5

Discussion

In this study, we have shown the expression of voltage-gated Ca^{2+} channels (VGCCs) in NG2 glia in different brain regions during the development, and the successful deletion using a tamoxifen inducible CreERT2 system. The conditional double knockout (dKO) of Cav1.2 and Cav1.3 in NG2 glia led to reduced but not diminished Ca^{2+} signaling in NG2 glia, indicating the potential upregulation of T-type Ca^{2+} channels. In dKO mice, cortical proliferation of NG2 glia was significantly inhibited, while their differentiation and myelination was not disturbed. In addition, Cav1.2/1.3 deficient NG2 glia had an overall changed morphology with less branched fine processes, probably due to the upregulated expression level of α-Tubulin. Furthermore, the length of paired paranodes in corpus callosum of dKO mice was shortened but the axon conduction velocity was not affected. We also found that NMDA-dependent long term depression (LTD) was not able to be elicited in the hippocampus and medial prefrontal cortex of dKO mice, however, the synaptic input from axons to NG2 glia remained unaltered. Behavioral analysis highlighted that Cav1.2/1.3 deficient mice displayed an anxiety-like disorder, although their overall motor behavior was not affected.

Two populations of NG2 glia, complex and passive as previously described in the hippocampus, were also found in the cortex. Both complex and passive NG2 glia in young mice ($<$ P16) displayed a comparable quantity, but the complex subpopulation decreased their number in wild type mice with increasing age.

5.1 Conditional inactivation of Cav1.2 and Cav1.3 specifically in NG2 glia

Our preliminary data showed that cortical NG2 glia exhibited inward currents upon depolarization *ex-vivo* in the presence of voltage-gated K^+ channel blockers 4-AP (Table 3.1), TEA, internal Cs^+ and fast Na^+ channel blocker TTX (Table 3.1) when extracellular [Ca^{2+}] was increased to 5 mM. The current-voltage curves of NG2 glia displayed a V shape and their peak currents appeared at about 0 mV. These inward currents were mostly inhibited by the L-type VGCC blocker Nimodipine, while only slightly by the T-type VGCC blocker Mibefradil, suggesting that L-type VGCCs were predominantly expressed in NG2 glia. Moreover, the expression of VGCCs in NG2 glia are non-specific region-dependent during the development but age-dependent. Hence, following questions were raised: What are the functions of L-type Ca^{2+} channels in NG2 glia and what is the underlying mechanism? To answer these questions, we deleted Cav1.2 and Cav1.3 specially from NG2 glia by crossbreeding homozygous floxed Cav1.2 (Moosmang et al., 2005, 2003) and flexed Cav1.3 (Satheesh et al., 2012) to NG2-CreERT2 knock-in mice (Huang et al., 2014).

Cav1.2 and Cav1.3 were successfully deleted from NG2 glia in neonatal and adolescent mice, when tamoxifen was administered at three different developmental time points. Ca^{2+} currents of cortical NG2 glia were significantly reduced in Cav1.2/1.3 deficient mice (P7 + 3 weeks and P21 + 7 weeks). However, T-type VGCCs could be upregulated subsequently after the complete ablation of the L-type Ca^{2+} channel isoforms Cav1.2 and Cav1.3. When the conditional knockout was induced at P21, the peak currents at 0 mV were completely reduced while another peak current appeared at -40 mV, indicating T-type VGCC involvement (Poetschke et al., 2015).

However, when the conditional knockout was induced in 4-5 weeks old mice, Ca^{2+} currents could still be detected in NG2 glia, inhibited by Nimodipine. It was published before that membrane-bound proteins can have a long half life (Hare and Taylor, 1991; Saab et al., 2012). Ablation of membrane proteins exhibits a degradation kinetic increasing with age by Western blot and immunohistochemistry analysis, despite DNA recombination occurring within the first 8h after induction (Saab et al., 2012). Therefore, the time window between induction of gene deletion and analysis might be not long enough for cleavage of Cav1.2 and Cav1.3 proteins in NG2 glia.

In addition, the expression level of the endogenous NG2 protein also displays a dynamic fluctuation. During the first postnatal week, both the density and the number of $NG2^+$ cells increased, reaching a maximum at the second postnatal week and declining

in the number thereafter (Butt et al., 2002; Levine et al., 1993; Nishiyama et al., 1996). Immunohistochemical analysis revealed that the level of NG2 and PDGFRα was greatly reduced in the corpus callosum and cortex of P30 mice (Nishiyama et al., 1996). Northern blot analysis showed that NG2 mRNA can be detected at E15 and then gradually increases its density during development. The highest levels of expression of mRNA encoding NG2 are seen between P3 and P7, after which the levels decline, but the transcripts continue to be detected in the adult brain. Although compared to the maximal expression at P7, NG2 mRNA is markedly weak at P37 and adult mice (Nishiyama et al., 1996). Therefore, with slow degradation of Cav1.2 and Cav1.3 proteins as well as reduced NG2 promotor activity in adult mice, late tamoxifen administration (in 4-5 weeks old mice) might require a larger time window to delete Cav1.2 and Cav1.3 from NG2 glia.

5.2 Reduced proliferation and no changes in differentiation in Cav1.2/1.3 deficient NG2 glia

In vitro studies have shown that L-type VGCCs are playing crucial roles in OPC development (Cheli et al., 2015; Paez et al., 2012, 2009a,b). In Cav1.2/1.3 deficient mice, the dividing NG2 glia in the cortex were reduced as compared to controls, which was in line with recently published data (Cheli et al., 2016). The decreased number of dividing cells was not due to cell death. The cell density of NG2 glia in the corpus callosum and cortex did not differ between dKO and control mice. Furthermore, caspase 3 staining also showed no difference in the number of apoptotic cells between CTL and dKO mice (data not shown). Therefore, Cav1.2/1.3 deficient NG2 glia might have a reduced rate of cell division in the cortex or a prolonged cell cycle. However, in the corpus callosum, a similar percentage of proliferating NG2 glia was observed in both CTL and dKO mice at 10 weeks. The proliferation properties of NG2 glia have shown regional differences (Dimou and Gallo, 2015; Hill et al., 2014; Vigano et al., 2013). Although almost all NG2 glia are dividing in both white and gray matter in an age-dependent manner during development, cumulative BrdU or EdU-labeling in mice revealed that NG2 glia in white matter display a much shorter cell cycle length compared to gray matter cells (2.7 days vs 18.6 days at postnatal day P21 and 9.5 d vs 36.3 d at P60 in corpus callosum and cortex respectively) (Clarke et al., 2012; Dimou and Gallo, 2015; Kang et al., 2010; Simon et al., 2011; Young et al., 2013). Therefore, Cav1.2 and 1.3 might also variously regulate NG2 glial proliferation in different brain regions.

However, Cav1.2/1.3 deficient mice did not show any change in differentiation, in

terms of mature OLs numbers, compared to controls. This result is contrary to the recently published work claiming that the conditional single knockout of Cav1.2 led to decreased differentiation of NG2 glia *in vivo* (Cheli et al., 2016). Double knockout of Cav1.2 and Cav1.3 in NG2 glia led to up-regulation of T-type Ca^{2+} channels, which might be not seen in single knockout of Cav1.2. Eventually, T-type Ca^{2+} channels might compensate the lost function of L-type VGCCs on cell differentiation. Another possibility is that the different CreERT2 driver lines (Huang et al., 2014; Zhu et al., 2008a) might influence cell type specific recombination.

NG2 glia are mainly generated from the dorsal and not the lateral wall of the ventricle (Ortega et al., 2013). Independently from their origin, NG2 glia can migrate from the subventricular zone (SVZ) into white matter, where they undergo extensive proliferation before they terminally differentiate into myelinating OLs (Dimou and Gallo, 2015). It has been shown that about 80% of OL lineage cells in the postnatal corpus callosum are generated locally in the cortical ventricular zone (VZ), the remaining 20% migrating in from the ventral forebrain, while the gray matter of the cerebral cortex almost entirely consists of dorsally derived cells (Tripathi et al., 2011). When ventrally or dorsally derived OL populations were separately ablated by targeted expression of diphtheria toxin, OLs were compensated by the surviving cells migration to fill up the space (Kessaris et al., 2006). Hence, the loss of OLs in the corpus callosum of dKO mice might be compensated by newly migrated cells from other brain regions, such as SVZ, resulting in unchanged OLs numbers. However, in the cortex, the NG2 glia population is mostly maintained by local proliferation of existing NG2 cells (Hill et al., 2014; Hughes et al., 2013). No recombined OLs can be detected in the cortex of Nestin-CreER transgenic mice when tamoxifen was injected at P10 and analyzed at P30 (Naruse et al., 2016), showing that only few NG2 glia migrate out of the ventricular zone (VZ)/ subventricular zone (SVZ) to the cerebral cortex and differentiate to OLs after birth. Therefore, the cortical population of NG2 glia is not affected by any foreign NG2 glia, contrary to that in the corpus callosum.

5.3 Myelination was not affected by knockout of Cav1.2/1.3 in NG2 glia

The known main function of NG2 glia is to differentiate into OLs in gray and white matter throughout the life span (Huang et al., 2014; Kang et al., 2010; Zhu et al., 2008a). OLs form myelin wrapping around the axons, which is essential for the rapid propagation of action potentials (Bercury and Macklin, 2015). In Cav1.2/1.3 deficient mice, myelination

was not impaired in different white matter regions including corpus callosum, spinal cord and optic nerve. Western blot analysis revealed no significant differences in the expression of myelin proteins, MBP (Myelin basic protein), PLP (Proteolipid protein) and MOG (Myelin oligodendrocyte glycoprotein) in corpus callosum and cortex between CTL and dKO mice. However, we observed that the length of paired paranodes was shortened in the corpus callosum of dKO mice but not in the spinal cord and optic nerve. The callosal conduction velocity of axons was not altered in dKO mice. Our results are contrary to a recently published work showing that the loss of Cav1.2 remarkably inhibited myelination in the corpus callosum at an earlier postnatal stage by conditional knockout of Cav1.2 specifically in NG2 glia (Cheli et al., 2016). L-type VGCCs might be only involved in the initiation of myelination (Kirischuk et al., 1995) but do not influence compacted myelin. However, we did not observe any change of myelination in dKO mice (P7 + 23 days and P7 + 9 weeks) in terms of MBP and MOG immunostaining (data not shown) as well as biochemical analysis. This apparent contradiction might be due to the different genetic background of used mice for gene deletion (Huang et al., 2014; Zhu et al., 2008a). In the published studies, they deleted Cav1.2 from NG2 glia in C57BL/6J mice which is a substrain of C57BL/6. These mice show their own specific characteristics and different behavior from our C57BL/6N (Bryant et al., 2008; Mekada et al., 2009). Another possibility could be that the upregulated T-type VGCCs compensate the lost function of L-type VGCCs in our dKO mice. Therefore, myelination impairment could not be detectable in our dKO mice.

But not all white matter structures in the CNS were affected equally. We could not observe similar phenotypes in other myelin concentrated regions (spinal cord and optic nerve). The myelination of the spinal cord and optic nerve occurs early in development (Foran and Peterson, 1992). NG2-positive OPCs in the spinal cord, first appear in highly restricted regions of the ventral neuroepithelium around embryonic day 12.5 (Lu et al., 2002; Woodruff et al., 2001). In the optic nerve, at embryonic day 18, it has been reported that NG2 immunoreactivity within the posterior optic chiasm is associated with cells scattered at the midline and other cells lying dorsal and lateral to the diverging optic tracts (Chen et al., 2002). Therefore, we presumed that the timing of our tamoxifen treatments was too late to reveal a role for L-VGCCs in these NG2 glia.

5.4 Ablation of Cav1.2 and Cav1.3 impaired the cytoskeleton network

NG2 glia elaborate numerous, highly branched processes and make contact with surrounding axons (Bergles et al., 2010; Dawson et al., 2003), but the factors governing their process extension are unknown. Unexpectedly, Western blot analysis showed that α-Tubulin expression in the corpus callosum of dKO mice was remarkably enhanced compared to controls while nothing was changed in the cerebral cortex. Our data suggests that the deletion of Cav1.2 and Cav1.3 genes disturbed the microtubule cytoskeleton. Sholl analysis and binary analysis data demonstrated that Cav1.2/1.3 deficient NG2 glia lost some fine processes and exhibited less complex morphology.

Associations with cytoskeletal proteins play a central role in regulating the number and function of VGCCs in the plasma membrane (Gandini and Felix, 2015; Johnson and Byerly, 1993). Tubulin polymers, or microtubules, along with actin microfilaments and intermediate filaments, make up the cytoskeletal framework, which provides structure and dynamics to cells (Marchisella et al., 2016). The organization and filamentous state of these proteins provide the cell with a network of structures that are highly dynamic and stable and essential for cellular processes such as cellular morphology, adhesion, motility or intracellular trafficking (Gandini and Felix, 2015). Microtubules are hollow tubular rods, polymerized from tubulin dimers by α and β heterodimers. Their assembly process is coupled to GTP cleavage, the polymerized form containing bound GDP. Ca^{2+} ions cause microtubule depolymerization probably via promoting hydrolysis of GTP to GDP or inactivating of free GTP-tubulin subunit by binding to it (O'Brien et al., 1997). A number of accessory proteins (MAPs-microtubule associated proteins) are also found in microtubules with important roles in the assembly process and the stabilization of microtubules (Bennett and Weeds, 1986). Ca^{2+} ions flowing along the microtubule can be utilized by MAP2 molecules (Sataric et al., 2015). In addition, α-actinin stabilizes Cav1.2 at the plasma membrane and its displacement by Ca^{2+}-calmodulin triggers Ca^{2+}-induced endocytosis of Cav1.2 in neurons, thus, providing an important negative feedback mechanism for Ca^{2+} influx (Hall et al., 2013). The interaction with calmodulin and MAP-2B is regulated by Ca^{2+} ions, which could also be supplied by localized pulses conveyed by actin filaments as polyelectrolytes (Todorov et al., 2001). CNS myelin wrapping is driven by actin disassembly and subsequent myelin wrapping coincides with the upregulation of actin disassembly proteins and rapid disassembly of the oligodendrocyte actin cytoskeleton (Zuchero et al., 2015). Our Ca^{2+} imaging data showed that Ca^{2+} elevations were

significantly reduced upon depolarization in Cav1.2/1.3 deficient NG2 glia. Therefore, $[Ca^{2+}]_i$ fluctuation induced by the knockout of L-type VGCC isoforms in NG2 glia might disturb the depolymerization of microtubules and cause increased the expression level of α-tubulin, eventually leading to the changes of NG2 glia morphology as well as callosal myelinated structures.

5.5 The neuronal network was strongly influenced in Cav1.2 and Cav1.3 knockout mice

Morphological and physiological interaction between NG2 glia, astrocytes and neurons, such as extension of glutamatergic synapses onto NG2 glia in the hippocampus (Bergles et al., 2000), are well described (Wigley et al., 2007). NG2 glia play important roles in maintaining CNS homeostasis by mediating astrocytic glutamate uptake and neuronal glutamatergic signaling, partially through secreted factors, like fibroblast growth factor 2 (FGF2) (Birey et al., 2015). Neuron to NG2 glia communication has been often studied. NG2 glia can receive synaptic input from both excitatory and inhibitory neurons in the gray matter. In white matter NG2 glia receive the excitatory synaptic input from axon collaterals, but lose their synaptic input when they differentiate into oligodendrocytes with a decrease in glutamate receptor expression (De Biase et al., 2010; Dimou and Gallo, 2015; Kukley et al., 2007, 2010). Our data showed that deletion of Cav1.2 and Cav1.3 genes did not alter the EPSC amplitudes of NG2 glia and its components, which were still predominantly mediated by Ca^{2+} permeable AMPA receptors, consistent with previous studies (Ge et al., 2006). NG2 glia also continue to receive AMPAR-mediated synaptic inputs in conditional NR1 knockout mice (De Biase et al., 2011). Therefore L-type VGCC isoforms Cav1.2 and Cav1.3 as well as NMDA receptors are not required for synaptic communication between neurons and NG2 glia. In addition, neuron-NG2 glia synapses also formed even in the absence of the NG2 protein. Short-term plasticity, synaptic connectivity, postsynaptic AMPAR current kinetics, and density were not affected by NG2 deletion (Passlick et al., 2016). Neuron-glia synapses undergo activity-dependent modifications analogous to long-term potentiation (LTP) at excitatory synapses, a hallmark of neuronal plasticity (Ge et al., 2006). Induction and expression of LTP at neuron-NG2 synapses involve Ca^{2+}-permeable AMPA receptors on NG2 glia in the CA1 region of the hippocampus.

Not only neuron to NG2 glia but also NG2 glia to neuron communication has been reported. Pharmacological inhibition of NG2 or genetic ablation of NG2 protein results

in striking reduction in NMDA receptor dependent LTP in pyramidal neurons of the somatosensory cortex and diminished NMDA and AMPA receptor-dependent current amplitudes in these neurons (Sakry et al., 2014). It demonstrates for the first time a bidirectional cross-talk between OPCs and the surrounding neuronal network and a novel physiological role of NG2 glia in regulating information processing at neuronal synapses. In Cav1.2/1.3 deficient mice, LTD failed to be elicited by LFS and NMDA perfusion in a non-region dependent manner. LTD induced by LFS leads to a modest activation of NMDA receptors and subsequently to an slight increase in postsynaptic Ca^{2+} influx (Luscher and Malenka, 2012). NMDA transiently abolishes synaptic responses by a depolarization of neurons, followed by recovery and relaxation to a stable depressed response, compared to the relative initial baseline value (Lee et al., 1998). Therefore, in our dKO mice, NMDA receptors of postsynaptic neurons in the hippocampus and mPFC might be impaired under the loss of NG2 glial L-type VGCC activation.

A triad of brain regions, including the PFC, hippocampus, and amygdala, form an essential brain circuit involved in fear conditioning and extinction. Within this circuit, the PFC is thought to exert top-down control over subcortical structures to regulate appropriate behavioral responses (Giustino and Maren, 2015). Whereas numerous evidences convincingly demonstrate a role of mPFC in fear or anxiety, electrophysiology is correlative (Arruda-Carvalho and Clem, 2014; Bi et al., 2013; Giustino et al., 2016; Herry and Garcia, 2003; Sui et al., 2008). Therefore, the LTD deficit in dKO mice results in chaos of CNS homeostasis, which might eventually lead to mood disorders.

5.6 Anxiety-like behavior in Cav1.2/1.3 deficient mice after several stimulation

NG2 glia are considered as a critical mediator which modulate CNS homeostasis as well as behavior. Loss of NG2 protein induces LTP reduction in cortical pyramidal neurons and the impairment of sensorimotor gating in mice (Sakry et al., 2014). Ablation of NG2 glia causes deficits in the excitatory glutamatergic synaptic transmission in the PFC of adult brain which results in depressive-like behaviors (Birey et al., 2015). Our electrophysiological data also pointed out NMDA receptor dependent LTD deficits in the hippocampus and mPFC, which might predispose to mood disorders in Cav1.2/1.3 deficient mice. The behavioral tests on the ErasmusLadder have shown that Cav1.2/1.3 deficient mice displayed anxiety-like disorders, while their motor learning and motor coordination were not influenced by the knockout of Cav1.2 and Cav1.3. Although the ErasmusLadder is gen-

erally used to evaluate motor learning and motor performance capabilities of mice in a noninvasive manner (Cupido, 2009; Saab et al., 2012; Schonewille et al., 2011). After four days of training, both control and dKO mice learned to leave the goal box and run over the ladder, indicated as decreased percentages of missteps. They ran on the ladder more confidently and freely as indicated by the reduced number of short steps and increased number of long steps. In perturbation sessions, dKO mice showed similar numbers of missteps to controls and reacted as fast as controls when they encountered stimuli. All these data suggest that dKO mice had no disturbed motor learning and motor coordination. However, dKO mice moved slower and spent more time on the ladder than controls, especially in undisturbed trials, after the start of perturbation sessions. Altogether, dKO mice displayed obviously no motoric behavior phenotype but showed enhanced anxiety, stress and fear-like behavior after several stimulation in line with the electrophysiological data. To further confirm this finding, other behavioral tests relative to mood disorders like fear-conditioning have to be performed.

However, the underlying mechanism is still unknown. NG2 glia-derived FGF2 remains as a factor that plays a crucial role in the emergence of depressive phenotypes in the NG2 glia ablation and social defeat models due to FGF2 stimulation can increase GLAST levels, glutamate uptake and phosphorylation of GluR (Birey et al., 2015). FGF2 has been found at low levels in major depression disorder and can rescue depressive-like behaviors in chronic stress models (Elsayed et al., 2012; Perez et al., 2009), suggesting FGF2 as a key factor in the pathophysiology of mood disorders. It is known that the activity of voltage-gated Ca^{2+} channels can be finely regulated by neurotransmitters and growth factors (Bean, 1989b; Squecco et al., 2016; Wu et al., 2002). The chronical treatment with BDNF (Brain Derived Neurotrophic Factor) and FGF2 neurotrophins definitely affected the voltage-gated Ca^{2+} current occurrence, likely ascribable to a sustained TrkB (Tropomyosin receptor kinase B) activation (Squecco et al., 2016). All these clues imply that the knockout of L-type VGCCs in NG2 glia might cause FGF2 fluctuation in the brain, consequently results in anxiety-like behavior deficits. However, whether the deletion of Cav1.2 and Cav1.3 induces the impairment of FGF2 secretion from NG2 glia should be further investigated.

5.7 Hypothetical functions of VGCCs in NG2 glia.

Recent transcriptomic profiling studies have revealed that NG2 glia express a number of genes previously considered as neuron-specific genes (Nishiyama et al., 2016). Notably,

SNARE proteins (soluble Nethylmaleimide-sensitive factor attachment receptor), SNAP-25, Synaptophysin and Synaptotagmin 1 have been detected in NG2 glia (Hamilton et al., 2010; Kukley et al., 2007). SNARE proteins mediate fusion of the vesicular and plasma membrane and are also involved in all trafficking steps of the secretory pathway, including neurotransmission (Palfreyman M.T., 2008). In the current study, we found that FM1-43 positive vesicles were detected in the somata and processes of NG2 glia upon membrane depolarization with high extracellular K^+. Futhermore, Ca^{2+}-dependent secretion of neuroactive factors from NG2 glia would allow rapid feedback regulation of neuronal functions with an increase in strength after the induction of potentiation, which was termed as glial LTP (Ge et al., 2006).

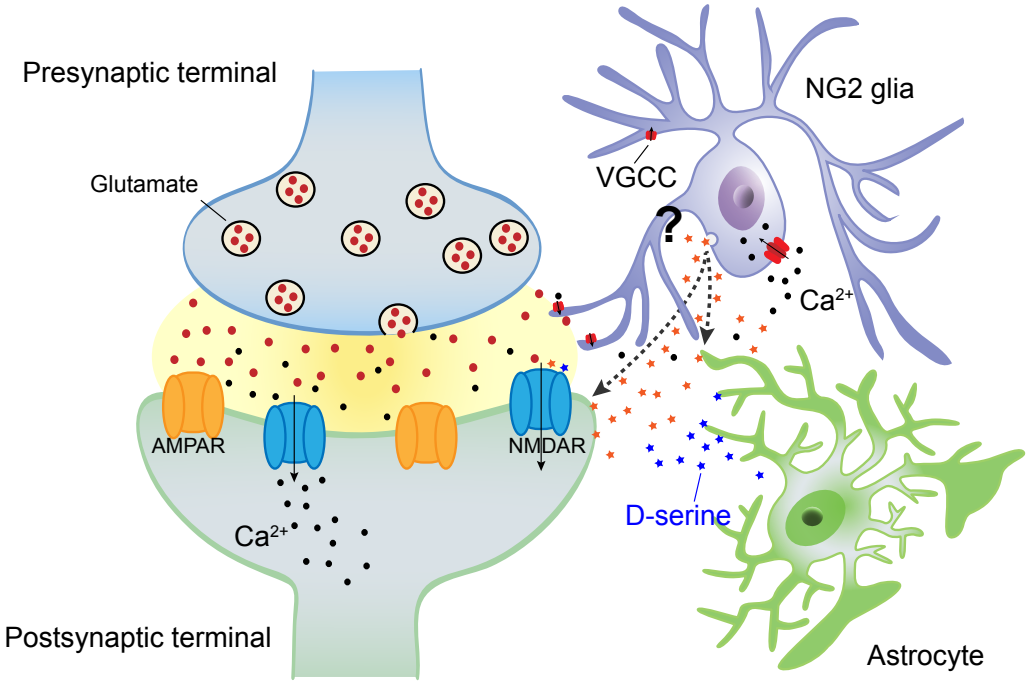

Figure 5.1 Hypothetical functions of VGCCs in NG2 glia. Upon activation of L-type VGCCs, NG2 glia could release neuromodulators or secrete neurotrophins and subsequently can communicate with neurons or other glial cells, e.g., astrocytes, and finally modulate CNS homeostasis.

Considering all these clues, we therefore hypothesize that NG2 glia release neuromodulators and thus communicate with neurons or astrocytes, which affect CNS homeostasis and animal behavior. The release of these potential neuromodulators is triggered by the activation of L-type VGCCs (Fig.5.1). In Cav1.2/1.3 deficient mice, no obvious difference in the quantity of FM1-43 positive vesicles could be found, but the vesicular release from NG2 glia might be impaired. That could explain why LTD were not elicited in

the mPFC and the hippocampus of Cav1.2 and Cav1.3 knockout mice and that these mice displayed anxiety-like disorders after given challenges. The knockout of L-type VGCCs in NG2 glia could prevent Ca^{2+} induced release of neuromodulators which will be further confirmed by live imaging in acutely isolated brain slices.

What NG2 glia release, how this process is initialized and how these factors modulate CNS homeostasis, however, are still open questions. It has been reported that NG2 glia can secrete FGF2, NGF (Nerve Growth Factor), IGF-1 (Insulin-like growth factor 1) and TGF (Transforming Growth Factor) (Birey et al., 2015; Butt et al., 2002; Hinks and Franklin, 1999). As a key factor, for example, astrocyte-secreted ATP is involved in astrocytic modulation of depressive-like behavior in adult mice by genetically blocking the release of astrocytic ATP (Cao et al., 2013). Similarly, astrocytic TNFα has been causally linked to hippocampus-mediated long-term memory (Han et al., 2013). The emergence of anxiety-like behaviors following ablation of L-type VGCC isoforms Cav1.2 and Cav1.3 in NG2 glia identifies a homeostatic loss of functions in the adult CNS. In line with this idea, next we ought to identify the potential factors released by NG2 glia that the release might be impaired by the loss of Cav1.2 and Cav1.3 proteins in NG2 glia while ultimately contributing to the maladaptive behaviors.

Chapter 6

Outlook

Our work has shown that voltage-gated Ca^{2+} channels are expressed in NG2 glia in gray and white matter in the mouse forebrain during CNS development. By crossbreeding floxed Cav1.2 and flexed Cav1.3 transgenic mice with NG2-CreERT2 knockin mice, Cav1.2 and Cav1.3 genes can be deleted specifically in NG2-expressing cells in the CNS after tamoxifen administration. Therefore, this triple transgenic mouse line is a powerful tool to investigate the functions of L-type VGCCs in NG2 glia during development.

Here we observed the phenotypes in proliferation, morphology, electrophysiology and mouse behavior in Cav1.2/1.3 deficient mice, however we cannot conclude these phenotypes are induced by Cav1.2 or Cav1.3 knockout so far. Hence, it is necessary to generate the single Cav1.2 and Cav1.3 conditional knockout mice for further studies.

Our Western blot analysis did not show any differences in the expression of β-actin or any of the tubulin and actin related proteins. Due to the morphological changes of NG2 glia occurring in dKO mice, it would be interesting to analyze these proteins on a biochemical level. However, sorting of NG2 glia by magnetic-activated cell sorting (MACS) is necessary because of high expression in the other neural cells . Here we also would like to investigate which genes are up- and down-regulated under the knockout of L-type VGCCs by RNA sequencing of sorted NG2 glia.

The behavioral results on the ErasmusLadder suggests that dKO mice showed mood disorders like stress, anxiety and fear after given challenges. However they still perform as well as control mice on motor learning and motor coordination. To confirm the anxiety phenotype, other behavioral tests exposing more details about mood disorders like fear conditioning, elevated plus maze, light-dark box and open field combined with an acute stress sensor should be investigated (Birey et al., 2015; Bourin and Hascoet, 2003; Martinowich et al., 2012).

Our hypothesis is that NG2 glia could release neuromodulators regulating neuronal activities and subsequently mouse behavior, triggered by the activation of L-type VGCCs. After deleting Cav1.2 and Cav1.3, the Ca^{2+} induced release might be impaired, and then leading to LTP deficiency in mPFC and hippocampus, and mood disorders afterwards. Therefore the released modulators should be identified to rescue the deficient LTD and abnormal behavior in Ca1.2/1.3 knockout mice. For this, we also have to appeal to RNAseq profiling.

Chapter 7

Appendix

7.1 Cav1.2/1.3 deficient mice behaved anxiety-like disorders

Our behavior results (context Fig. 4.44) showed that dKO mice moved slower on the ladder than control mice after perturbation session started. The system is designed that

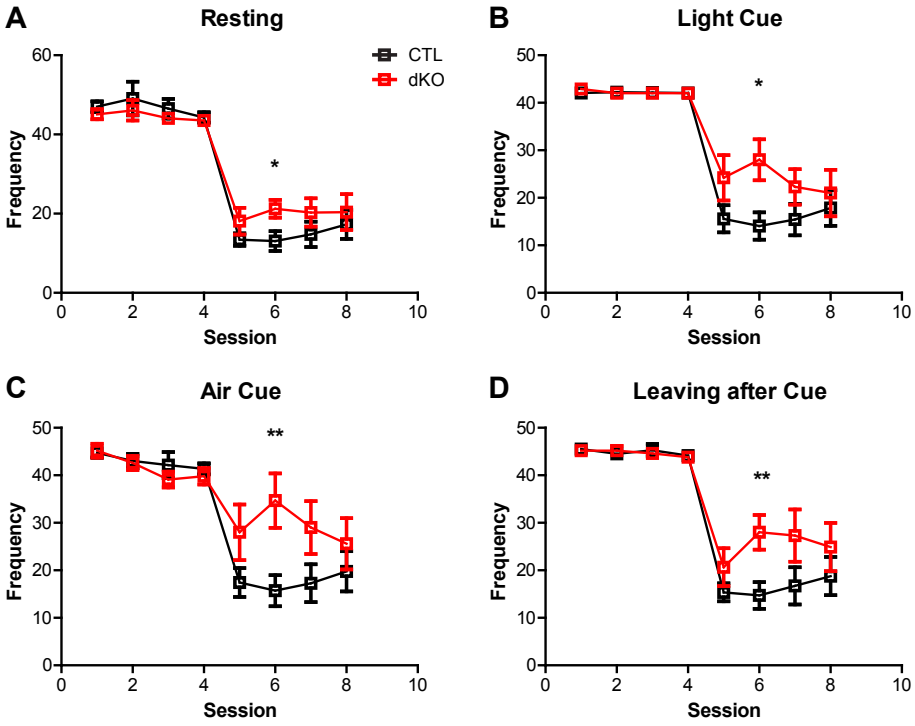

Figure 7.1 dKO mice made more undisturbed trials due to irregular walking on the ladder. A-D, The number of undisturbed trials were indicated by sorting the trial types of the parameters: resting (A), light cue (B), air cue (C) and leaving after cue (D) between CTL (black) and dKO (red) mice. dKO mice showed higher numbers of undisturbed trials in perturbation sessions than controls. CTL, n=14 mice; dKO, n=10 mice. *P$<$0.05, **P$<$0.01.

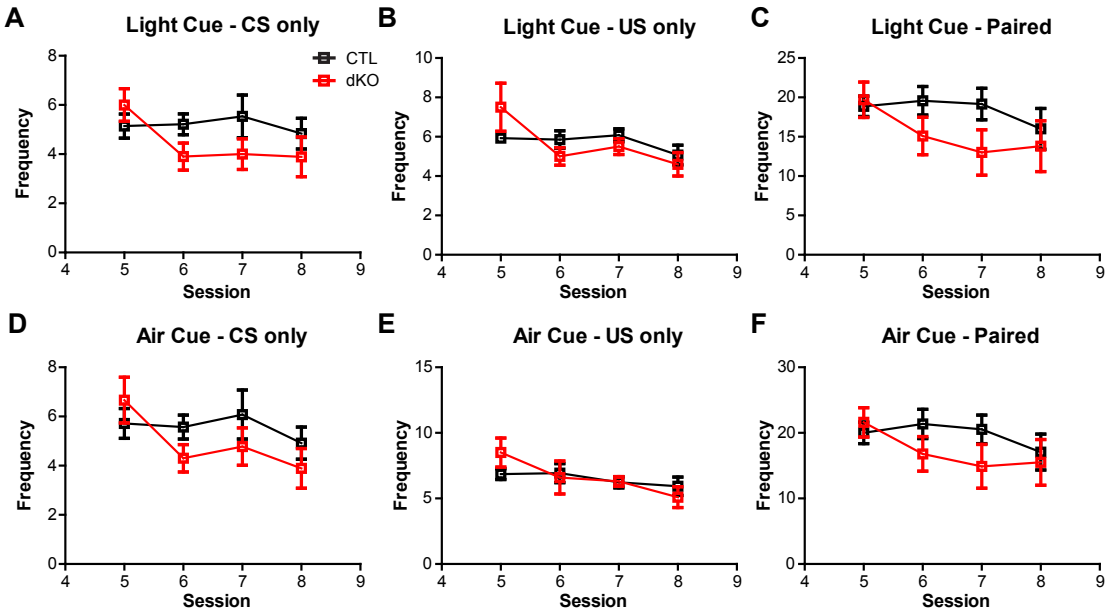

Figure 7.2 dKO mice triggered less perturbation trials. A-F, The number of different perturbation trials (CS only (A, D), US only (B, E) and paired (C, F)) were indicated by sorting the trial types of the parameters: light cue and air cue in each session between CTL (black) and dKO (red) mice. CTL, n=14 mice; dKO, n=10 mice.

only when the mice walked on the ladder at a relatively constant speed and step size, it was possible to predict the next step and which obstacle rung was raised up. Otherwise the default trial with stimulus was temporarily changed to undisturbed trial. dKO mice generated higher numbers of undisturbed trials reflected by these parameters, including frequency of resting (Fig. 7.1A), light cue (Fig. 7.1B), air cue (Fig. 7.1C) and leaving after cue (Fig. 7.1D). These results indicated that dKO mice walked more irregularly on the ladder, so that they could not reach the requirements to trigger the stimuli. However, the frequency of light cue and air cue activation in CS only (Fig. 7.2A, D), US only (Fig. 7.2B, E) and paired (Fig. 7.2C, F) trials per session in dKO mice were slightly lower than in control mice, although without any significant difference. All these results implies that dKO mice were in a stressful status on the ladder after challenged by perturbations.

During the training, mice learnt to run over the ladder, so both CTL and dKO mice showed decreased percentages of short steps (Fig. 7.3A) and increased percentages of long steps (Fig. 7.5A), indicating that mice walked more confidently on the ladder. No difference was detected between CTL and dKO mice in the training sessions. When perturbations were introduced, all the mice corrected their steps immediately by making jumps on the EramusLadder rungs (Fig. 7.7), however, dKO mice increased the percentage of short steps (Fig. 7.3) as well as the duration of short steps (Fig. 7.4) and long

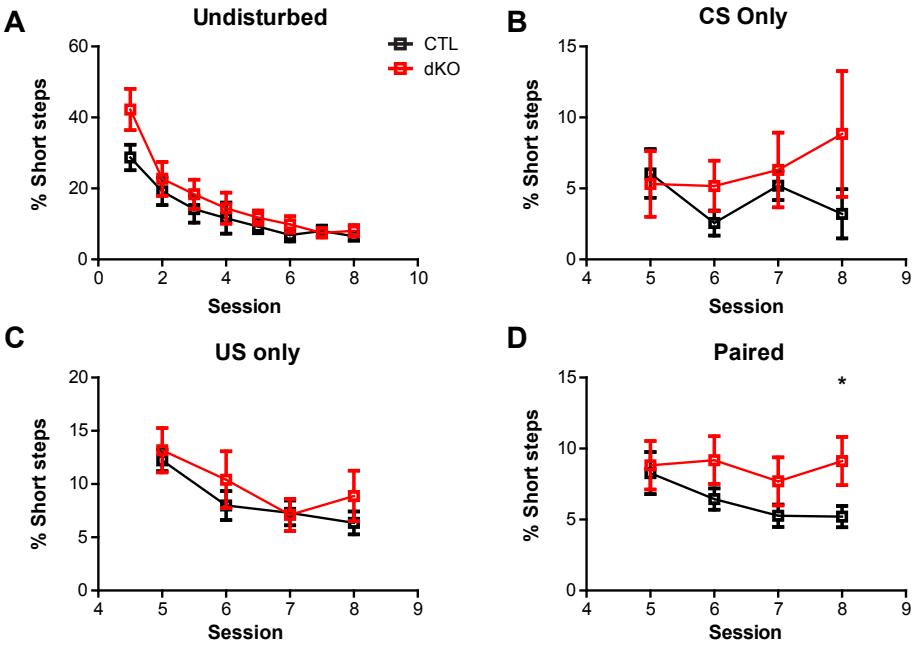

Figure 7.3 dKO mice increased the percentage of short steps in perturbation trials. A-D, The percentage of short steps in undisturbed (A), CS only (B), US only (C) and paired (D) trials in each session between CTL (black) and dKO (red) mice showed dKO mice had more short steps than controls, indicating that dKO mice displayed cautions and hesitations. CTL, n=14 mice; dKO, n=10 mice. *P$<$0.05.

steps (Fig. 7.6) in all trials compared to controls. Particularly, in undisturbed trials, even without any stimulus, dKO mice still moved slowly as indicated by increased duration of short steps (Fig. 7.4A) and long steps (Fig. 7.6A). No difference was observed in the percentage of long steps between WT and dKO mice (Fig. 7.5). However, the comparative percentage of missteps (context Fig. 4.42) demonstrated that motor learning was not impaired in dKO mice. These data implies the appearance of perturbation stimulated dKO mice in an anxiety-like status, therefore, they moved on the ladder more cautiously and nervously than control mice. These observations were well in line with our LTD results from electrophysioliogical investigations, which displayed a good consistency in indicating the important roles of Cav1.2/Cav1.3 of NG2 glia on modulation of neural network.

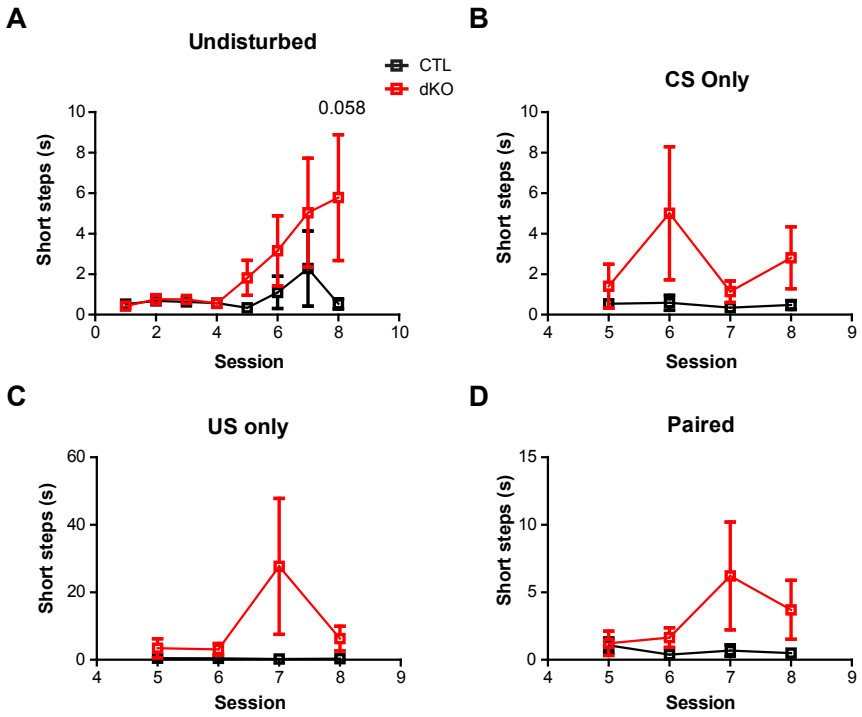

Figure 7.4 dKO mice moved slower with short steps during perturbation sessions. A-D, The duration of short steps on the ladder in undisturbed (A), CS only (B), US only (C) and paired (D) trials in each session between CTL (black) and dKO (red) mice. CTL, n=14 mice; dKO, n=10 mice.

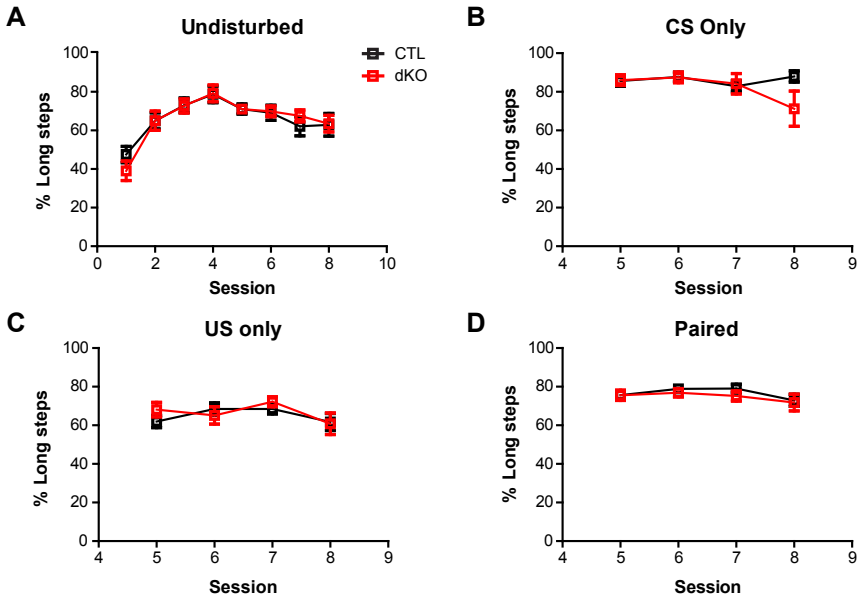

Figure 7.5 No difference of the percentage of long steps between CTL and dKO mice. A-D, The percentage of long steps in undisturbed (A), CS only (B), US only (C) and paired (D) trials in each session between CTL (black) and dKO (red) mice. CTL, n=14 mice; dKO, n=10 mice.

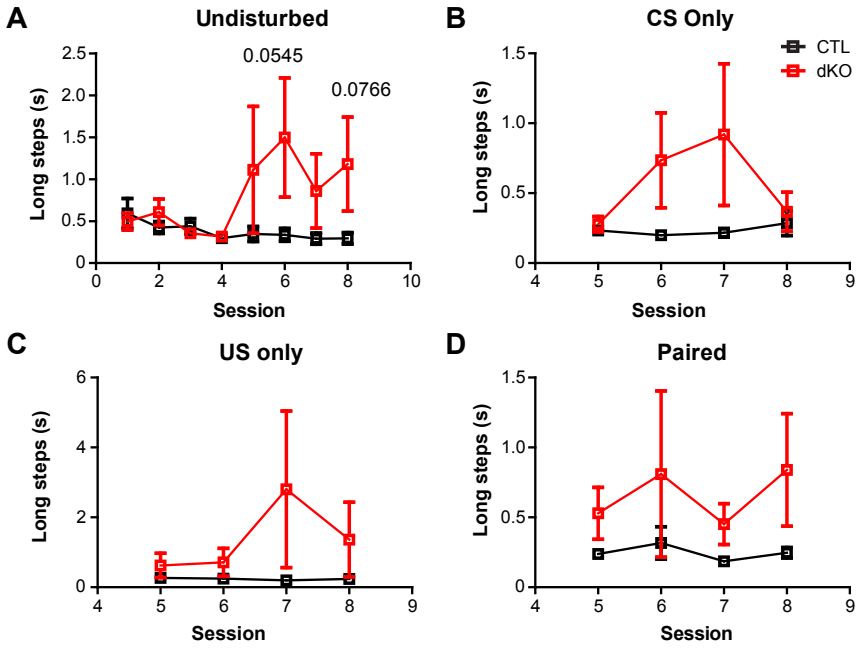

Figure 7.6 dKO mice walked slowly with long steps during perturbation sessions. The duration of long steps in undisturbed (A), CS only (B), US only (C) and paired (D) trials each session between CTL (black) and dKO (red) mice. CTL, n=14 mice; dKO, n=10 mice.

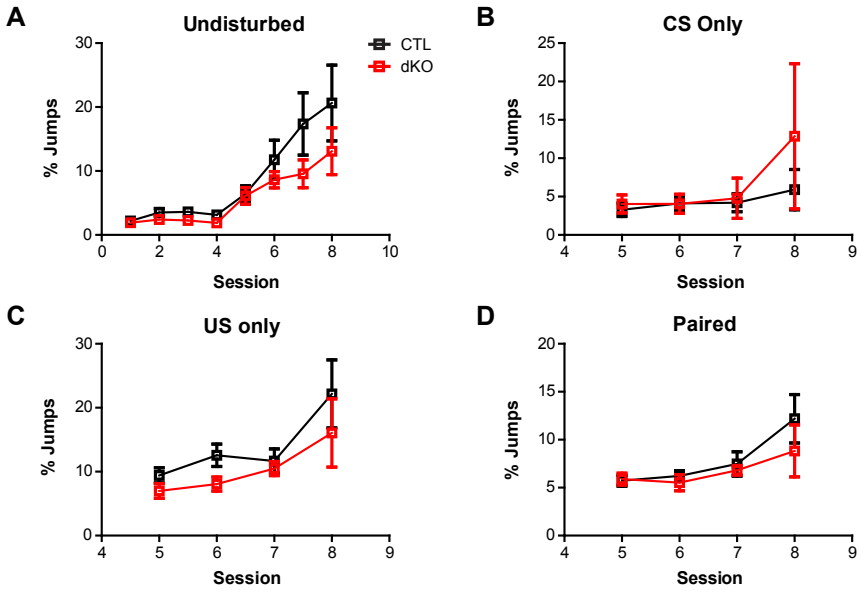

Figure 7.7 dKO mice did not show any difference on the percentage of Jumps from CTL mice. A-D, The percentage of Jumps in undisturbed (A), CS only (B), US only (C) and paired (D) trials in each session between CTL (black) and dKO (red) mice. CTL, n=14 mice; dKO, n=10 mice.

References

Agrawal, S. K., Nashmi, R., and Fehlings, M. G. (2000). Role of l- and n-type calcium channels in the pathophysiology of traumatic spinal cord white matter injury. *Neuroscience* 99, 179–88

Amaral, E., Guatimosim, S., and Guatimosim, C. (2011). Using the fluorescent styryl dye fm1-43 to visualize synaptic vesicles exocytosis and endocytosis in motor nerve terminals. *Methods in molecular biology (Clifton, N.J.)* 689, 137–148

Arruda-Carvalho, M. and Clem, R. L. (2014). Pathway-selective adjustment of prefrontal-amygdala transmission during fear encoding. *The Journal of Neuroscience* 34, 15601–15609

Attali, B., Wang, N., Kolot, A., Sobko, A., Cherepanov, V., and Soliven, B. (1997). Characterization of delayed rectifier kv channels in oligodendrocytes and progenitor cells. *J Neurosci* 17, 8234–45

Bai, X., Zhao, N., Huang, W., Caudal, L. C., Catalin, B., Cupido, A., et al. (Under review). After traumatic brain injury oligodendrocytes can regain a plastic phenotype and become astrocytes. *Unpublished*

Barres, B. A., Koroshetz, W. J., Swartz, K. J., Chun, L. L., and Corey, D. P. (1990). Ion channel expression by white matter glia: the o-2a glial progenitor cell. *Neuron* 4, 507–24

Bean, B. P. (1989a). Classes of calcium channels in vertebrate cells. *Annu Rev Physiol* 51, 367–84

Bean, B. P. (1989b). Neurotransmitter inhibition of neuronal calcium currents by changes in channel voltage dependence. *Nature* 340, 153–156

Bennett, J. and Weeds, A. (1986). Calcium and the cytoskeleton. *Br Med Bull* 42, 385–90

Bercury, K. K. and Macklin, W. B. (2015). Dynamics and mechanisms of cns myelination. *Dev Cell* 32, 447–58

Berger, T., Schnitzer, J., and Kettenmann, H. (1991). Developmental changes in the membrane current pattern, k+ buffer capacity, and morphology of glial cells in the corpus callosum slice. *J Neurosci* 11, 3008–24

Berger, T., Schnitzer, J., Orkand, P. M., and Kettenmann, H. (1992). Sodium and calcium currents in glial cells of the mouse corpus callosum slice. *Eur J Neurosci* 4, 1271–1284

Bergles, D. E., Jabs, R., and Steinhauser, C. (2010). Neuron-glia synapses in the brain. *Brain Res Rev* 63, 130–7

Bergles, D. E., Roberts, J. D., Somogyi, P., and Jahr, C. E. (2000). Glutamatergic synapses on oligodendrocyte precursor cells in the hippocampus. *Nature* 405, 187–91

Bi, L. L., Wang, J., Luo, Z. Y., Chen, S. P., Geng, F., Chen, Y. H., et al. (2013). Enhanced excitability in the infralimbic cortex produces anxiety-like behaviors. *Neuropharmacology* 72, 148–56

Birey, F., Kloc, M., Chavali, M., Hussein, I., Wilson, M., Christoffel, D. J., et al. (2015). Genetic and stress-induced loss of ng2 glia triggers emergence of depressive-like behaviors through reduced secretion of fgf2. *Neuron* 88, 941–56

Blankenfeld Gv, G. V., Verkhratsky, A. N., and Kettenmann, H. (1992). Ca2+ channel expression in the oligodendrocyte lineage. *Eur J Neurosci* 4, 1035–1048

Bourin, M. and Hascoet, M. (2003). The mouse light/dark box test. *Eur J Pharmacol* 463, 55–65

Bryant, C. D., Zhang, N. N., Sokoloff, G., Fanselow, M. S., Ennes, H. S., Palmer, A. A., et al. (2008). Behavioral differences among c57bl/6 substrains: implications for transgenic and knockout studies. *J Neurogenet* 22, 315–31

Budde, T., Meuth, S., and Pape, H. C. (2002). Calcium-dependent inactivation of neuronal calcium channels. *Nat Rev Neurosci* 3, 873–83

Butt, A. M. (2006). Neurotransmitter-mediated calcium signalling in oligodendrocyte physiology and pathology. *Glia* 54, 666–75

Butt, A. M. and Kalsi, A. (2006). Inwardly rectifying potassium channels (kir) in central nervous system glia: a special role for kir4.1 in glial functions. *J Cell Mol Med* 10, 33–44

Butt, A. M., Kiff, J., Hubbard, P., and Berry, M. (2002). Synantocytes: new functions for novel ng2 expressing glia. *J Neurocytol* 31, 551–65

Cao, X., Li, L. P., Wang, Q., Wu, Q., Hu, H. H., Zhang, M., et al. (2013). Astrocyte-derived atp modulates depressive-like behaviors. *Nat Med* 19, 773–7

Chavis, P., Fagni, L., Lansman, J. B., and Bockaert, J. (1996). Functional coupling between ryanodine receptors and l-type calcium channels in neurons. *Nature* 382, 719–22

Cheli, V. T., Santiago Gonzalez, D. A., Namgyal Lama, T., Spreuer, V., Handley, V., Murphy, G. G., et al. (2016). Conditional deletion of the l-type calcium channel cav1.2 in oligodendrocyte progenitor cells affects postnatal myelination in mice. *J Neurosci* 36, 10853–10869

Cheli, V. T., Santiago Gonzalez, D. A., Spreuer, V., and Paez, P. M. (2015). Voltage-gated ca2+ entry promotes oligodendrocyte progenitor cell maturation and myelination in vitro. *Exp Neurol* 265, 69–83

Chen, S., Ren, Y. Q., Bing, R., and Hillman, D. E. (2000). Alpha 1e subunit of the r-type calcium channel is associated with myelinogenesis. *J Neurocytol* 29, 719–28

Chen, Z. J., Negra, M., Levine, A., Ughrin, Y., and Levine, J. M. (2002). Oligodendrocyte precursor cells: Reactive cells that inhibit axon growth and regeneration. *Journal of Neurocytology* 31, 481 ppl=–495

Chittajallu, R., Aguirre, A., and Gallo, V. (2004). Ng2-positive cells in the mouse white and grey matter display distinct physiological properties. *J Physiol* 561, 109–22

Chittajallu, R., Aguirre, A. A., and Gallo, V. (2005). Downregulation of platelet-derived growth factor-alpha receptor-mediated tyrosine kinase activity as a cellular mechanism for k+-channel regulation during oligodendrocyte development in situ. *J Neurosci* 25, 8601–10

Clarke, L. E., Young, K. M., Hamilton, N. B., Li, H., Richardson, W. D., and Attwell, D. (2012). Properties and fate of oligodendrocyte progenitor cells in the corpus callosum, motor cortex, and piriform cortex of the mouse. *J Neurosci* 32, 8173–85

Coppi, E., Maraula, G., Fumagalli, M., Failli, P., Cellai, L., Bonfanti, E., et al. (2013). Udp-glucose enhances outward k(+) currents necessary for cell differentiation and stimulates cell migration by activating the gpr17 receptor in oligodendrocyte precursors. *Glia* 61, 1155–71

Crawford, D. K., Mangiardi, M., and Tiwari-Woodruff, S. K. (2009). Assaying the functional effects of demyelination and remyelination: revisiting field potential recordings. *J Neurosci Methods* 182, 25–33

Cupido, A. (2009). *Detecting Cerebellar Phenotypes with the Erasmus Ladder*. Phd thesis, University of Erasmus

Czeh, B., Muller-Keuker, J. I., Rygula, R., Abumaria, N., Hiemke, C., Domenici, E., et al. (2007). Chronic social stress inhibits cell proliferation in the adult medial prefrontal cortex: hemispheric asymmetry and reversal by fluoxetine treatment. *Neuropsychopharmacology* 32, 1490–503

Dawson, M. R., Levine, J. M., and Reynolds, R. (2000). Ng2-expressing cells in the central nervous system: are they oligodendroglial progenitors? *J Neurosci Res* 61, 471–9

Dawson, M. R., Polito, A., Levine, J. M., and Reynolds, R. (2003). Ng2-expressing glial progenitor cells: an abundant and widespread population of cycling cells in the adult rat cns. *Mol Cell Neurosci* 24, 476–88

De Biase, L. M., Kang, S. H., Baxi, E. G., Fukaya, M., Pucak, M. L., Mishina, M., et al. (2011). Nmda receptor signaling in oligodendrocyte progenitors is not required for oligodendrogenesis and myelination. *J Neurosci* 31, 12650–62

De Biase, L. M., Nishiyama, A., and Bergles, D. E. (2010). Excitability and synaptic communication within the oligodendrocyte lineage. *J Neurosci* 30, 3600–11

Dimou, L. and Gallo, V. (2015). Ng2-glia and their functions in the central nervous system. *Glia* 63, 1429–51

Einheber, S., Zanazzi, G., Ching, W., Scherer, S., Milner, T. A., Peles, E., et al. (1997). The axonal membrane protein caspr, a homologue of neurexin iv, is a component of the septate-like paranodal junctions that assemble during myelination. *J Cell Biol* 139, 1495–506

Elsayed, M., Banasr, M., Duric, V., Fournier, N. M., Licznerski, P., and Duman, R. S. (2012). Antidepressant effects of fibroblast growth factor-2 in behavioral and cellular models of depression. *Biological Psychiatry* 72, 258 – 265

Foran, D. R. and Peterson, A. C. (1992). Myelin acquisition in the central nervous system of the mouse revealed by an mbp-lac z transgene. *J Neurosci* 12, 4890–7

Fuenzalida, L. C., Keen, K. L., and Terasawa, E. (2011). Colocalization of fm1-43, bassoon, and gnrh-1: Gnrh-1 release from cell bodies and their neuroprocesses. *Endocrinology* 152, 4310–21

Gallo, V., Zhou, J. M., McBain, C. J., Wright, P., Knutson, P. L., and Armstrong, R. C. (1996). Oligodendrocyte progenitor cell proliferation and lineage progression are regulated by glutamate receptor-mediated k+ channel block. *J Neurosci* 16, 2659–70

Gandini, M. A. and Felix, R. (2015). Molecular and functional interplay of voltage-gated ca(2)(+) channels with the cytoskeleton. *Curr Mol Pharmacol* 8, 69–80

Ge, W. P., Yang, X. J., Zhang, Z., Wang, H. K., Shen, W., Deng, Q. D., et al. (2006). Long-term potentiation of neuron-glia synapses mediated by ca2+-permeable ampa receptors. *Science* 312, 1533–7

Ge, W. P., Zhou, W., Luo, Q., Jan, L. Y., and Jan, Y. N. (2009). Dividing glial cells maintain differentiated properties including complex morphology and functional synapses. *Proc Natl Acad Sci U S A* 106, 328–33

Giustino, T. F., Fitzgerald, P. J., and Maren, S. (2016). Fear expression suppresses medial prefrontal cortical firing in rats. *PLoS One* 11, e0165256

Giustino, T. F. and Maren, S. (2015). The role of the medial prefrontal cortex in the conditioning and extinction of fear. *Frontiers in Behavioral Neuroscience* 9

Guo, F., Maeda, Y., Ma, J., Xu, J., Horiuchi, M., Miers, L., et al. (2010). Pyramidal neurons are generated from oligodendroglial progenitor cells in adult piriform cortex. *J Neurosci* 30, 12036–49

Haberlandt, C., Derouiche, A., Wyczynski, A., Haseleu, J., Pohle, J., Karram, K., et al. (2011). Gray matter ng2 cells display multiple ca2+-signaling pathways and highly motile processes. *PLoS One* 6, e17575

Hall, D. D., Dai, S., Tseng, P. Y., Malik, Z., Nguyen, M., Matt, L., et al. (2013). Competition between alpha-actinin and ca(2)(+)-calmodulin controls surface retention of the l-type ca(2)(+) channel ca(v)1.2. *Neuron* 78, 483–97

Hamilton, N., Vayro, S., Wigley, R., and Butt, A. M. (2010). Axons and astrocytes release atp and glutamate to evoke calcium signals in ng2-glia. *Glia* 58, 66–79

Han, X., Chen, M., Wang, F., Windrem, M., Wang, S., Shanz, S., et al. (2013). Forebrain engraftment by human glial progenitor cells enhances synaptic plasticity and learning in adult mice. *Cell Stem Cell* 12, 342–353

Hare, J. F. and Taylor, K. (1991). Mechanisms of plasma membrane protein degradation: recycling proteins are degraded more rapidly than those confined to the cell surface. *Proc Natl Acad Sci U S A* 88, 5902–6

Herry, C. and Garcia, R. (2003). Behavioral and paired-pulse facilitation analyses of long-lasting depression at excitatory synapses in the medial prefrontal cortex in mice. *Behav Brain Res* 146, 89–96

Hill, R. A. and Nishiyama, A. (2014). Ng2 cells (polydendrocytes): listeners to the neural network with diverse properties. *Glia* 62, 1195–210

Hill, R. A., Patel, K. D., Goncalves, C. M., Grutzendler, J., and Nishiyama, A. (2014). Modulation of oligodendrocyte generation during a critical temporal window after ng2 cell division. *Nat Neurosci* 17, 1518–27

Hill, R. A., Patel, K. D., Medved, J., Reiss, A. M., and Nishiyama, A. (2013). Ng2 cells in white matter but not gray matter proliferate in response to pdgf. *J Neurosci* 33, 14558–66

Hinks, G. L. and Franklin, R. J. (1999). Distinctive patterns of pdgf-a, fgf-2, igf-i, and tgf-beta1 gene expression during remyelination of experimentally-induced spinal cord demyelination. *Mol Cell Neurosci* 14, 153–68

Hirrlinger, J., Hulsmann, S., and Kirchhoff, F. (2004). Astroglial processes show spontaneous motility at active synaptic terminals in situ. *Eur J Neurosci* 20, 2235–9

Huang, W., Zhao, N., Bai, X., Karram, K., Trotter, J., Goebbels, S., et al. (2014). Novel ng2-creert2 knock-in mice demonstrate heterogeneous differentiation potential of ng2 glia during development. *Glia* 62, 896–913

Hughes, E. G., Kang, S. H., Fukaya, M., and Bergles, D. E. (2013). Oligodendrocyte progenitors balance growth with self-repulsion to achieve homeostasis in the adult brain. *Nat Neurosci* 16, 668–76

Johnson, B. D. and Byerly, L. (1993). A cytoskeletal mechanism for ca2+ channel metabolic dependence and inactivation by intracellular ca2+. *Neuron* 10, 797–804

Kang, S. H., Fukaya, M., Yang, J. K., Rothstein, J. D., and Bergles, D. E. (2010). Ng2+ cns glial progenitors remain committed to the oligodendrocyte lineage in postnatal life and following neurodegeneration. *Neuron* 68, 668–81

Karadottir, R., Hamilton, N. B., Bakiri, Y., and Attwell, D. (2008). Spiking and nonspiking classes of oligodendrocyte precursor glia in cns white matter. *Nat Neurosci* 11, 450–6

Karram, K., Goebbels, S., Schwab, M., Jennissen, K., Seifert, G., Steinhuser, C., et al. (2008). Ng2-expressing cells in the nervous system revealed by the ng2-eyfp-knockin mouse. *Genesis* 46, 743–57

Kessaris, N., Fogarty, M., Iannarelli, P., Grist, M., Wegner, M., and Richardson, W. D. (2006). Competing waves of oligodendrocytes in the forebrain and postnatal elimination of an embryonic lineage. *Nat Neurosci* 9, 173–9

Kirchhoff, F. and Kettenmann, H. (1992). Gaba triggers a [ca2+]i increase in murine precursor cells of the oligodendrocyte lineage. *Eur J Neurosci* 4, 1049–1058

Kirischuk, S., Scherer, J., Moller, T., Verkhratsky, A., and Kettenmann, H. (1995). Subcellular heterogeneity of voltage-gated ca2+ channels in cells of the oligodendrocyte lineage. *Glia* 13, 1–12

Knutson, P., Ghiani, C. A., Zhou, J. M., Gallo, V., and McBain, C. J. (1997). K+ channel expression and cell proliferation are regulated by intracellular sodium and membrane depolarization in oligodendrocyte progenitor cells. *J Neurosci* 17, 2669–82

Kressin, K., Kuprijanova, E., Jabs, R., Seifert, G., and Steinhuser, C. (1995). Developmental regulation of na+ and k+ conductances in glial cells of mouse hippocampal brain slices. *Glia* 15, 173–87

Kukley, M., Capetillo-Zarate, E., and Dietrich, D. (2007). Vesicular glutamate release from axons in white matter. *Nat Neurosci* 10, 311–20

Kukley, M., Nishiyama, A., and Dietrich, D. (2010). The fate of synaptic input to ng2 glial cells: neurons specifically downregulate transmitter release onto differentiating oligodendroglial cells. *J Neurosci* 30, 8320–31

Lalo, U., Palygin, O., Rasooli-Nejad, S., Andrew, J., Haydon, P. G., and Pankratov, Y. (2014). Exocytosis of atp from astrocytes modulates phasic and tonic inhibition in the neocortex. *PLoS Biol* 12, e1001747

Larson, V. A., Zhang, Y., and Bergles, D. E. (2016). Electrophysiological properties of ng2(+) cells: Matching physiological studies with gene expression profiles. *Brain Res* 1638, 138–60

Lee, H. K., Kameyama, K., Huganir, R. L., and Bear, M. F. (1998). Nmda induces long-term synaptic depression and dephosphorylation of the glur1 subunit of ampa receptors in hippocampus. *Neuron* 21, 1151–62

Levine, J. M., Stincone, F., and Lee, Y. S. (1993). Development and differentiation of glial precursor cells in the rat cerebellum. *Glia* 7, 307–21

Lu, Q. R., Sun, T., Zhu, Z., Ma, N., Garcia, M., Stiles, C. D., et al. (2002). Common developmental requirement for olig function indicates a motor neuron/oligodendrocyte connection. *Cell* 109, 75–86

Luscher, C. and Malenka, R. C. (2012). Nmda receptor-dependent long-term potentiation and long-term depression (ltp/ltd). *Cold Spring Harb Perspect Biol* 4

Lytle, J. M., Chittajallu, R., Wrathall, J. R., and Gallo, V. (2009). Ng2 cell response in the cnp-egfp mouse after contusive spinal cord injury. *Glia* 57, 270–85

Maldonado, P. P., Velez-Fort, M., and Angulo, M. C. (2011). Is neuronal communication with ng2 cells synaptic or extrasynaptic? *J Anat* 219, 8–17

Maldonado, P. P., Velez-Fort, M., Levavasseur, F., and Angulo, M. C. (2013). Oligodendrocyte precursor cells are accurate sensors of local k+ in mature gray matter. *J Neurosci* 33, 2432–42

Marchisella, F., Coffey, E. T., and Hollos, P. (2016). Microtubule and microtubule associated protein anomalies in psychiatric disease. *Cytoskeleton (Hoboken)* 73, 596–611

Martinowich, K., Schloesser, R. J., Lu, Y., Jimenez, D. V., Paredes, D., Greene, J. S., et al. (2012). Roles of p75(ntr), long-term depression, and cholinergic transmission in anxiety and acute stress coping. *Biol Psychiatry* 71, 75–83

Mekada, K., Abe, K., Murakami, A., Nakamura, S., Nakata, H., Moriwaki, K., et al. (2009). Genetic differences among c57bl/6 substrains. *Exp Anim* 58, 141–9

Milosevic, N. T. and Ristanovic, D. (2007). The sholl analysis of neuronal cell images: semi-log or log-log method? *J Theor Biol* 245, 130–40

Miyata, S., Taniguchi, M., Koyama, Y., Shimizu, S., Tanaka, T., Yasuno, F., et al. (2016). Association between chronic stress-induced structural abnormalities in ranvier nodes and reduced oligodendrocyte activity in major depression. *Sci Rep* 6, 23084

Moosmang, S., Haider, N., Klugbauer, N., Adelsberger, H., Langwieser, N., Müller, J., et al. (2005). Role of hippocampal cav1.2 ca2+ channels in nmda receptor-independent synaptic plasticity and spatial memory. *Journal of Neuroscience* 25, 9883–9892

Moosmang, S., Schulla, V., Welling, A., Feil, R., Feil, S., Wegener, J. W., et al. (2003). Dominant role of smooth muscle l-type calcium channel cav1.2 for blood pressure regulation. *The EMBO Journal* 22, 6027–6034

Moshrefi-Ravasdjani, B., Dublin, P., Seifert, G., Jennissen, K., Steinhauser, C., Kafitz, K. W., et al. (2016). Changes in the proliferative capacity of ng2 cell subpopulations during postnatal development of the mouse hippocampus. *Brain Struct Funct*

Nakamura, T., Colbert, M. C., and Robbins, J. (2006). Neural crest cells retain multipotential characteristics in the developing valves and label the cardiac conduction system. *Circ Res* 98, 1547–54

Naruse, M., Ishizaki, Y., Ikenaka, K., Tanaka, A., and Hitoshi, S. (2016). Origin of oligodendrocytes in mammalian forebrains: a revised perspective. *J Physiol Sci*

Neusch, C., Rozengurt, N., Jacobs, R. E., Lester, H. A., and Kofuji, P. (2001). Kir4.1 potassium channel subunit is crucial for oligodendrocyte development and in vivo myelination. *J Neurosci* 21, 5429–38

Nicholls, R. E., Alarcon, J. M., Malleret, G., Carroll, R. C., Grody, M., Vronskaya, S., et al. (2008). Transgenic mice lacking nmdar-dependent ltd exhibit deficits in behavioral flexibility. *Neuron* 58, 104–17

Nishiyama, A., Boshans, L., Goncalves, C. M., Wegrzyn, J., and Patel, K. D. (2016). Lineage, fate, and fate potential of ng2-glia. *Brain Res* 1638, 116–28

Nishiyama, A., Komitova, M., Suzuki, R., and Zhu, X. (2009). Polydendrocytes (ng2 cells): multifunctional cells with lineage plasticity. *Nat Rev Neurosci* 10, 9–22

Nishiyama, A., Lin, X. H., Giese, N., Heldin, C. H., and Stallcup, W. B. (1996). Co-localization of ng2 proteoglycan and pdgf alpha-receptor on o2a progenitor cells in the developing rat brain. *J Neurosci Res* 43, 299–314

Noldus (2015). Erasmusladder. *Noldus Information Technology Reference Manual, Version 1.1*

Nowycky, M. C., Fox, A. P., and Tsien, R. W. (1985). Three types of neuronal calcium channel with different calcium agonist sensitivity. *Nature* 316, 440–3

O'Brien, E. T., Salmon, E. D., and Erickson, H. P. (1997). How calcium causes microtubule depolymerization. *Cell Motil Cytoskeleton* 36, 125–35

Orduz, D., Maldonado, P. P., Balia, M., Velez-Fort, M., de Sars, V., Yanagawa, Y., et al. (2015). Interneurons and oligodendrocyte progenitors form a structured synaptic network in the developing neocortex. *Elife* 4

Ortega, F., Gascon, S., Masserdotti, G., Deshpande, A., Simon, C., Fischer, J., et al. (2013). Oligodendrogliogenic and neurogenic adult subependymal zone neural stem cells constitute distinct lineages and exhibit differential responsiveness to wnt signalling. *Nat Cell Biol* 15, 602–13

Paez, P. M., Cheli, V. T., Ghiani, C. A., Spreuer, V., Handley, V. W., and Campagnoni, A. T. (2012). Golli myelin basic proteins stimulate oligodendrocyte progenitor cell proliferation and differentiation in remyelinating adult mouse brain. *Glia* 60, 1078–93

Paez, P. M., Fulton, D., Colwell, C. S., and Campagnoni, A. T. (2009a). Voltage-operated ca(2+) and na(+) channels in the oligodendrocyte lineage. *J Neurosci Res* 87, 3259–66

Paez, P. M., Fulton, D. J., Spreuer, V., Handley, V., Campagnoni, C. W., and Campagnoni, A. T. (2009b). Regulation of store-operated and voltage-operated ca2+ channels in the proliferation and death of oligodendrocyte precursor cells by golli proteins. *ASN Neuro* 1

Paez, P. M., Fulton, D. J., Spreur, V., Handley, V., and Campagnoni, A. T. (2010). Multiple kinase pathways regulate voltage-dependent ca2+ influx and migration in oligodendrocyte precursor cells. *J Neurosci* 30, 6422–33

Palfreyman M.T., J. E. (2008). *Roles of SNARE Proteins in Synaptic Vesicle Fusion* (Humana Press)

Passlick, S., Trotter, J., Seifert, G., Steinhauser, C., and Jabs, R. (2016). The ng2 protein is not required for glutamatergic neuron-ng2 cell synaptic signaling. *Cereb Cortex* 26, 51–7

Perez, J. A., Clinton, S. M., Turner, C. A., Watson, S. J., and Akil, H. (2009). A new role for fgf2 as an endogenous inhibitor of anxiety. *Journal of Neuroscience* 29, 6379–6387

Pivonkova, H., Benesova, J., Butenko, O., Chvatal, A., and Anderova, M. (2010). Impact of global cerebral ischemia on k+ channel expression and membrane properties of glial cells in the rat hippocampus. *Neurochem Int* 57, 783–94

Poetschke, C., Dragicevic, E., Duda, J., Benkert, J., Dougalis, A., DeZio, R., et al. (2015). Compensatory t-type ca2+ channel activity alters d2-autoreceptor responses of substantia nigra dopamine neurons from cav1.3 l-type ca2+ channel ko mice. *Sci Rep* 5, 13688

Rivers, L. E., Young, K. M., Rizzi, M., Jamen, F., Psachoulia, K., Wade, A., et al. (2008). Pdgfra/ng2 glia generate myelinating oligodendrocytes and piriform projection neurons in adult mice. *Nat Neurosci* 11, 1392–401

Saab, A. S., Neumeyer, A., Jahn, H. M., Cupido, A., Simek, A. A., Boele, H. J., et al. (2012). Bergmann glial ampa receptors are required for fine motor coordination. *Science* 337, 749–53

Sahel, A., Ortiz, F. C., Kerninon, C., Maldonado, P. P., Angulo, M. C., and Nait-Oumesmar, B. (2015). Alteration of synaptic connectivity of oligodendrocyte precursor cells following demyelination. *Front Cell Neurosci* 9, 77

Sakry, D., Neitz, A., Singh, J., Frischknecht, R., Marongiu, D., Biname, F., et al. (2014). Oligodendrocyte precursor cells modulate the neuronal network by activity-dependent ectodomain cleavage of glial ng2. *PLoS Biol* 12, e1001993

Sataric, M. V., Sekulic, D. L., Sataric, B. M., and Zdravkovic, S. (2015). Role of nonlinear localized ca(2+) pulses along microtubules in tuning the mechano-sensitivity of hair cells. *Prog Biophys Mol Biol* 119, 162–74

Satheesh, S. V., Kunert, K., Rttiger, L., Zuccotti, A., Schnig, K., Friauf, E., et al. (2012). Retrocochlear function of the peripheral deafness gene cacna1d. *Hum Mol Genet* 21, 3896–909

Schmidt, K., Eulitz, D., Veh, R. W., Kettenmann, H., and Kirchhoff, F. (1999). Heterogeneous expression of voltage-gated potassium channels of the shaker family (kv1) in oligodendrocyte progenitors. *Brain Res* 843, 145–60

Schneider, C. A., Rasband, W. S., and Eliceiri, K. W. (2012). Nih image to imagej: 25 years of image analysis. *Nat Methods* 9, 671–5

Schonewille, M., Gao, Z., Boele, H. J., Veloz, M. F., Amerika, W. E., Simek, A. A., et al. (2011). Reevaluating the role of ltd in cerebellar motor learning. *Neuron* 70, 43–50

Schools, G. P., Zhou, M., and Kimelberg, H. K. (2003). Electrophysiologically "complex" glial cells freshly isolated from the hippocampus are immunopositive for the chondroitin sulfate proteoglycan ng2. *J Neurosci Res* 73, 765–77

Sholl, D. A. (1953). Dendritic organization in the neurons of the visual and motor cortices of the cat. *J Anat* 87, 387–406

Simms, B. and Zamponi, G. (2014). Neuronal voltage-gated calcium channels: Structure, function, and dysfunction. *Neuron* 82, 24 – 45

Simon, C., Gotz, M., and Dimou, L. (2011). Progenitors in the adult cerebral cortex: cell cycle properties and regulation by physiological stimuli and injury. *Glia* 59, 869–81

Snaidero, N., Mbius, W., Czopka, T., Hekking, L. H., Mathisen, C., Verkleij, D., et al. (2014). Myelin membrane wrapping of cns axons by pi(3,4,5)p3-dependent polarized growth at the inner tongue. *Cell* 156, 277–90

Sontheimer, H., Perouansky, M., Hoppe, D., Lux, H. D., Grantyn, R., and Kettenmann, H. (1989). Glial cells of the oligodendrocyte lineage express proton-activated na+ channels. *J Neurosci Res* 24, 496–500

Squecco, R., Idrizaj, E., Morelli, A., Gallina, P., Vannelli, G. B., and Francini, F. (2016). An electrophysiological study on the effects of bdnf and fgf2 on voltage dependent ca(2+) currents in developing human striatal primordium. *Mol Cell Neurosci* 75, 50–62

Steinhauser, C., Berger, T., Frotscher, M., and Kettenmann, H. (1992). Heterogeneity in the membrane current pattern of identified glial cells in the hippocampal slice. *Eur J Neurosci* 4, 472–484

Steinhauser, C., Kressin, K., Kuprijanova, E., Weber, M., and Seifert, G. (1994). Properties of voltage-activated na+ and k+ currents in mouse hippocampal glial cells in situ and after acute isolation from tissue slices. *Pflugers Arch* 428, 610–20

Sui, L., Wang, J., and Li, B. M. (2008). Role of the phosphoinositide 3-kinase-akt-mammalian target of the rapamycin signaling pathway in long-term potentiation and trace fear conditioning memory in rat medial prefrontal cortex. *Learn Mem* 15, 762–76

Sun, W., Matthews, E. A., Nicolas, V., Schoch, S., and Dietrich, D. (2016). Ng2 glial cells integrate synaptic input in global and dendritic calcium signals. *Elife* 5, e16262

Tanaka, Y., Tozuka, Y., Takata, T., Shimazu, N., Matsumura, N., Ohta, A., et al. (2009). Excitatory gabaergic activation of cortical dividing glial cells. *Cereb Cortex* 19, 2181–95

Tang, X., Taniguchi, K., and Kofuji, P. (2009). Heterogeneity of kir4.1 channel expression in glia revealed by mouse transgenesis. *Glia* 57, 1706–15

Tatsumi, K., Takebayashi, H., Manabe, T., Tanaka, K. F., Makinodan, M., Yamauchi, T., et al. (2008). Genetic fate mapping of olig2 progenitors in the injured adult cerebral cortex reveals preferential differentiation into astrocytes. *J Neurosci Res* 86, 3494–502

Todorov, P. T., HARDISTY, R. E., and BROWN, S. D. M. (2001). Myosin viia is specifically associated with calmodulin and microtubule-associated protein-2b (map-2b). *Biochemical Journal* 354, 267–274

Tong, X. P., Li, X. Y., Zhou, B., Shen, W., Zhang, Z. J., Xu, T. L., et al. (2009). Ca(2+) signaling evoked by activation of na(+) channels and na(+)/ca(2+) exchangers is required for gaba-induced ng2 cell migration. *J Cell Biol* 186, 113–28

Tripathi, R. B., Clarke, L. E., Burzomato, V., Kessaris, N., Anderson, P. N., Attwell, D., et al. (2011). Dorsally and ventrally derived oligodendrocytes have similar electrical properties but myelinate preferred tracts. *J Neurosci* 31, 6809–19

Tripathi, R. B., Rivers, L. E., Young, K. M., Jamen, F., and Richardson, W. D. (2010). Ng2 glia generate new oligodendrocytes but few astrocytes in a murine experimental autoimmune encephalomyelitis model of demyelinating disease. *J Neurosci* 30, 16383–90

Tuckwell, H. C. (2012). Quantitative aspects of l-type ca2+ currents. *Prog Neurobiol* 96, 1–31

Vigano, F., Mobius, W., Gotz, M., and Dimou, L. (2013). Transplantation reveals regional differences in oligodendrocyte differentiation in the adult brain. *Nat Neurosci* 16, 1370–1372

von Bohlen und Halbach, O. (2007). Immunohistological markers for staging neurogenesis in adult hippocampus. *Cell and Tissue Research* 329, 409–420

Wigley, R., Hamilton, N., Nishiyama, A., Kirchhoff, F., and Butt, A. M. (2007). Morphological and physiological interactions of ng2-glia with astrocytes and neurons. *J Anat* 210, 661–70

Woodruff, R. H., Tekki-Kessaris, N., Stiles, C. D., Rowitch, D. H., and Richardson, W. D. (2001). Oligodendrocyte development in the spinal cord and telencephalon: common themes and new perspectives. *Int J Dev Neurosci* 19, 379–85

Wu, L., Bauer, C. S., Zhen, X.-g., Xie, C., and Yang, J. (2002). Dual regulation of voltage-gated calcium channels by ptdins(4,5)p2. *Nature* 419, 947–952

Young, K. M., Psachoulia, K., Tripathi, R. B., Dunn, S. J., Cossell, L., Attwell, D., et al. (2013). Oligodendrocyte dynamics in the healthy adult cns: evidence for myelin remodeling. *Neuron* 77, 873–85

Yuan, X., Chittajallu, R., Belachew, S., Anderson, S., McBain, C. J., and Gallo, V. (2002). Expression of the green fluorescent protein in the oligodendrocyte lineage: a transgenic mouse for developmental and physiological studies. *J Neurosci Res* 70, 529–45

Zhang, Y., Chen, K., Sloan, S. A., Bennett, M. L., Scholze, A. R., O'Keeffe, S., et al. (2014). An rna-sequencing transcriptome and splicing database of glia, neurons, and vascular cells of the cerebral cortex. *J Neurosci* 34, 11929–47

Zhou, M., Schools, G. P., and Kimelberg, H. K. (2006). Development of glast(+) astrocytes and ng2(+) glia in rat hippocampus ca1: mature astrocytes are electrophysiologically passive. *J Neurophysiol* 95, 134–43

Zhu, X., Bergles, D. E., and Nishiyama, A. (2008a). Ng2 cells generate both oligodendrocytes and gray matter astrocytes. *Development* 135, 145–57

Zhu, X., Hill, R. A., and Nishiyama, A. (2008b). Ng2 cells generate oligodendrocytes and gray matter astrocytes in the spinal cord. *Neuron Glia Biol* 4, 19–26

Zhu, X., Zuo, H., Maher, B. J., Serwanski, D. R., LoTurco, J. J., Lu, Q. R., et al. (2012). Olig2-dependent developmental fate switch of ng2 cells. *Development* 139, 2299–307

Ziskin, J. L., Nishiyama, A., Rubio, M., Fukaya, M., and Bergles, D. E. (2007). Vesicular release of glutamate from unmyelinated axons in white matter. *Nat Neurosci* 10, 321–30

Zonouzi, M., Renzi, M., Farrant, M., and Cull-Candy, S. G. (2011). Bidirectional plasticity of calcium-permeable ampa receptors in oligodendrocyte lineage cells. *Nat Neurosci* 14, 1430–8

Zuchero, J. B., Fu, M. M., Sloan, S. A., Ibrahim, A., Olson, A., Zaremba, A., et al. (2015). Cns myelin wrapping is driven by actin disassembly. *Dev Cell* 34, 152–67

Publications and presentations

Publication

1. Bai X, **Zhao N**, Huang W, Caudal L, Catalin B, Cupido A, Zhao R, Hirrlinger J, Walz W, Kirchhoff F, Scheller A. (2017) After traumatic brain injury oligodendrocytes can regain a plastic phenotype and become astrocytes. (Nature neuroscience, under review)

2. Huang W, **Zhao N**, Bai X, Karram K, Trotter J, Goebbels S, Scheller A, Kirchhoff F. (2014) Novel NG2-CreERT2 knock-in mice demonstrate heterogeneous differentiation potential of NG2 glia during development. Glia; 62(6):896-913.

3. **Zhao N** et al., Effects of long-term administration of levo-thyroxine on ICa,L density in remodeled rat hearts. Journal of China Pharmaceutical University, 2007, 38(4):352-355.

Poster presentations

1. **Zhao N**, Huang W, Catalin B, Scheller A, Kirchhoff F (2015) The role of L-type Ca^{2+} channel subtypes 1.2 and 1.3 in NG2 glia. 12th Euroglia Meeting on Glial cells in Health and Disease. Bilbao, Spain.

2. **Zhao N**, Huang W, Scheller A, Kirchhoff F (2014) The role of L-type Ca^{2+} channel subtypes 1.2 and 1.3 in NG2 glia. DAAD-CAPES workshop in Brasilia, Brazil.

3. **Zhao N**, Huang W, Scheller A, Kirchhoff F (2013) The role of L-type Ca^{2+} channel subtypes 1.2 and 1.3 in NG2 glia. 11th Euroglia Meeting on Glial cells in Health and Disease. Berlin, Germany.

Acknowledgement

Firstly, I would like to express my sincere gratitude to my supervisor Prof. Frank Kirchhoff for the continuous support of my PhD study and related research, for his patience, motivation, and immense knowledge. His guidance helped me in all the time of research and writing of this thesis. I could not have imagined having a better supervisor and mentor for my PhD study.

Besides my supervisor, I would like to thank Prof. Dr. Peter Lipp, for agreeing to be the second correspondent of my thesis.

My sincere thanks also goes to Dr. Anja Scheller, who helped me with my scientific research and corrected my thesis. I am deeply grateful to Dr. Wenhui Huang, my colleague and my best friend for more than ten years for introducing me to Prof. Kirchhoff's lab and helping me establishment of my knowledge on neuroscience from zero. Many thanks for helping me with the experiments of Western blots and behavioral tests and many interesting discussion as well as reading my thesis and valuable advices. Without your precious support it would not be possible to conduct this research.

I would especially like to thank Daniel Rhode and all the members who working in the animal facility, for taking care of my lovely mice and always helping me to carry out all kinds of experiments.

I thank my fellow labmates Dr. Xianshu Bai, Laura Schlosser, Carmen Bohn and Laura Caudal for your close collaboration and many kind helps. I will never forget you giving me a birthday surprise. I am especially grateful to Bogdan Catalin for his help with morphology analysis and his jokes. I would like to thank Andrea Pantiru for polishing my writing.

My gratitudes also go to Frank Rhode for his great technical support for my research, for his kindness to help me solve the difficulties in my life and for his tasty cakes. I am also grateful to our secretary Ute Legler for taking care of the paperwork during my study and her kind help in my life.

I would like to thank Prof. Yuriy Pankratov for showing me electrophysiology experi-

ments on synaptic signaling.

I appreciate all the people who helped me during these years!

Lastly, I would like to thank my family for all their love and encouragement. For my parents who raised me with a love of science and supported me in all my pursuits. My deepest gratitude goes to Qinghai Tian for your greatest support in my study and my life. Thank you so much for supervising my Ca^{2+} imaging experiments and your programs as well as formatting my thesis.